

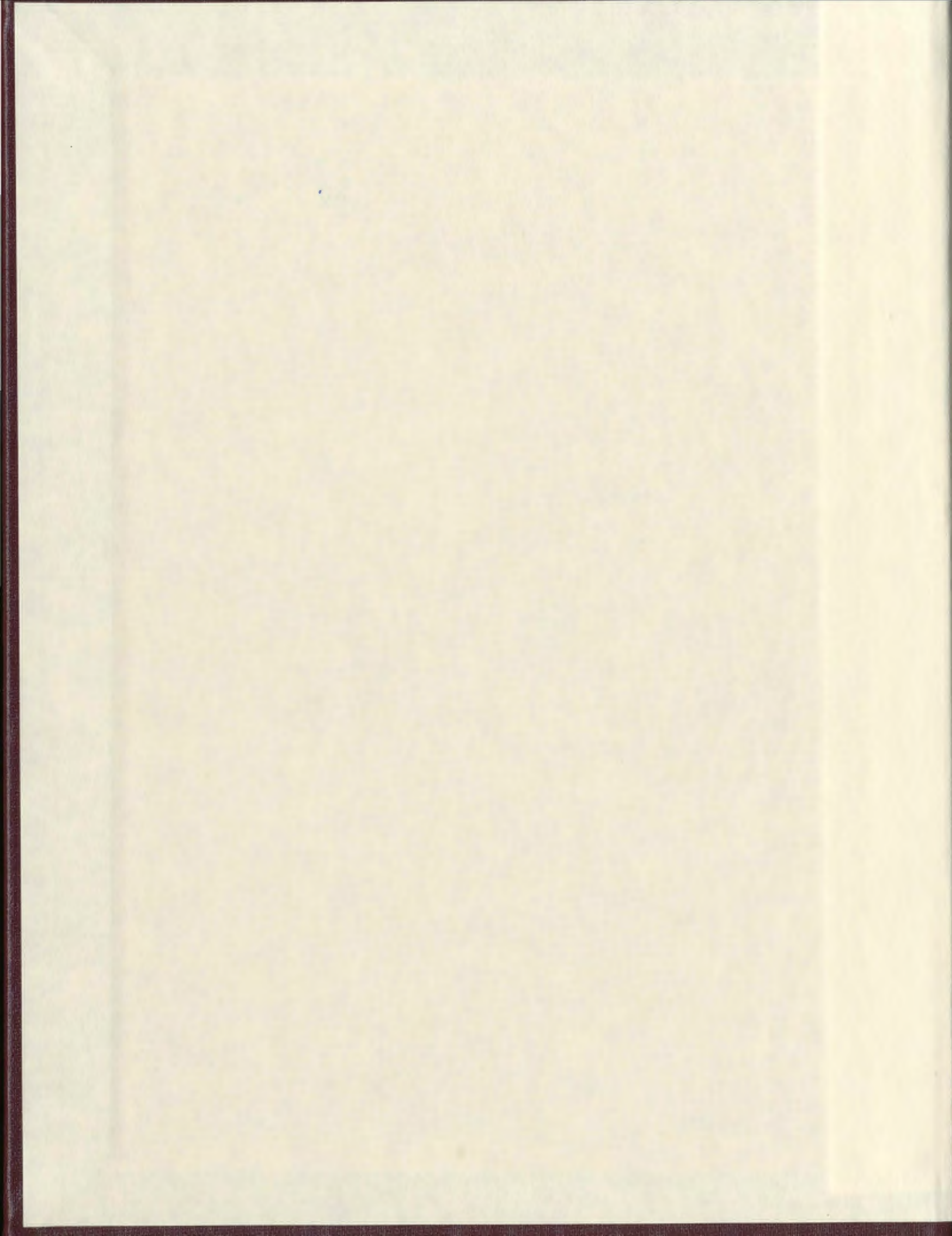
THE DEVELOPMENT AND GEOLOGICAL APPLICATION
OF A WHOLE ROCK - LA - ICP - MS TECHNIQUE
FOR THE DETERMINATION OF HIGH FIELD
STRENGTH ELEMENTS

CENTRE FOR NEWFOUNDLAND STUDIES

**TOTAL OF 10 PAGES ONLY
MAY BE XEROXED**

(Without Author's Permission)

JOY EMILY REID



1981
The author has granted a non-exclusive license allowing the National Library of Canada to reproduce, loan, distribute or sell copies of this thesis in microform, paper or other non-durable format.



The author has granted a non-exclusive license allowing the National Library of Canada to reproduce, loan, distribute or sell copies of this thesis in microform, paper or other non-durable format.

L'auteur a autorisé une licence non exclusive permettant à la Bibliothèque nationale du Canada de reproduire, prêter, distribuer ou vendre des copies de cette thèse sous la forme de microfiche/film, de reproduction sur papier ou sur format électronique.

The author retains copyright and the copyright in this thesis. Neither the thesis nor substantial extracts therefrom may be reproduced or otherwise disseminated without the author's permission.

L'auteur conserve la propriété du droit de copyright qui protège cette thèse. Ni la thèse ni des extraits substantiels de celle-ci ne doivent être reproduits ou autrement diffusés sans la permission de l'auteur.



National Library
of Canada

Acquisitions and
Bibliographic Services

395 Wellington Street
Ottawa ON K1A 0N4
Canada

Bibliothèque nationale
du Canada

Acquisitions et
services bibliographiques

395, rue Wellington
Ottawa ON K1A 0N4
Canada

Your file Votre référence

Our file Notre référence

The author has granted a non-exclusive licence allowing the National Library of Canada to reproduce, loan, distribute or sell copies of this thesis in microform, paper or electronic formats.

The author retains ownership of the copyright in this thesis. Neither the thesis nor substantial extracts from it may be printed or otherwise reproduced without the author's permission.

L'auteur a accordé une licence non exclusive permettant à la Bibliothèque nationale du Canada de reproduire, prêter, distribuer ou vendre des copies de cette thèse sous la forme de microfiche/film, de reproduction sur papier ou sur format électronique.

L'auteur conserve la propriété du droit d'auteur qui protège cette thèse. Ni la thèse ni des extraits substantiels de celle-ci ne doivent être imprimés ou autrement reproduits sans son autorisation.

0-612-42434-0

THE DEVELOPMENT AND GEOLOGICAL APPLICATION
OF A WHOLE ROCK – LA – ICP – MS TECHNIQUE FOR THE
DETERMINATION OF HIGH FIELD STRENGTH ELEMENTS

by

Joy Emily Reid, BSc (hons)

A thesis submitted to the
School of Graduate Studies
in partial fulfilment of the
requirements for the degree of
Master of Science

Earth Science Department, Centre of Earth Resource Research,
Memorial University of Newfoundland

May, 1998

St John's

Newfoundland

TABLE OF CONTENTS

TABLE OF CONTENTS.....	0-1
LIST OF FIGURES.....	0-5
LIST OF TABLES.....	0-8
LIST OF ACRONYMS.....	0-9
ABSTRACT.....	0-10
ACKNOWLEDGEMENTS.....	0-12
CHAPTER 1 . INTRODUCTION	1-1
CHAPTER 2 . REVIEW OF THE PHYSICAL CHEMISTRY AND PETROLOGIC IMPLICATIONS OF HFSE.....	2-1
2.1 PHYSICAL AND CHEMICAL PROPERTIES OF THE HFSE	2-1
2.1.1 <i>Niobium and tantalum</i>	2-1
2.1.2 <i>Zirconium and hafnium</i>	2-3
2.2 PETROLOGICAL SIGNIFICANCE OF HFSES	2-4
2.2.1 <i>General element classification</i>	2-4
2.2.2 <i>The petrological significance of the HFSE</i>	2-5
2.2.3 <i>Petrologic significance of the Nb/Ta ratio</i>	2-7
2.3 SUMMARY	2-11
CHAPTER 3 . ANALYTICAL PROBLEMS ASSOCIATED WITH HIGH FIELD STRENGTH ELEMENTS	3-1
3.1 CONTAMINATION THROUGH CRUSHING	3-2
3.2 USING X-RAY FLUORESCENCE (XRF) FOR THE DETERMINATION OF Nb AND Zr.....	3-2
3.3 USING INSTRUMENTAL NEUTRON ACTIVATION ANALYSIS (INAA) FOR THE DETERMINATION OF TA AND HF	3-4

3.4 INDUCTIVELY COUPLED PLASMA - MASS SPECTROSCOPY: A HIGHLY SENSITIVE, MULTI-ELEMENT TECHNIQUE.....	3-5
3.5 INDUCTIVELY COUPLED PLASMA – OPTICAL EMISSION SPECTROMETRY AND SPARK SOURCE MASS SPECTROMETRY.....	3-7
3.5.1 ICP-OES.....	3-7
3.5.2 SSMS.....	3-8
3.6 THE INSTABILITY OF HFSE IN SOLUTIONS OF DILUTE MINERAL ACIDS.....	3-9
3.7 SUMMARY.....	3-11

CHAPTER 4 . WHOLE ROCK LA-ICP-MS AND AN INVESTIGATION INTO THE USE OF ISOTOPE DILUTION AS A MEANS TO IMPROVE THE PRECISION AND ACCURACY OF WHOLE ROCK LA-ICP-MS ANALYSIS4-1

4.1 STRIP HEATING AS A RAPID METHOD OF PRODUCING HOMOGENEOUS GLASS BEADS.....	4-1
4.1 STRIP HEATER SET-UP.....	4-2
4.2 SAMPLE PREPARATION	4-4
4.3 HOMOGENEITY OF SYNTHETIC GLASSES	4-6
4.4 STRIP CLEANING BETWEEN SAMPLES.....	4-6
4.5 IMPURITIES IN THE METAL STRIP	4-7
4.6 ANALYTICAL PROCEDURE.....	4-8
4.6.1 ICP-MS.....	4-8
4.6.2 Laser ablation set-up.....	4-9
4.6.3 Data collection and reduction	4-10
4.6.4 Interferences	4-10
4.6.5 Results of whole rock - LA-ICP-MS on selected reference materials.....	4-11
4.7 ISOTOPE DILUTION - LA-ICP-MS: A NEW TECHNIQUE	4-12
4.7.1 Application of isotope dilution to whole rock LA-ICP-MS.....	4-14
4.7.1.1 Spike calibration:.....	4-17

4.7.2 Results of ID-LA-ICP-MS on selected standard reference materials	4-18
4.7.2.1 Precision	4-18
4.7.2.2 Accuracy	4-20
4.7.3 Conclusion	4-22
4.8 SUMMARY	4-23

CHAPTER 5. HIGH FIELD STRENGTH ELEMENT BEHAVIOUR: EVIDENCE FROM A VARIETY OF ROCK SUITES ANALYSED BY WHOLE ROCK - LA-ICP-MS.....5-1

5.1. Nb/Ta AND Zr/Hf VARIATION IN EACH TECTONIC ENVIRONMENT INVESTIGATED: RESULTS.....	5-2
5.1.1 MORB.....	5-2
5.1.2 Ocean Island Volcanic Rocks	5-3
5.1.3 Continental Crust	5-3
5.1.4 Destructive Margin Volcanic Rocks	5-3
5.1.3 Back-arc Basin and Related Volcanic Rocks.....	5-4
5.1.4 Boninites and Related Rocks	5-5
5.1.4.1 Dabi Tholeiites	5-5
5.1.4.2 Paquet Harbour Group, Newfoundland	5-6
5.1.5 Ultramafic Rocks	5-7
5.2 DISCUSSION	5-7
5.2.1 Nb/Ta variation within the samples analysed.....	5-9
5.2.2 Zr/Hf variation within the samples analysed.....	5-16
5.2 CONCLUSION.....	5-17

Appendix I . Tectonic settings and geographical locations..... I-i

A.1 MORB	I-I
A.1.1 Macquarie Island.....	I-i
A.1.2 ODP Leg 82 - MORB	I-ii
A.2 DESTRUCTIVE MARGIN VOLCANIC ROCKS.....	I-II
A.2.1 Sunda arc volcanics (Indonesia).....	I-iii

A.2.2 Vanuatu Island arc (<i>New Hebrides Anglo-French condominium</i>).....	I-iv
A.2.3 Tonga Ridge	I-v
A.3 BACK-ARC BASIN VOLCANIC ROCKS.....	I-V
A.3.1 Lau Basin, SW Pacific.....	I-v
A.3.2 Valu Fa Ridge	I-vi
A.3.3 Ata Island.....	I-vii
A.4 BONINITES AND RELATED ROCKS	I-VIII
A.4.1 Dabi Volcanics, Cape Vogel, Papua New Guinea	I-ix
A.4.2 Pacquet Harbour Group, Newfoundland, Canada.....	I-ix
A.4.3 Boninites from Bonin Island and Boninite-Related Rocks from Japan	I-x
A.5 OCEAN ISLAND VOLCANIC ROCKS	I-XI
A.6 CONTINENTAL CRUST	I-XII
A.7 ULTRAMAFIC SAMPLES	I-XIII
A.7.1 Xenoliths.....	I-xiii
A.7.2 Troodos Ophiolite, Cyprus.....	I-xiii
Appendix II . Data tables.....	II-i
REFERENCES.....	III

LIST OF FIGURES

Figure 2.1: A flow chart illustration of the various classification schemes used in geochemistry.....	2-17
Figure 2.2: Primitive mantle normalized plot.....	2-18
Figure 2.3: Graph to show a model of the variation of Nb/Ta ratios with partial melting of a garnet lherzolite.....	2-19
Figure 3.1: Solubility of K_2NbOF_5 and K_2TaF_7 in solutions of HF.....	3-15
Figure 3.2 a: A comparison of XRF and solution nebulisation ICP-MS determinations for Zr analysed at Memorial University of Newfoundland, Canada.....	3-16
Figure 3.2 b: A comparison of XRF and solution nebulisation ICP-MS determinations for Nb analysed at Memorial University of Newfoundland, Canada	3-17
Figure 3.2 c: A comparison of the Sr determinations by XRF and solution nebulisation ICP-MS for a variety of geological samples analysed at Memorial University	3-18
Figure 3.2 d: A comparison of the Rb determinations by XRF and solution nebulisation ICP-MS for a variety of geological samples analysed at Memorial University.....	3-19
Figure 4.1: Schematic sketch of strip-heater and sample.....	4-30
Figure 4.2: Photographs taken of synthetic glasses under a petrographic microscope using plane polarized light.....	4-31
Figure 4.3: The precision of the analyses of two synthetic geostandard glasses analysed using LA-ICP-MS.....	4-32

Figure 4.4: Semi-quantitative impurity concentrations in a >99.95% (Alpha Aesar) tungsten-strip.....	4-33
Figure 4.5: Time resolved LA-ICP-MS analysis of Gran Canaria synthetic glass.....	4-34
Figure 4.6: CrAr ⁺ interference on Nb.....	4-35
Figure 4.7: Suspected interference on Nb in Al-rich rocks analyzed by solution nebulisation ICP-MS.....	4-36
Figure 4.8: The effect of over- and under-spiking on the resulting accuracy of a BCR-2 analysis by ID-LA-ICP-MS.....	4-37
Figure 4.9: Accuracy of Zr and Hf ID-LA-ICP-MS determinations.....	4-38
Figure 4.10: Chondrite normalised REE plot for geostandards Jb-2 and Jb-3.....	4-39
Figure 5.1: The variation of Nb/Ta with Nb for all island arc and non-arc related suites and non-arc related rock suites.....	5-19
Figure 5.2: The variation of Zr/Hf with Zr for all island arc and non-arc related suites and non-arc related rock suites.....	5-20
Figure 5.3: N-MORB normalised extended plot for E-MORB samples from Macquarie Island	5-21
Figure 5.4: Primitive mantle normalised extended plot for all island arc samples	5-22
Figure 5.5: N-MORB normalised extended plot for synthetic and natural glasses from Southern Lau Basin.....	5-23
Figure 5.6: N-MORB normalised extended plot for natural glasses from Central Lau Basin.....	5-24

Figure 5.7: Primitive mantle normalised REE plot for all boninites and related rocks from Bonin Island, Japan, Papua New Guinea and Newfoundland.....	5-25
Figure 5.8: Primitive mantle normalised extended plot for boninites and related rocks	5-26
Figure 5.9: Nb/Ta variation with Nb and Ta for Dabi tholeiites, Cape Vogel.....	5-27
Figure 5.10: Nb/Ta variation with Nb and Ta for Pacquet Harbour Group boninites...	5-27
Figure A.1: Macquarie Island map.....	I-i
Figure A.2: The Sunda and Banda arcs of Indonesia map.....	I-iii
Figure A.3: Vanuatu Island arc map.....	I-iii
Figure A.4: Ambrym Island, Vanuatu map.....	I-iv
Figure A.5: Tanna Island, Vanuatu map.....	I-iv
Figure A.6: Map showing the location of and spatial relationship between Vanuatu, Tonga and Lau Basin.....	I-iv
Figure A.7: Tonga Ridge and Lau Basin.....	I-v

LIST OF TABLES

Table 2.1: Physical Properties of Niobium and Tantalum.....	2-13
Table 2.2: The chemical composition of selected niobium and tantalum bearing minerals	2-14
Table 2.3: Physical Properties of Zirconium and Hafnium.....	2-15
Table 2.4: A compilation of partition coefficient data for Nb and Ta between various crystal phases and melt chemistries.....	2-16
Table 3.1: The routine performance of XRF in the analysis of Nb and Zr.....	3-13
Table 3.2: The routine performance of INAA in the analysis of Ta and Hf.....	3-13
Table 3.3: The limits of detection (LOD) of ICP-OES and ICP-MS.....	3-13
Table 3.4: A comparison of the expected precision and accuracy of ID-SSMS and SSMS	3-14
Table 4.1: Major element homogeneity in a synthetic BCR-2 glass.....	4-24
Table 4.2: Results of geological standard synthetic glass analyses by whole rock - LA- ICP-MS.....	4-25
Table 4.3: Calculated concentrations of spike solutions and stock solution.....	4-27
Table 4.4: Precision (RSD) of background corrected ratios of duplicate BCR-2 analyses and NIST SRM 612 glass compared to Poisson counting statistics.....	4-28
Table 4.5: Duplicate analyses of SRM BCR-2.....	4-29
Table 5.1: A review of the samples analysed by whole rock LA-ICP-MS; number of samples analysed, tectonic setting and geographical location, and HFSE ratio characteristics.	5-18

LIST OF ACRONYMS

Acronym	Translation
BAB	Back-arc basin
E-MORB	Enriched - MORB
IAB	Island-arc basalt
ICP-MS	Inductively coupled plasma – mass spectrometry
ICP-OES	Inductively coupled plasma – optical emission spectrometry
ID	Isotope dilution
INAA	Instrumental neutron activation analysis
MORB	Mid-ocean ridge basalt
N-MORB	Normal - MORB
OIB	Ocean island basalt
SSMS	Spark source mass spectrometry
XRF	X-ray fluorescence

ABSTRACT

Whole rock, laser ablation - inductively coupled plasma - mass spectrometry (LA-ICP-MS) was carried out on synthetic and natural glasses in an attempt to improve the precision and accuracy of the determination of high field strength element (HFSE) abundances. Compared to more conventional methods of analysis, such as X-ray fluorescence and ICP-optical emission spectrometry, ICP-MS offers lower limits of detection. Neutron activation analysis typically has worse precision than ICP-MS and is more labour intensive. The determination of HFSE by solution nebulisation ICP-MS is compromised by problems associated with solution instability and the possibility of incomplete digestion of mineral phases in acid. To avoid the problems inherent in solution nebulisation ICP-MS, a solid-sampling technique was developed by preparing synthetic glasses that were fused using an iridium strip heater and analysed with LA-ICP-MS. The results for fused geostandard reference materials (G-2, NBS688, MRG-1, SY-2, SY-3, and AGV-1) have an accuracy of within 11% of literature values for REE determinations and within 7% for HFSE determinations. The average precision (1σ) of analysis is within 5% for REE determinations and within 4% for HFSE determinations.

An investigation was carried out on the application of isotope dilution (ID) to whole rock LA-ICP-MS through spiking the sample powder with an isotopically enriched solution (^{91}Zr , ^{179}Hf , ^{145}Nd , ^{151}Eu , ^{161}Dy and ^{171}Yb) before fusion. The results for geostandards BHVO-1, MRG-1, AGV-1 and BCR-2 analysed with this ID-LA-ICP-MS

technique show an accuracy of within 4% of literature values for Zr and Hf. The ID-Zr values determined by isotope dilution were used as an internal standard, with external calibration on NIST SRM 612 glass, for the determination of Nb, Ta, La, Ce, Pr, Sm, Gd, Ho, Tm and Lu. The accuracy achieved with this methodology is within 3% for Nb, 6% for Ta and 8% for REE determinations.

Over 100 geological samples from a variety of tectonic settings have been analysed by whole rock LA-ICP-MS in order to determine accurate and precise HFSE values. The main emphasis of this study was to investigate the variation of Nb/Ta and Zr/Hf ratios and assess the potential for these element pairs to fractionate within geological systems. The Nb/Ta ratios for virtually all of the mid-ocean ridge and ocean island basalt samples, and a majority of the island arc samples, overlapped within the chondritic range (17.5 ± 2). Because Nb/Ta does not appear to fractionate among very diverse tectonic settings (such as MORB, OIB and most arcs), the non-chondritic values found for a few of the arc samples (Nb/Ta = 11 to 26), and all of the boninitic (Nb/Ta = 9 to 12) and continental crust samples (Nb/Ta = 4 to 9), suggest that very unusual mantle processes characterise the genesis of these rocks. These processes might include fractionation related to metasomatism or the existence of an accessory phase such as rutile or amphibole. In comparison to Nb/Ta, Zr/Hf ratios showed a greater tendency to fractionate below the chondritic margin of error (36.3 ± 4) with overall values from 19 to 45 and a mean value of 31. This may reflect the greater tendency of Zr to fractionate from Hf related to the greater difference in the bulk partition coefficients of these elements.

ACKNOWLEDGEMENTS

The author would like to acknowledge the financial support of the Natural Science and Engineering Research Council of Canada (NSERC), which provided equipment grants to fund the purchase of the ICP-MS and laser ablation system at Memorial University. NSERC also provided infrastructure and major facility access grant support that ensures the long term operation and management of the facility. Memorial University also provided technical support through the department of Technical Services machine shop and electronic personnel. Mike Tubrett greatly contributed to the maintenance and daily alignment of the instruments and Lakmali Hewa contributed in the preparation of standard solutions. Gratitude is also extended to Roberta L. Rudnick and William F. McDonough for their interest in this project and for the use of the LA-ICP-MS facilities at Harvard University. Gaby Loock is acknowledged for her work in the collection of Lau Basin natural glasses, which were analysed a part of this study.

Many thanks go to Henry Longerich for the time and energy spent in explaining the fundamentals of analytical thinking and the practicalities of a good scientific approach. I am indebted to Ingo Horn for being my closest teacher, supervisor, and friend. Many thanks also go to all those who helped during the course of this study, especially Mark Wilson and, my supervisor, George Jenner, who provided inspiration and guidance at critical times. Thanks also to Roger Mason, Murry Brooker, Greg Dunning, Maggy Pirania and David Lange for their patience and instruction. Thanks also to Javier Fernandez-Saurez, Caroline Petibon, Lisa Miller and Steve Piercey who provided support and advise.

Chapter 1. INTRODUCTION

The main emphasis of this study was to improve the precision and accuracy of the determinations of the high field strength elements (HFSE) (niobium (Nb), tantalum (Ta), zirconium (Zr) and hafnium (Hf)), in rocks by inductively-coupled-plasma-mass spectrometry (ICP-MS). The motivation for this study largely reflects the extensive use of HFSE in geochemistry: relative concentrations of these elements compared to elements with more affinity for silicate phases are often used as tectonic discriminators (Rollinson, 1993); relative depletions of Nb and Ta are characteristic of destructive plate margin magmatism and of the continental crust (Pearce and Peate, 1995); Hf isotopes derived from the radiogenic system lutetium-hafnium are increasingly used as tools to interpret mantle depletion episodes and their chronology with respect to that of the Earth's genesis (Lee and Halliday, 1995). Of particular interest, there is a lack of data on the distribution of Nb/Ta ratios and to a lesser extent of Zr/Hf ratios within the Earth's crust and upper mantle. These element pairs behave in a very similar geochemical manner due to their nearly identical physio-chemical properties and it has been assumed by many that their ratios remain constant within analytical error (Hofmann, 1988).

The measurement of HFSE is compromised in a number of ways by the analytical techniques available. For example, determination of Nb by X-ray fluorescence (XRF) is not precise for concentrations below $5 \mu\text{g g}^{-1}$ (detection limit of many instruments) and instrumental neutron activation analysis (INAA) for Ta and Hf is time consuming and work intensive with a typical precision of 10% (Potts, 1987). The analytical capabilities of ICP-MS and ICP-optical emission spectrometry (-OES) for the analysis of HFSE are

compromised by the instability of these elements in solution and their tendency towards irreversible hydrolysis (Gibalo, 1970; Fairbrother, 1967). This study employed solid sampling using a laser ablation-(LA-) ICP-MS technique to provide analyses with high accuracy and precision, thereby eliminating problems associated with solution instability and removing the issue of incomplete acid digestion of resistant phases containing the HFSE (*e.g.* zircon, titanates and oxides). This technique has been shown to be a rapid method for the determination of trace elements in silicate rocks using flux-free fused glass beads (Fedorowich *et al.*, 1993; Odling, 1995).

The analytical techniques used in this study are laser ablation ICP-MS (LA-ICP-MS), solution nebulisation (after acid digestion) ICP-MS, isotope dilution LA-ICP-MS (ID-LA-ICP-MS) and electron microprobe. Sample preparation for LA-ICP-MS involves fusion of a powder using a strip heater built in-house. Solution ICP-MS was used for the calibration of enriched isotopes used in ID-LA-ICP-MS. A database for all acid digest ICP-MS, sinter ICP-MS and XRF runs carried out at Memorial University of Newfoundland over the last ten years was re-organised and investigated. Review of this database allowed the long-term precision of these techniques to be evaluated for different elements in a variety of samples.

The text of this thesis is structured as follows: The behaviour and classification of the HFSE will be examined in Chapter Two, including both an overview of the physical chemistry of Nb, Ta, Zr and Hf and their behaviour in geological systems; Chapter Three includes an overview of the analytical techniques used to measure concentrations of the HFSE (INAA, XRF, ICP-MS, ICP-OES and spark source mass spectrometry) and

problems associated with each; Chapter Four describes the rationale and approach behind the whole rock LA-ICP-MS methodology used in this study and the results of the quality control experiments carried out; Chapter Five presents the results for a number of geological samples analysed by this method and an interpretation of the results, including an investigation of the feasibility of using Nb/Ta and Zr/Hf ratios for the tectonic discrimination of different rocks. Within these chapters, the text comes first followed by the tables and figures, to facilitate review of the material. Complete tables of analytical data obtained can be found in the appendices.

CHAPTER 2. REVIEW OF THE PHYSICAL CHEMISTRY AND PETROLOGIC IMPLICATIONS OF HFSE

2.1 Physical and chemical properties of the HFSE

2.1.1 Niobium and tantalum

Niobium and tantalum are transition metals of Group V in the periodic table. From Table 2.1 it can be seen that although the atomic weights of the elements differ by a factor of two they have nearly identical ionic radius/charge ratios ($\text{Nb} = 0.64 \text{ \AA} / 5^+$ and $\text{Ta} = 0.64 \text{ \AA} / 5^+$) in the six-fold co-ordination state (Shannon, 1976). The ionic radius/charge ratio of Nb and Ta is less than 0.2, classifying these elements as “high field strength elements” (HFSE) (Saunders *et al.*, 1980). A similar ionic radius/charge ratio gives Nb and Ta very similar chemical characteristics. However, Nb is slightly more electronegative than Ta (Krauskopf, 1967) and, therefore, should exhibit a stronger preference for lower oxidation states. Wolff (1984), in a study of the petrogenesis of Canary Island phonolites, suggested that the presence of Nb^{3+} was the cause of the observed fractionation between Nb and Ta. The ionic radius of Nb is 0.72 \AA in the trivalent, six-fold co-ordination state, giving it an ionic radius ratio/charge of 0.24 ($0.72 \text{ \AA} / 3^+$) (Shannon, 1976).

Nb and Ta are rare metals with estimated abundances in the Earth’s crust of $14 \mu\text{g g}^{-1}$ Nb and $1 \mu\text{g g}^{-1}$ Ta (Plank and Langmuir, 1998), or $25 \mu\text{g g}^{-1}$ Nb and $2.2 \mu\text{g g}^{-1}$ Ta (Taylor and McLennan, 1985). These elements do not occur as native metals or as sulphides, however, there are 72 minerals known where Nb and Ta occur as the main constituents and more than 60 known where they occur as trace constituents (Gibalo,

1970). Most of these minerals are complex oxides and silicates (Table 2.2) where other metals such as the lanthanides, uranium and thorium are often of more economic interest. Most of the commercial production of Nb and Ta has been derived from the columbite-tantalite series of minerals (Table 2.2) (Fairbrother, 1967); the ore is called *columbite* if the Nb content is greater than the Ta content and *tantalite* if the Ta content is greater. The mineral pyrochlore may contain up to 70 wt% of Nb₂O₅ and is interesting in that it contains virtually no Ta.

Nb is mainly used in arc-welding rods for stabilised grades of stainless steel (Fairbrother, 1967). Superconductive magnets have been made with Nb-Zr wire, which has superconductivity in strong magnetic fields (Lide, 1996). The metal Ta has many uses due to its high melting point and chemical resistance. It is used in the manufacture of electronics, alloys and glass and, due to its chemical resistance, also in surgery (Fairbrother, 1967). The metal is also widely used to fabricate chemical process equipment, nuclear reactors, aircraft, and missile parts (Lide, 1996). Scientists at Los Alamos have produced a tantalum carbide graphite composite material, which is said to be one of the hardest materials ever made with a melting point of 3738°C (Lide, 1996).

Despite the industrial demand for Nb and Ta, the main geochemical interest in these elements lies in their trace element abundance in rocks and minerals. The Nb/Ta ratios in rocks remains within the error of the chondritic ratio (17.5 ± 2 , Sun and McDonough, 1989) in the vast majority of tectonic settings (this study).

2.1.2 Zirconium and hafnium

Zirconium and hafnium are transition metals belonging to Group IV in the periodic table. Like Nb and Ta these elements are often considered to be geological "twins" (Table 2.3), with very similar ionic radius to charge ratio ($Zr = 0.72\text{\AA} / 4^+$ and $Hf = 0.71\text{\AA} / 4^+$) in the six-fold co-ordination state (Shannon, 1976). Estimated abundances in the Earth's crust are $100\ \mu\text{g/g}$ Zr and $3.0\ \mu\text{g/g}$ Hf (Taylor and McLennan, 1985).

Compared to Nb and Ta, the distribution of Zr and Hf is more fully understood because they often concentrate in more evolved igneous rocks and in metamorphic assemblages as the minerals zircon (relative cation abundance 94% ZrO_2 , 1.2% HfO_2 , Mukherji, 1970) or, less commonly, baddeleyite. The ratio of Zr/Hf is not thought to deviate strongly from the chondritic ratio of 36.3 (Sun and McDonough, 1989).

Zr is very resistant to corrosion by many common acids and alkalis and is used extensively by the chemical industry. Zr is also used as a "getter" in vacuum tubes, as an alloying agent in steel, in surgical appliances, photoflash bulbs, explosive primers, rayon spinnerets and lamp filaments (Lide, 1996). Zirconium oxide has a high index of refraction and is used as a gem material. The impure oxide, zirconia, is used for laboratory crucibles, for linings of metallurgical furnaces, and by the glass and ceramic industries (Lide, 1996). Hf is used for reactor control rods in nuclear submarines due to its good absorption cross section for thermal neutrons (almost 600 times that of zirconium) (Lide, 1996). It also has excellent mechanical properties and is extremely resistant to corrosion (Mukherji, 1970).

2.2 Petrological significance of HFSEs

2.2.1 General element classification

A summary of basic, element classification schemes that can be used in geochemistry is illustrated in Figure 2.1. The classification schemes can be used in any combination as they are based on different physical and chemical properties. However, it is possible to correlate between the groupings, for example, it is often assumed that low field strength elements (LFSE) are *mobile* (transported in aqueous fluids) under most circumstances. Properties such as compatibility and mobility are, of course, a function of the environment prevailing, and conditions such as composition, pressure, temperature, oxygen fugacity and volatile content need to be specified. The terms *compatible* and *incompatible* are used commonly in a very general sense to give a feel for how these elements behave during partial melting of a peridotitic composition at moderate pressures (30Kbars). With the conditions at the time of equilibration specified, an element is compatible if the bulk partition coefficient ($D = \frac{\sum \text{concentration of element in all solid phases}}{\text{concentration of element in melt}}$, Rollinson, 1993) is greater than 1 and incompatible if D is less than 1. In Figure 2.1, the appropriate classification boxes are outlined for the element Nb; it is a refractory, lithophile, trace abundant, high field strength element, which is typically incompatible and immobile. This is also the case for Ta, Zr, Hf and Ti (can also be a major element).

2.2.2 The petrological significance of the HFSE

The factors that contribute to the composition of a melt derived from the mantle or crust are the degree of partial melting that occurred, the composition and mineralogy

of the source, the volatile content of the source and the pressure prevailing at melt segregation (Takahashi, 1986; Baker *et al.*, 1995). These factors can be deduced from the trace and major elements, fluid inclusion and isotopic compositions and petrography of the resulting rock. For mafic rocks the HFSE are important because of their high incompatibility in residual phases and, therefore, their preference to fractionate into the melt. If any subsequent fluid interaction occurs then these elements are unlikely to be affected as they are highly immobile in fluids (Brenan *et al.*, 1993; Keppler, 1996). If the source composition is known, then the degree of partial melting at the source can be deduced from a combined knowledge of the concentration of HFSE in the derivative rock and the partition coefficients that are thought to be relevant for the prevailing pressure and temperature of segregation. From a different perspective, if the degree of partial melting is otherwise constrained, the HFSE concentration of the source can be deduced. Comparing this to the primitive mantle composition (Sun and McDonough, 1989) gives an indication of the level of source depletion. For example, mid-ocean ridge basalts (MORB) are derived from a depleted mantle source and have a relatively low abundance of incompatible elements in the derived basalts. In contrast, ocean island basalts, such as Hawaiian basalts, are relatively enriched in incompatible elements, derived from a more enriched mantle source. Complications in the interpretation of trace elements of mafic magmas can arise from processes such as crustal contamination, fractional crystallisation, metasomatism and magma mixing. The crust is highly enriched in incompatible elements but has a sub-chondritic Nb/Ta ratio (< 17.5 , Sun and McDonough, 1989) and a negative Nb anomaly with respect to other incompatible elements and so, if assimilated into a

melt, can change the mantle signature. It is useful to use isotopic information, such as $^{87}\text{Sr}/^{86}\text{Sr}$ ratios, to indicate if there has been any crustal contamination (Faure, 1986). Fractional crystallisation involves the removal of crystalline phases from a melt as it cools from its liquidus to its solidus temperature. Due to the high solubilities of HFSE in basaltic melt, it is not until more felsic compositions are reached that HFSE-enriched accessory minerals precipitate (Green and Pearson, 1986). Nb and Ta partition strongly into Ti-rich accessory phases such as sphene and rutile, whereas Zr and Hf commonly precipitate in the form of zircons. In a suite of rock compositions related by fractional crystallisation, trace element chemistry can be used to model the crystallisation sequence of major and accessory phases.

The HFSE are commonly used as a means to discriminate among rocks of different tectonic settings, especially mafic-intermediate volcanic rocks (Harris *et al.*, 1986; Pearce *et al.*, 1984; Floyd and Winchester, 1975; Pearce, 1982; Canabis and Lecolle, 1989; Wood, 1980). For example, it is known that island arc basalts are typically depleted in HFSE but enriched in large ion lithophile elements (LILE), relative to mid-ocean ridge basalts, whereas ocean island basalts are relatively enriched in all incompatible elements.

One of the most common ways of presenting geochemical data is by way of a primitive mantle-normalised plot. The elements are plotted in a sequence reflecting the bulk distribution coefficients during partial melting of a peridotitic mantle that gives rise to normal mid-ocean ridge basalt (Jenner, 1996). The bulk distribution coefficients increase from the left to right on the plot reflecting an increasing compatibility of the

elements plotted. Theoretically there should be a smooth trend between the elements reflecting their increasing or decreasing compatibility in the source residue however, there are occasions when “anomalies” occur. For example, if the oxidation state is unusually reducing Eu will enter the 2⁺ valence state and may therefore enter into plagioclase, causing a negative Eu anomaly in the residue and a positive Eu anomaly in a plagioclase cumulate. One of the most characteristic trace element signatures of island arc magmatism can be seen on a primitive mantle-normalised plot as a negative Nb and Ta anomaly (Figure 2.2). There is a plethora of speculation as to the origin of this signature (discussed in Chapter Five).

2.2.3 Petrologic significance of the Nb/Ta ratio

Due to the chemical similarities of Nb and Ta (section 2.1.1) it has been thought that the ratio of their concentrations within the Earth’s crust remains roughly constant at the chondritic value of Nb/Ta = 17.5 ± 2.0 (Sun and McDonough, 1989) or 17.6 ± 2 (Jochum *et al.*, 1986, 1989a,b). Any variation of this ratio was commonly thought to result from analytical error (section 3). However, with improvements in geochemical analysis it has been possible to investigate the fractionation of these elements in rocks and minerals from different tectonic settings with a reasonable degree of accuracy and precision (Green, 1995; Stolz *et al.*, 1995; Eggins *et al.*, 1997; and Munker, 1998). The only rock suites that remain difficult to analyse precisely are those with low Nb and Ta concentrations such as in many granites, island arc and ultramafic suites (Green, 1995).

It can be seen from Table 2.4 that Nb and Ta are highly incompatible elements with partition coefficients (K_{dNb} and K_{dT_a} , Rollinson, 1993) less than unity for most

phases. The ratio K_{dNb}/K_{dTaNb} illustrates the potential of a mineral phase to fractionate Nb and Ta from each other. Sphene, rutile and garnet are phases which show a significant difference in their compatibility's for Nb and Ta (K_{dNb}/K_{dTaNb} sphene = 0.3; rutile = 0.6-0.7 and garnet = 0.3). In the majority of studies, Ta is more compatible than Nb ($K_{dNb}/K_{dTaNb} < 1$), and so fractional crystallisation or small degrees of partial melting would result in an increase in the Nb/Ta ratio of the melt. However, a study by Brenan *et al.* (1994) on the partitioning of Nb, Ta, Hf, Zr, U between rutile and aqueous fluid, found that niobium was more compatible than Ta in the rutile. This is in contrast to the higher compatibility of Ta in rutile when in equilibrium with a silicate melt (Green and Pearson, 1987). These results have important implications because an aqueous fluid derived from a rutile-bearing source would provide a metasomatising agent that would effectively decrease the Nb/Ta ratio of affected source regions. Another mechanism which is thought to decrease the Nb/Ta ratio is assimilation of continental crust which has a relatively low Nb/Ta ratio of 11 (Taylor and McLennan, 1985), to 14, (Plank and Langmuir, 1998). As yet there are no generally accepted mechanisms to explain the low Nb/Ta ratios of boninites (this work) or the continental crust.

Nb and Ta are commonly used as petrogenetic indicators with the assumption that the Nb/Ta ratio of the mantle source region has a constant chondritic value with no subsequent fractionation. The data above suggests that fractionation may take place and that the variation in Nb/Ta of rocks from different tectonic settings may reflect such processes as:

1. metasomatism by aqueous fluids, carbonatitic melts or silicate melts (Sweeney *et al.*, 1992; Green, 1995);
2. fractionation of a Ti-rich phase such as rutile or sphene from a melt (Green 1995);
3. low degrees of partial melting from a source containing a titanite or silicate phase which can fractionate Nb from Ta (Stolz *et al.* 1996); and
4. contrasting solubilities of Nb and Ta in peralkaline and subaluminous melt compositions (Linnen and Keppler, 1997).

It is thought that crystal fractionation of silicate minerals such as garnet, amphibole and clinopyroxene may explain small-scale variation but not crust-mantle variation (Green, 1995).

The high K_{dNb}/K_{dTa} ratios for garnet (Green *et al.*, 1989) suggest that small degrees of partial melting from a garnet-bearing source could result in a melt with a super-chondritic Nb/Ta ratio. This melt could then percolate upward, altering the Nb/Ta ratios of source regions for crustal magmas. To test this model, the computer program, *Newpet*, was used constrained by the following parameters: The initial source rock was a garnet lherzolite, taken from a world wide average xenolith study (Maaløe and Aoki, 1977) and consisting of 63% olivine, 30% enstatite, 2% diopside and 5% garnet. The change of Nb and Ta concentrations with partial melting was carried out assuming an initial composition of 0.713 $\mu\text{g/g}$ Nb and 0.041 $\mu\text{g/g}$ Ta (Sun and McDonough, 1989). Two melting scenarios were tested with different proportions of phases contributing to the melt: (1) 5% olivine, 5% enstatite, 10% diopside and 80% garnet and (2) 10% olivine, 10% enstatite, 40% diopside and 40% garnet. In each case, there was a similar decrease

in Nb and Ta concentrations in the derived melt with increase in partial melting. The Nb/Ta ratio variation was controlled by the garnet and decreased exponentially from very high ratios at very small degrees of partial melting to lower, less variable ratios, at larger degrees of melting (Figure 2.3). When garnet was completely removed from the residue the Nb/Ta ratio variation with partial melting was insignificant.

Recently, experiment work by Linnen and Keppler (1997) investigated the solubility of Nb- and Ta-rich phases (MnNb_2O_6 and MnTa_2O_6) in granitic melts. The results showed that the equilibrium fractionation of Nb and Ta between silicate melts and mineral phases is strongly dependent on melt composition. There was an increase in the ratio $K_{\text{dNb}}/K_{\text{dTaN}}$ (between rutile and silicate melt) from andesite to trachyte to peralkaline and peraluminous granite related to changes in the activity of Nb and Ta in the melt. It is estimated by Linnen and Keppler that the $K_{\text{dNb}}/K_{\text{dTaN}}$ should increase by a factor of 4-5 when going from andesitic to subaluminous or peraluminous granitic melts. Although there is no systematic variation of Nb/Ta with percentage fractionation for several alkaline and calc-alkaline lava suites, ranging from basaltic to rhyolitic in composition, there is a systematic decrease in Nb/Ta with increasing fractionation of peraluminous granites and rhyolites (Linnen and Keppler, 1997). This process is thought to contribute to the sub-chondritic Nb/Ta ratio of the continental crust.

The similar relative Nb depletions of island arc and continental crust rocks are perhaps the strongest evidence that the continental crust was formed at subduction zones (Thirlwall *et al.*, 1994). However, it can be seen that island arc magmatism is typically depleted in both Nb and Ta, with marked Nb and Ta anomalies on primitive mantle

normalised extended plots and variable Nb/Ta ratios which are both sub- and super-chondritic. The continental crust, however, has consistently sub-chondritic Nb/Ta ratios caused by Nb negative anomalies and Ta concentrations that are consistent with elements of similar compatibility. This would suggest that there is not a clear relationship between continental crust genesis and island arc magmatism.

2.3 Summary

The HFSE are of importance to geochemists. The incompatibility of HFSE in mantle phases combined with their immobility enables them to be used as tectonic discriminators with minimal effect from metasomatic or hydrothermal alteration systems. Prehistory of fractional crystallisation and degrees of partial melting of a source can be estimated from a combined knowledge of the source composition and partition coefficients of HFSE between residue and segregating melt. The similar behaviour of Nb-Ta and Zr-Hf may provide indication of subtle metasomatic effects such as that found for Zr/Hf ratios by Rudnick *et al.* (1991) in Tanzanian xenoliths and those found in this study for Nb/Ta ratios in boninites.

Table 2.1: Physical Properties of Niobium and Tantalum

	Niobium	Tantalum	Reference
Atomic number	41	73	
Atomic weight	92.906	180.948	Sharp (1990)
Atomic Radius, Å	1.45	1.47	Gibalo (1970)
Ionic radius (VI), Å	(valency 5+) 0.64	(valency 5+) 0.64	Shannon (1976)
Electron configuration	Kr4d ⁴ 5s ¹	Xe4f ¹⁴ 5d ³ 6s ²	Fairbrother (1967)
Density (20°C) gcm ⁻³	8.57	16.62-16.66	Sharp (1990)
Melting point °C	2468	2996	Sharp (1990)
Boiling point, °C	4742	5425	Sharp (1990)
Crystal structure	bcc	bcc	Fairbrother (1967)

Table 2.2: The chemical composition of selected niobium and tantalum bearing minerals (Gibalo, 1970):

Wt %	Columbite	Tantalite	Pyrochlore	Microlite	Loparite
Nb₂O₅	56.43-77.97	2.50	37.54-70.0	7.74	11.06-11.48
Ta₂O₅	5.26-30.58	53.28-82.83	0-5.86	68.43-77.0	
TiO₂	0-1.50	0-0.71	0.83-12.25	0-1.58	39.22-39.24
SiO₂			0.09-3.78		0.27-0.72
SnO₂	0-0.73	0-1.51	0.25-0.55	0.8-4.0	
ZrO₂	0-0.54		0.53-4.99		
ThO₂			0.26-9.28		0.53
Fe₂O₃			0.36-4.30		0.06-0.72
ΣCe₂O₃			0.66-13.33	0.17-4.20	
ΣY₂O₃			0.24-11.34	0-0.23	39.30-34.61
UO₂			0.20-12.90	0-4.21	
UO₂			0.43-10.68	0-1.59	
CaO	1.27-0	0-0.17	2.82-20.01	10.48-15.03	4.22-5.76
Na₂O			2.52-6.93	1.66-5.03	7.88-9.06
K₂O					0.26-0.75
H₂O	0-0.40	0-0.16	0.47-11.35	0-5.70	
FeO	5.07-16.8	1.17-12.67			
MnO	2.39-10.41	1.33-14.15			
WO₃	0-1.07	0-0.3			
PbO₂	0-0.12				
Bi₂O₃				0-3.25	
Al₂O₃					0.72
SrO			1.07		3.0
F			0.49-4.31	0-2.85	

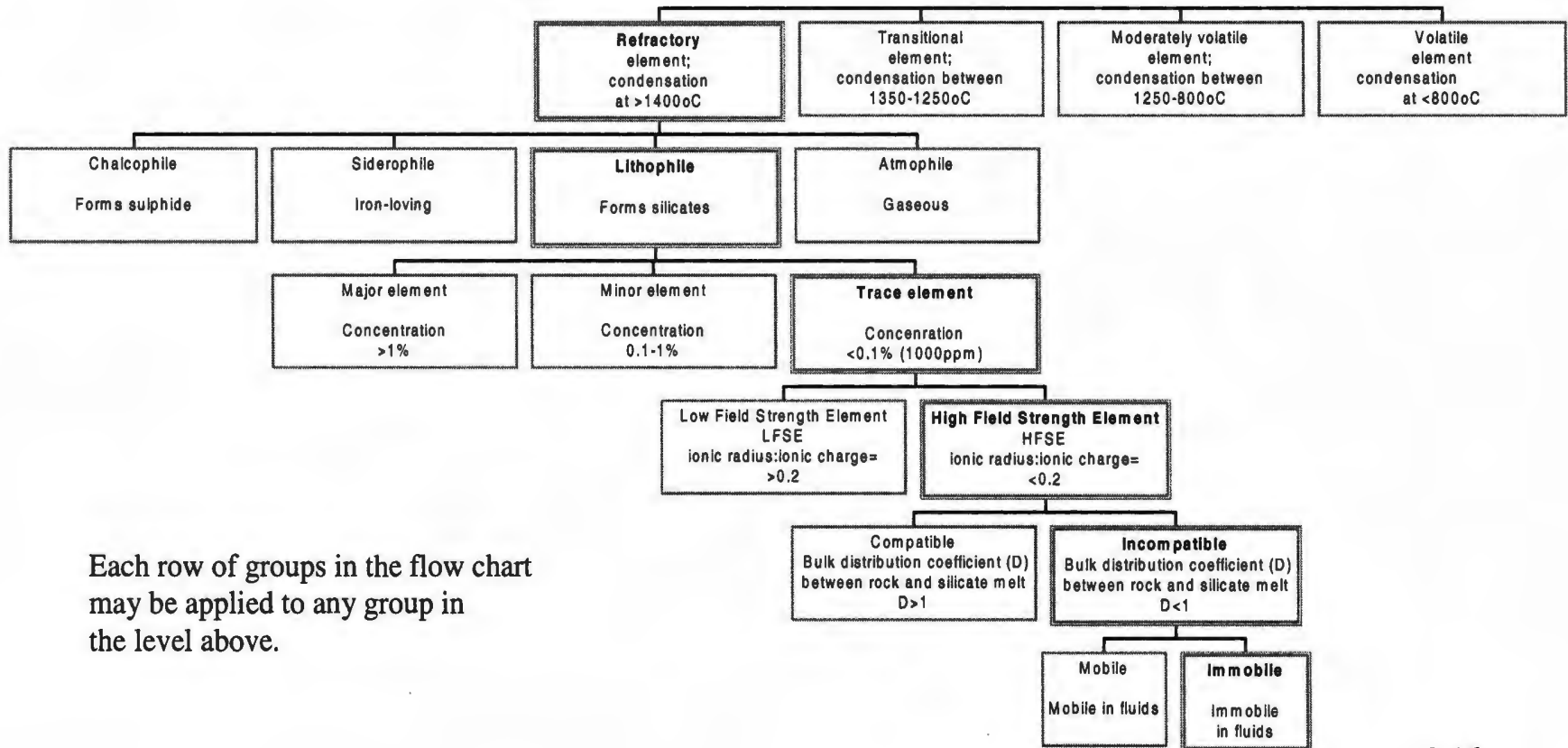
Table 2.3: Physical Properties of Zirconium and Hafnium

	Zirconium	Hafnium	Reference
Atomic number	40	72	Mukherji, 1970
Atomic weight	91.22	178.6	Mukherji, 1970
Atomic radius, Å	1.452	1.442	Mukherji, 1970
Ionic radius (VI), Å	(valency 4+) 0.72	(valency 4+) 0.71	Shannon (1976)
Electron configuration	Kr4d ² 5s ²	Xe4f ¹⁴ 5d ² 6s ²	
Density (20°C) gcm ⁻³	6.489-6.574	13.09+/-0.01	Mukherji, 1970
Melting point, °C	1852+/-2	2222	Mukherji, 1970
Boiling point, °C	3580	5400	Mukherji, 1970
Crystal structure (α)	hcp	hcp	Elinson and Petrov, 1969

Table 2.4: A compilation of partition coefficient data for Nb and Ta between various crystal phases and melt chemistries

Phase and melt type	Pressure / Temperature	Partition coefficient $K_{d_{Nb}}$	Partition coefficient $K_{d_{Ta}}$	$K_{d_{Nb}}/K_{d_{Ta}}$	Reference
Rutile with aqueous fluid	10Kb / 900°C	>100	>100	>1	Brenan <i>et al.</i> , 1994
Rutile with andesitic liquid	16Kb/1000°C	26.5	44.0	0.6	Green and Pearson, 1987
Rutile with trachyte liquid	~4Kb/1000°C	29.8	44.7	0.7	Green and Pearson, 1987
Ti-magnetite with basaltic andesite liquid	~4Kb/1000°C	0.7	0.8	0.9	Green and Pearson, 1987
Sphene with basaltic andesite liquid	7.5Kb/1000°C	3.5	10.8	0.3	Green and Pearson, 1987
Sphene with andesitic liquid	7.5Kb/1000°C	5.3	15.4	0.3	Green and Pearson, 1987
Sphene with trachyte liquid	7.5Kb/1000°C	5.4	15.7	0.3	Green and Pearson, 1987
Ilmenite with basaltic andesite liquid	7.5Kb/950°C	2.3	2.7	0.9	Green and Pearson, 1987
Ilmenite with andesitic liquid	~4Kb/1000°C	4.6	6.6	0.7	Green and Pearson, 1987
Orthopyroxene		0.027	0.048	0.56	Dunn and Sen, 1994
		0.001	0.0009	1.11	Horn, 1995
Clinopyroxene		0.005	0.013	0.38	Green <i>et al.</i> , 1989
Garnet		0.004	0.012	0.33	Adam <i>et al.</i> 1994
		0.015	0.051	0.29	Jenner <i>et al.</i> 1994
		0.02	0.06	0.33	Green <i>et al.</i> , 1989
Olivine		0.0016	0.065	0.025	Dunn and Sen, 1994
Spinel	1390°C/1atm.	0.006	0.007	1.33	Horn, 1995
		0.0853	0.1069	0.80	Foley <i>et al.</i> 1996
Amphibole		0.08	0.09	0.89	Adam <i>et al.</i> 1994
		0.19	0.21	0.90	Brenan <i>et al.</i> , 1994
Plagioclase		0.008	0.01	0.8	Dunn and Sen, 1994

Figure 2.1: A flow chart illustration of the various classification schemes used in geochemistry



Each row of groups in the flow chart may be applied to any group in the level above.

Figure 2.2: Primitive mantle normalized plot. Compatibility of element increases towards the right.

Taken from Hawsworth *et al.* (1993).

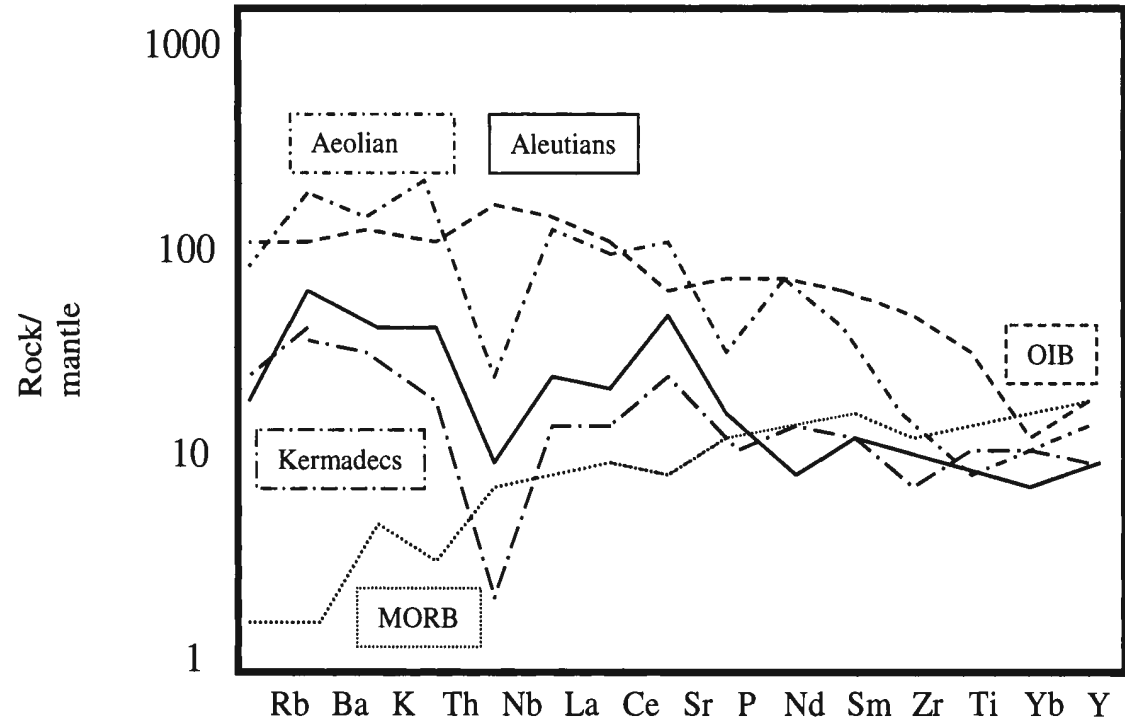
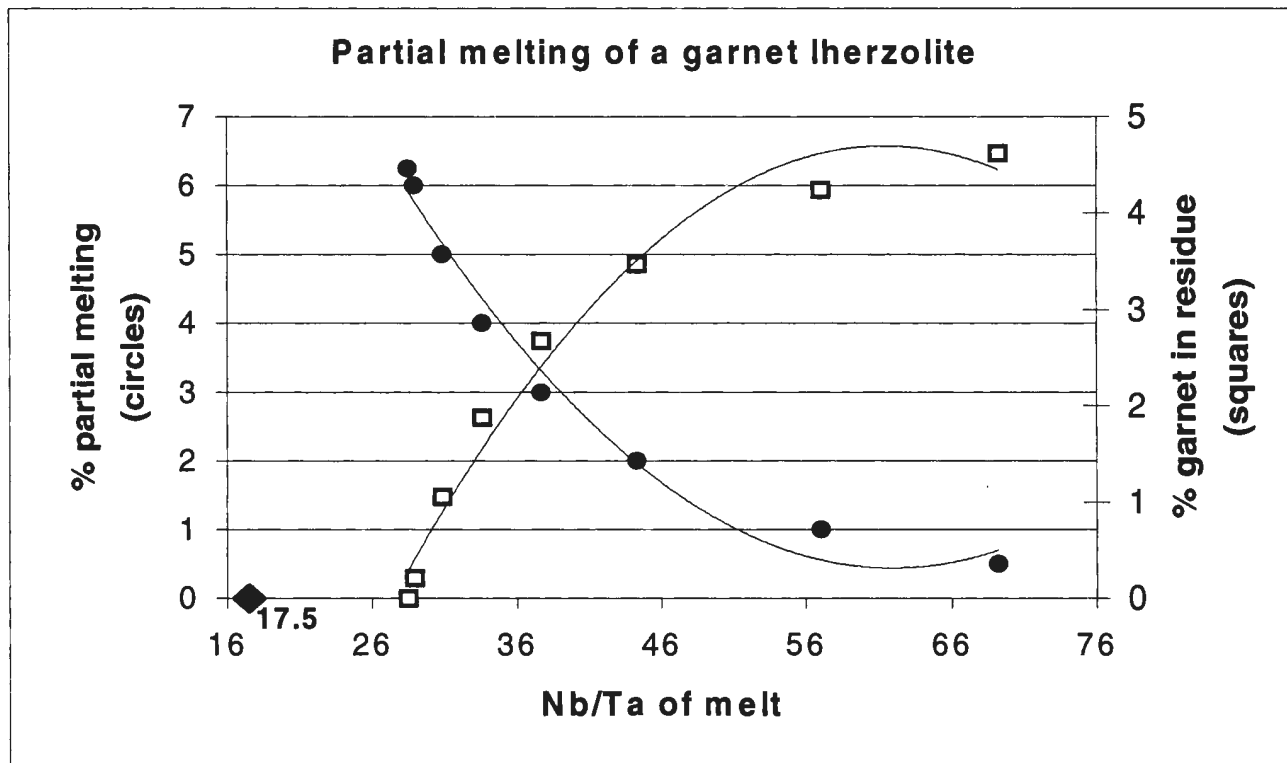


Figure 2.3: Graph to show a model of the variation of Nb/Ta ratios with partial melting of a garnet lherzolite.

It can be seen that as the % garnet in the residue is proportional to the change in Nb/Ta due to control of garnet on this ratio. The solid diamond refers to the initial Nb/Ta ratio of the source rock (17.5).



CHAPTER 3. ANALYTICAL PROBLEMS ASSOCIATED WITH HIGH FIELD STRENGTH ELEMENTS

The problem for many scientists interested in the behaviour of niobium and tantalum has been the paucity of reliable data in the literature due to the difficulty of measuring these elements with high precision and accuracy (Green, 1995; Poitrasson, 1993; Hall and Plant, 1992; Hall and Pelchat, 1990; Jochum *et al.*, 1990). Historically, the methods most commonly used to analyse niobium and tantalum concentrations have been XRF and INAA, respectively (Glaney *et al.*, 1990). However, owing to problems associated with these techniques (section 3.1 and 3.2) other methods of analysis are now preferred, for example:

- Inductively coupled plasma - mass spectrometry (ICP-MS) (section 3.4),
- Inductively coupled plasma - optical emission spectroscopy (ICP-OES) (section 3.3) and, to a lesser extent,
- Spark source – mass spectrometry (SSMS) (section 3.3).

The following chapter gives an outline of the techniques often used to measure the HFSE with the aim of highlighting the advantages and disadvantages of each method. Section 3.1 discusses the problem of Ta contamination caused by grinding samples in tungsten carbide mills, which is a problem potentially affecting all Ta determinations, regardless of the analytical technique. Section 3.5 will be devoted to the solution problems associated with the HFSE as this is one of the major disadvantages of using (solution sample introduction) ICP-MS and ICP-OES for the analysis of these elements.

3.1 Contamination through crushing

It is known that the use of tungsten carbide (WC) as a crushing and grinding mill material can impart a tantalum contamination into the sample being prepared (Potts, 1987; Stolz *et al.*, 1996). Potts (1987) carried out experiments where batches (0.5 g) of high purity SiO₂ were analysed after crushing twice in different mill vessels (agate, WC, Al₂O₃, boron carbide, aluminium ceramic, and leucite). The results for the SiO₂ ground twice in the WC vessel gave trace element concentrations of 8.6 µg g⁻¹ Co, 102 µg g⁻¹ Ti, and 5 µg g⁻¹ Ta. The results for the SiO₂ ground in the alumina ceramic mill gave significant contamination of Fe, Ga, Li, Ti and B. The agate mill contaminated the SiO₂ to a relatively small degree (2.3 µg g⁻¹ B, 3.9 µg g⁻¹ Cu) and is thought to be the most desirable grinding material. It is important that a rock in which Ta is to be analysed is ground in agate or ceramic mills.

3.2 Using X-Ray Fluorescence (XRF) for the determination of Nb and Zr

X-ray fluorescence (XRF) is one of the widely used routine instrumental methods of analysing rock samples for both major elements and selected trace elements (including Nb and Zr). XRF is a bulk sampling technique used typically for whole rock analysis. Samples are prepared as either pressed pellets or fused glass discs and are excited with X-ray radiation. This irradiation raises electrons from low to higher energy electron shells and the subsequent relaxation releases the excitation energy as x-rays characteristic of the element being measured. Most XRF instruments have wavelength dispersive spectrometers to detect the X-ray emission although the less expensive energy dispersive spectrometers have gained popularity as the technique has developed.

XRF is a technique of high precision. However, accuracy is more difficult to attain as it depends on the reliability of the attenuation-enhancement correction and calibration (Potts, 1987). The value of this technique cannot be overstated as it achieves high precision and accuracy to micrograms per gram ($\mu\text{g g}^{-1}$) detection limits for many elements with simple, robust sample preparation, requiring no dissolution.

In the past, XRF has been the technique commonly used to measure Nb and Zr in whole rocks. These elements have poor stability in dilute mineral acids and are subject to incomplete digestion so a technique requiring no sample dissolution is desirable. The measured concentrations of Nb and Zr in geological reference materials by different laboratory groups using XRF are shown in Table 3.1. Limits of detection for Nb and Zr using XRF are quoted as 1-2 $\mu\text{g g}^{-1}$ and 2-5 $\mu\text{g g}^{-1}$ respectively (Hall and Pelchat, 1990). Instruments using enhanced sensitivity XRF, such as the facility at Memorial University of Newfoundland, have limits of detection for Nb of approximately 0.6 $\mu\text{g g}^{-1}$. Sample concentrations an order of magnitude above this detection limit can be analysed with a precision of approximately 5 % (Table 3.1). XRF is therefore not a highly precise method of Nb determination at sub- $\mu\text{g g}^{-1}$ concentrations and another technique is preferable when determining concentrations in depleted samples such as island arc basalts and ultramafic rocks. Also, Ta and Hf are not measured by XRF at the concentrations commonly found in rocks ($< 1 \mu\text{g g}^{-1}$) and so the Nb/Ta and Zr/Hf ratios cannot be calculated using this technique alone.

3.3 Using Instrumental Neutron Activation Analysis (INAA) for the determination of Ta and Hf

INAA is a technique that has played an important role in Earth Science in the last 20 years, especially with regard to the analysis of rare earth elements. It is a simple, non-destructive technique requiring little sample preparation other than crushing in order to ensure homogeneity. INAA is used predominantly for the analysis of the REEs, Sc, Co, Cr, Cs, Hf, Ta, Th and U (Potts, 1987). Samples are irradiated (in a nuclear reactor) with neutrons and become radioactive by neutron capture-type nuclear reactions. It is the radioactive products of the neutron capture reaction that are used in INAA. It is important to allow unwanted, short-lived, radiation (*e.g.* ^{24}Na ; $T_{1/2} = 15$ hours) to fall in order to improve sensitivity of long-lived isotopes. The gamma-ray spectra from activated samples are measured using a solid-state, germanium, energy dispersive, gamma-ray detector (Potts, 1987).

Historically, Hf and Ta have been analysed using INAA. However, to reach a reasonable analytical precision each sample must be measured for 10-24 hours, 8-10 weeks after irradiation, due to the low Hf and Ta concentrations ($\text{sub-}\mu\text{g g}^{-1}$) in many rocks (Potts, 1987). INAA has had the reputation of a technique of variable precision perhaps due to the slight differences in instrument parameters and counting times used. Counting times and delay are important; in some cases, precision and sensitivity are compromised for more rapid and less expensive analyses. The routine performance of INAA in the analysis of Ta (and Hf) was illustrated by Potts (1987) by a compilation of

data for basalt USGS:BCR-1 from a variety of schemes (Table 3.2). These INAA results are compared with the consensus values of Gladney *et al.* (1983).

It can be seen from the results of Gladney *et al.* (1983) that the relative standard deviation for the consensus analysis for Ta is approximately 11%. This precision would be inadequate for some studies, which require greater precision in order to use Ta as an element for tectonic discrimination of rocks. A further disadvantage of INAA is the necessity of using an expensive nuclear reactor to irradiate the sample and the problem of the disposal of low-level radioactive waste after irradiation.

3.4 Inductively coupled plasma - mass spectroscopy: A highly sensitive, multi-element technique

The development of the inductively coupled plasma – mass spectrometer (ICP-MS) over the last fifteen years has provided an alternative method of analysis with sufficient precision and accuracy for the determination of a large number of trace elements including Nb and Ta (Jenner *et al.*, 1990). ICP-MS analysis utilises an argon plasma as a source of ionisation, the mass spectrum of which is measured using a quadrupole-based (or sector double focusing or time-of-flight) mass spectrometer. This was made possible by the development of an interface whereby plasma gases at atmospheric pressure can be physically sampled through an orifice, via a differential pumping unit and into the quadrupole mass filter at 10^{-5} - 10^{-6} torr (Potts, 1987). The high sensitivity and low backgrounds of the mass spectrometer allows low detection limits to be attained (ng g^{-1}) for many elements, depending on mass interferences, background and isotopic abundance. However, the precision of this technique (5-10 % 2σ) does not rival that of

thermal ionisation mass spectrometry and so quadrupole based ICP-MS is not suitable for the reliable determination of radiogenic isotopes used in geochronological studies. However, isotopic ratios can be measured to sufficient precision on the ICP-MS to allow isotope dilution analysis to be used. When optimal enriched-isotope concentrations are used, this greatly improves the accuracy and precision of analysis by removing the need for drift and matrix correction and by providing an ideal form of internal standardisation (Longerich, 1989) (section 6).

Sample introduction into the argon plasma is most easily carried out through solution nebulisation, where the sample is taken up into solution and aspirated into the plasma. Another more recent advance in the development of ICP-MS is the laser ablation microprobe as a means of sample introduction (LAM-ICP-MS) (Jackson *et al.*, 1992). This solid sampling technique now uses an ultra-violet laser beam to ablate microscopic holes into a sample. The ablated material (with particle sizes of 1-3 μm) is then carried in the argon flow into the plasma where it is ionised (Jeffries, 1996).

The quadrupole mass filter, with associated data collection electronics, enables the rapid scanning of selected mass ranges between 0-300 AMU. The quadrupole is a set of four, parallel metal rods positioned in such a way as to enable mass-charge discrimination. Each pair of rods has a potential difference across it creating a time-dependant, oscillating electric field between the rods, which causes a selected ion of specific mass/charge ratio to follow a stable path into the mass spectrometer detector. All other paths lead to collision into the side of the quadrupole and so the ions are not detected.

The detector can lead to a set of two amplifiers, one is an analogue amplifier suitable for signals of high intensity and one leads to a pulse counter (PC) and is suitable for signals of low intensity. For trace analysis, the multiplier operates in PC mode so that the arrivals of individual ions are counted. It is also possible to have dual detection where both detectors operate simultaneously. This avoids the problem of large signals flooding the PC mode as the detector can switch instantly to analogue mode.

3.5 Inductively coupled plasma – optical emission spectrometry and spark source mass spectrometry

3.5.1 ICP-OES

ICP-OES is a technique that uses the optical spectra given off by excited atoms and ions as a means of qualitative and quantitative analysis. The source of ionisation in ICP-OES is the argon plasma identical to that used in ICP-MS (section 3.3.2). The torch is vertical with the spectrometers tangential to the side of the plasma flame. The ICP-OES can be designed with “direct reader spectrometers”, which permit simultaneous multi-element determination. Twenty to sixty elements can be simultaneously detected in a cycle time of 2-3 minutes (Potts, 1987). One drawback of this technique is that sample introduction is via solution nebulisation and so all samples must be reproducibly dissolved (section 3.5).

ICP-OES is the instrument of choice for routine major and trace element determinations in many laboratories. However, the major drawback of this instrument for trace element analysis is the relatively high limits of detection for many elements compared to the ICP-MS. This is illustrated by Table 3.3, which compares the limits of

detection for the HFSE using ICP-OES and ICP-MS. It can be seen that, whereas ICP-MS can easily detect sub-ppm levels, ICP-OES has detection limits above approximately $6 \mu\text{g g}^{-1}$.

3.5.2 SSMS

SSMS is a technique with a balance of desirable and undesirable properties with respect to trace element analysis. It involves homogenising a small amount of powdered sample (<1 mg) with ultrapure graphite and packing it together to form an electrode. A high RF voltage is then applied across this and another “blank” electrode. This excitation process imparts a considerable range of kinetic energies to ions formed in the spark, up to 1000 eV (Potts, 1987). An electrostatic sector is used to select a mono-energetic beam of ions, which are then dispersed by an electromagnetic analyser. The entire spectrum is focused on a flat plate and detected by a photographic plate or a detector array. The advantages of this technique are that, typically, 30 elements can be detected simultaneously. It is one of the most sensitive techniques available for trace element analysis and has a precision ranging from 2-5% (1σ) (Potts, 1987). Limits of detection range from 0.1-0.001 $\mu\text{g g}^{-1}$ for whole rock analysis without chemical separation (Potts, 1987). There are small to negligible matrix effects and almost uniform sensitivity for a wide range of trace elements (Potts, 1987). However, despite these favourable characteristics SSMS remains a relatively uncommon method of analysis. This is due mainly to the high cost of the equipment and the low sample throughput (perhaps two samples a day). It is also suspected that, due to the small sample sizes of <1 mg, sampling

error may occur, especially when accessory minerals such as zircons are present. Care must be taken in the homogenisation of the sample before it is mixed with the graphite.

Jochum *et al.* (1988) showed that isotope dilution analyses could be applied to SSMS by spiking the graphite electrode with a known concentration of an enriched isotopic spike. It was shown that this improved the precision and accuracy of the analysis of certain elements by eliminating the effects of poor beam stability. The expected precision and accuracy of SSMS and ID-SSMS, for HFSE, is shown in Table 3.4.

3.6 The instability of HFSE in solutions of dilute mineral acids

HFSE are known to be unstable in solutions of dilute mineral acids (Gibalo, 1970; Poitrasson *et al.*, 1993). The most stable complexes formed by Nb, Ta, Zr and Hf are the fluoro- and oxyfluoro-complexes (NbOF_5^{2-} , TaF_7^{2-} , ZrF_6^{2-} and HfF_6^{2-}) (Fairbrother, 1967; Elinson and Petrov, 1965). The relative stabilities of these species are a function of hydrofluoric acid (HF) concentration, illustrated in Figure 3.1 for Nb and Ta complexes (Gibalo, 1970; Keller and Chetham-Strode, 1966). It can be seen that TaF_7^{2-} has a far lower stability in solution than NbOF_5^{2-} at low HF concentrations. Due to their high charge and small radius, the HFSE ions have a tendency to hydrolyse in aqueous solutions, even in the presence of a strong ligand such as fluoride ions, forming the insoluble precipitates $\text{Nb}(\text{OH})_5$, $\text{Ta}(\text{OH})_5$, $\text{Zr}(\text{OH})_4$ and $\text{Hf}(\text{OH})_4$ (Gibalo, 1970). The hydrolysis is an ageing reaction that is kinetically controlled by temperature and can be suppressed by freezing or refrigeration of the sample. It has also been shown that the rate of hydrolysis is a function of acid composition, for example, in perchloric acid solutions

of zirconium salts the rate of hydrolysis is less than in hydrochloric and nitric acid solutions (Elinson and Petrov, 1965).

The instability of HFSE soluble complexes in aqueous solution is partially the cause of the relatively poor reproducibility of the determination of these elements by analytical methods requiring sample digestion. Other causes of the poor reproducibility are incomplete digestion of mineral phases containing HFSE, such as zircon, and sampling error due to non-representative quantities of rock powder. Comparing a solid sampling technique of analysis (*e.g.* XRF) to one involving acid digestion (*e.g.* ICP-MS) illustrates the problems associated with incomplete digestion and solution instability. A database at Memorial University of Newfoundland has both XRF and ICP-MS data for samples analysed over the last ten years. XRF is considered the most accurate technique for concentrations above the limit of detection ($0.6 \mu\text{g g}^{-1}$) for Nb and ($1\text{-}2 \mu\text{g g}^{-1}$) Zr. Plots comparing the results of XRF and solution nebulisation ICP-MS analyses for Nb and Zr in a variety of samples are shown in Figure 3.2 (a) and (b). For comparison, equivalent plots for Sr and Rb are shown in Figure 3.2 (c) and (d). Assuming that both instruments are running under optimal operating conditions, the frequent underestimation of ICP-MS Zr analyses compared to XRF suggests that not all of the Zr is going into solution. It is known that zircons, which contain the majority of Zr in a sample, are difficult to dissolve especially if they are large, young and low in uranium. If they are not taken up into solution the concentration of Zr going into the ICP-MS is lower than in the original sample. Zircon is a more prevalent phase in felsic rocks as can be seen in Figure 3.2(a) where the felsic rocks show the greatest spread of underestimated Zr analyses. Nb

determinations do not show the same spread of results in the XRF – ICP-MS plot (Figure 3.2b) compared to Zr. However, there remains a tendency for ICP-MS results to underestimate the Nb concentrations. Nb and Ta are not readily associated with any accessory phase but are known to have a relatively high partition coefficient into oxide phases such as rutile, sphene and ilmenite (Green and Pearson, 1987). The problem in this case may be with the initial digestion of a mineral phase but it is even more likely that the problem involves keeping the Nb in solution once digested. The product of hydrolysis ($\text{Nb}(\text{OH})_5$) forms a colloidal precipitate with high adsorption characteristics (Gibalo, 1970). It is suspected that it is the adsorption and of these molecules onto the sides of tubes and glassware that causes the low precision in Nb results by ICP-MS. It has been observed that Ta backgrounds were unusually high during an ICP-MS solution nebulisation analysis using more HF in the sample introduction than is usual. This was probably due to the higher concentrations of HF scavenging Ta, which has been deposited onto the sides of tubes and glassware. The Ta backgrounds should gradually decrease with time if HF is flushed through the sample introduction system. The fact that Nb backgrounds were not a problem illustrates that the fluoro-complex of Ta is either less stable in solution or has far higher adsorptive properties than the fluoro-complex of Nb. It can be seen in Figure 3.1 that at lower HF concentrations TaF_7^{2-} is far less soluble than NbOF_5^{2-} .

3.7 Summary

There are a number of techniques of analyses that can be employed to determine HFSE concentrations in rocks. The most common of these are XRF, INAA, ICP-OES, ICP-MS and SSMS. However, despite the high precision and accuracy of analyses

possible using these techniques, the determination of HFSE is compromised by their instabilities in solution, the difficulty of digesting accessory phases rich in HFSE, the high cost and long counting times required for INAA and the time consuming and costly nature of SSMS. XRF is a highly suitable technique for the determination of Nb and Zr but has relatively high detection limits inhibiting the analysis of rocks containing low concentrations of HFSE, such as island arc volcanics and peridotites. The instability of the HFSE in solution is related to their tendency to irreversible hydrolysis to the $M(OH)_x$ species which is insoluble in dilute mineral acids.

Table 3.1: The routine performance of XRF in the analysis of Nb and Zr.

	Basalt CRPG:BR Govindaraju and de la Roche (1977).		Basalt CRPG:BR Schroeder <i>et al.</i> (1980)		Andesite USGS:AGV-1 Gladney <i>et al.</i> , (1983)	
	Expected ($\mu\text{g/g}$)	RSD (%)	Analysed ($\mu\text{g/g}$)	RSD (%)	Expected ($\mu\text{g/g}$)	RSD (%)
Nb	100	11	114.7	1.2	15	10
Zr	250	29	251.1	3.8	225	4

RSD = relative standard deviation (2σ)

Table 3.2: The routine performance of INAA in the analysis of Ta and Hf; modified from Potts (1987). RSD = relative standard deviation.

	Gladney <i>et al.</i> (1983) consensus analysis:		Potts <i>et al.</i> (1981):	
	Expected ($\mu\text{g/g}$)	RSD %	Analysed ($\mu\text{g/g}$)	RSD % (n=2)
Ta	0.79	11.4	0.79	0.9
Hf	4.9	6.1	4.76	1.8

RSD = relative standard deviation (2σ)

Table 3.3: The limits of detection (LOD) of ICP-OES and ICP-MS.

	ICP-OES**; LOD ($\mu\text{g/g}$)	ICP-MS*; LOD ($\mu\text{g/g}$)
Nb	10	0.009
Ta	10	0.008
Zr	6	0.045
Hf	6	0.023

* Memorial University of Newfoundland ICP-MS facility ($\text{LOD} = 3\sigma \sqrt{1/(n+1)}$).

** Taken from Potts (1987).

**Table 3.4: A comparison of the expected precision and accuracy of ID-SSMS and SSMS,
taken from Potts (1987) ♣♦ and Jochum *et al.* (1988)**

<LOD = concentrations below limit of detection.

Numbers in parentheses indicate the expected precision of analysis (RSD 2σ).

	BCR-1	BCR-1	W-1	W-1
	ID-SSMS	SSMS♣	ID-SSMS	SSMS♦
Nb	13.8 (3-10%)	13.4 (4-10%)	7.91 (3-10%)	9.5 (4-10%)
Ta	<LOD	<LOD	<LOD	<LOD
Zr	186 (5%)	180 (4-10%)	98.6 (5%)	105 (4-10%)
Hf	4.90 (5%)	4.5 (4-10%)	2.68 (5%)	2.7* (4-10%)

♣Abbey (1983)

♦ Taylor and Gorton (1977) (mean of 7 analyses)

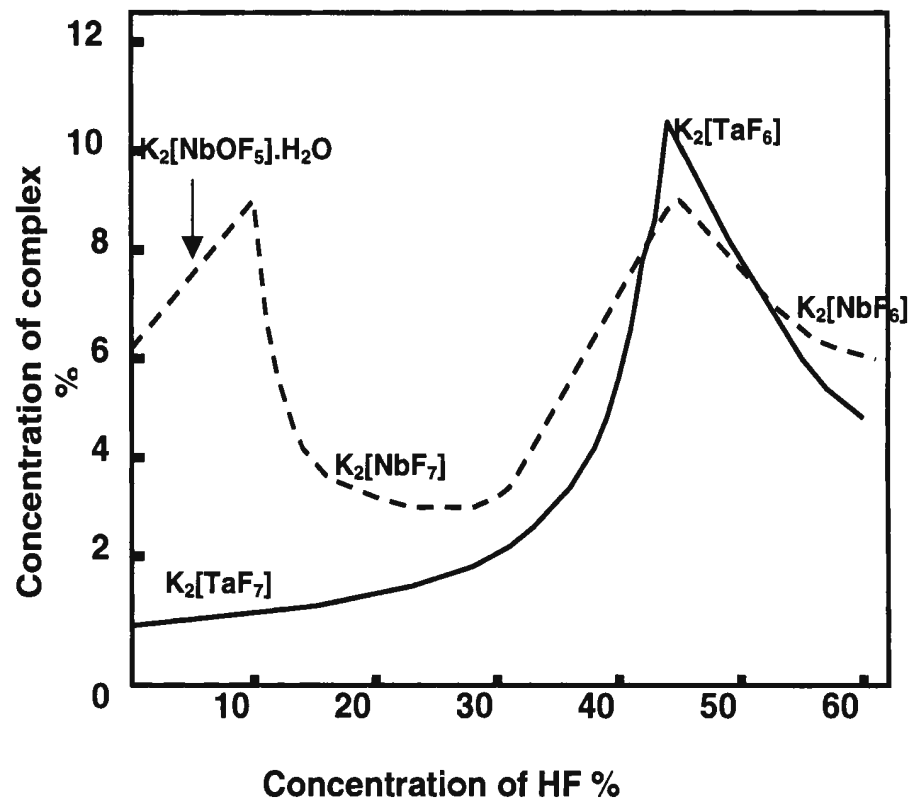


Figure 3.1: Solubility of K_2NbOF_5 and K_2TaF_7 in solutions of HF; taken from Gibalo (1970)

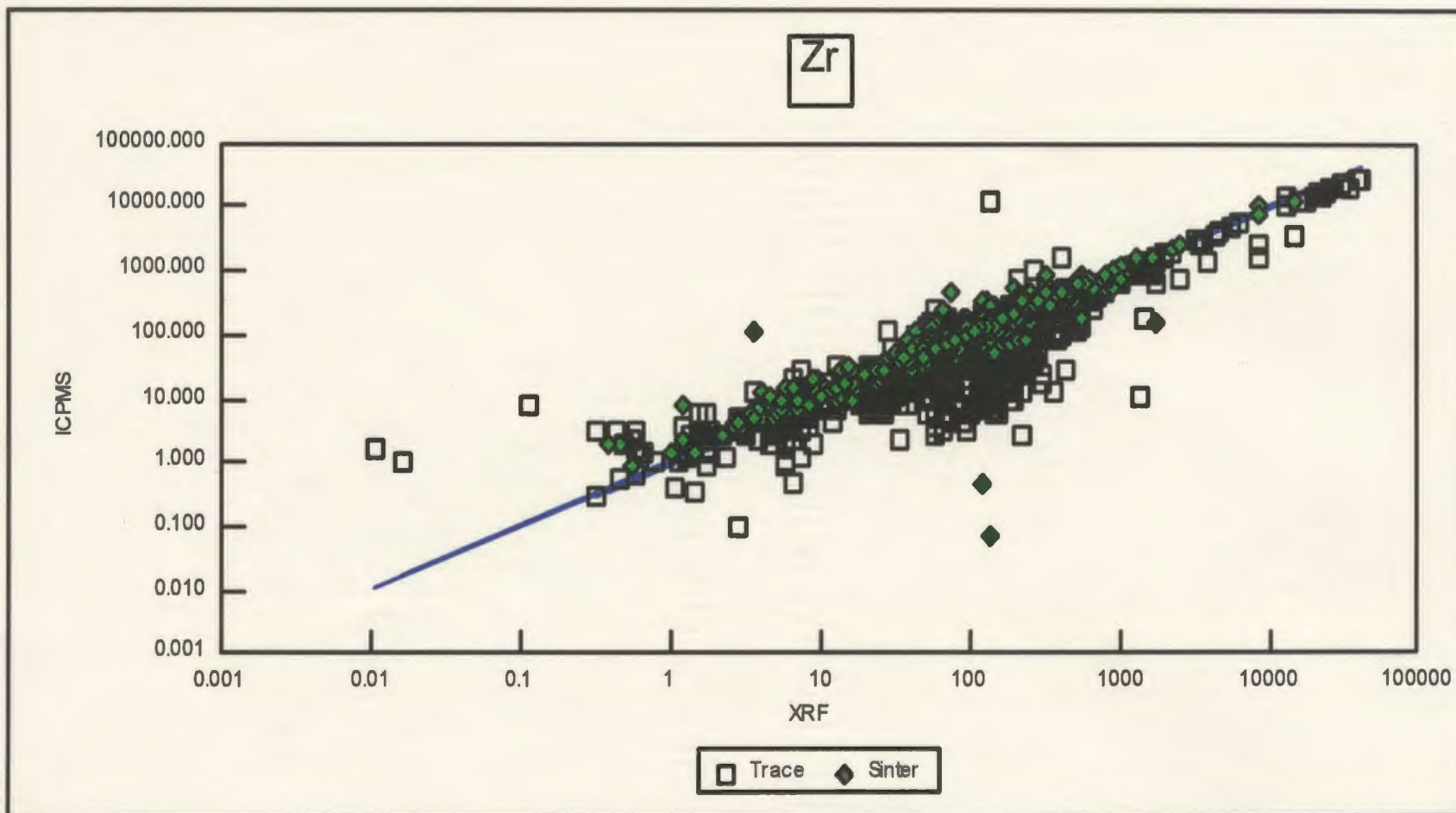


Figure 3.2 a: A comparison of XRF and solution nebulisation ICP-MS (acid digest, and Na_2O_2 sinter) determinations for Zr analysed at Memorial University of Newfoundland, Canada. Detection limits for XRF Zr are approximately $4 \mu\text{g g}^{-1}$.

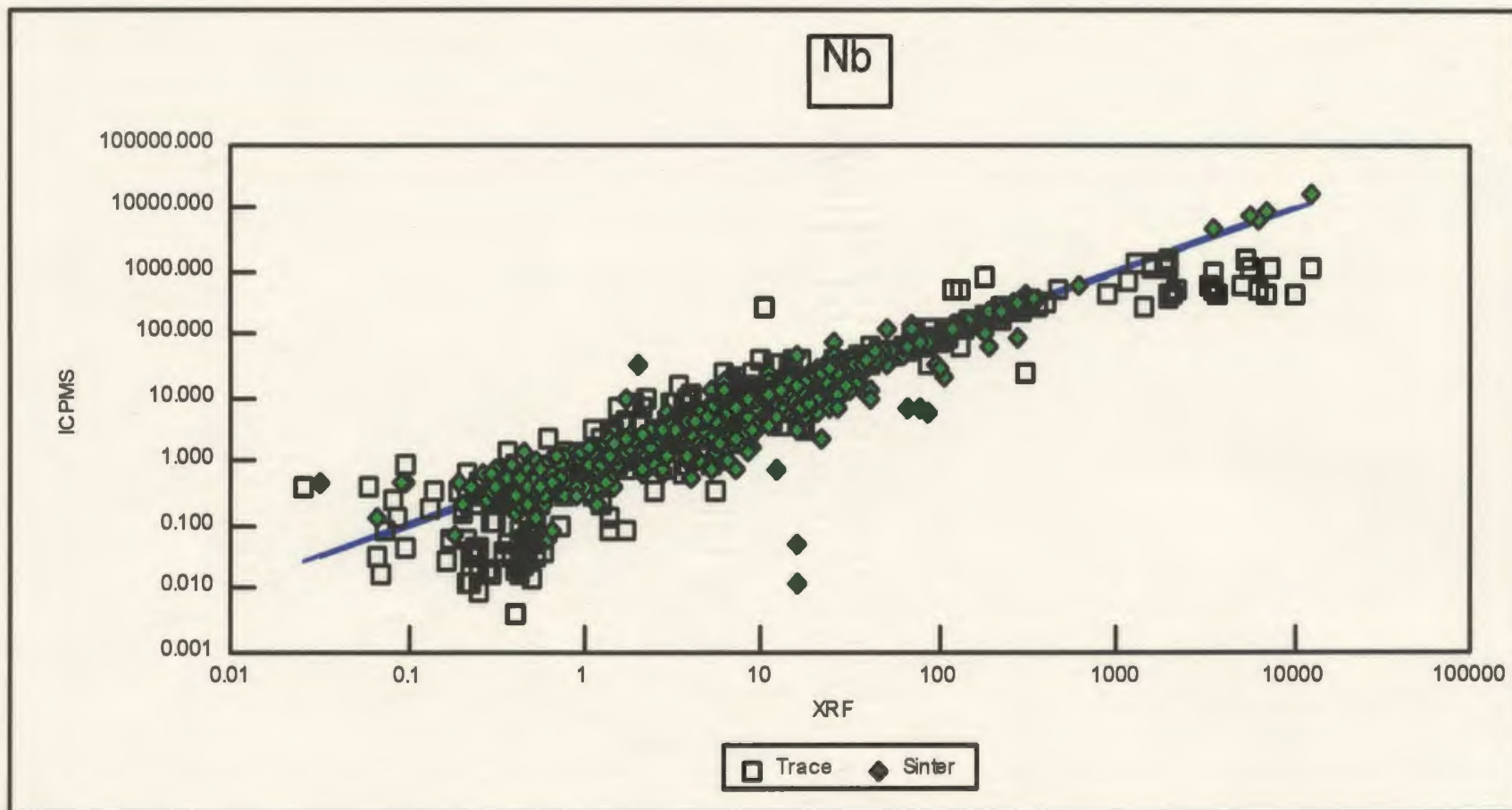


Figure 3.2 b: A comparison of XRF and solution nebulisation ICP-MS (acid digest and Na₂O₂ sinter) determinations for Nb analysed at Memorial University of Newfoundland, Canada. Detection limits for XRF Nb determinations are approximately 0.6 μg g⁻¹.

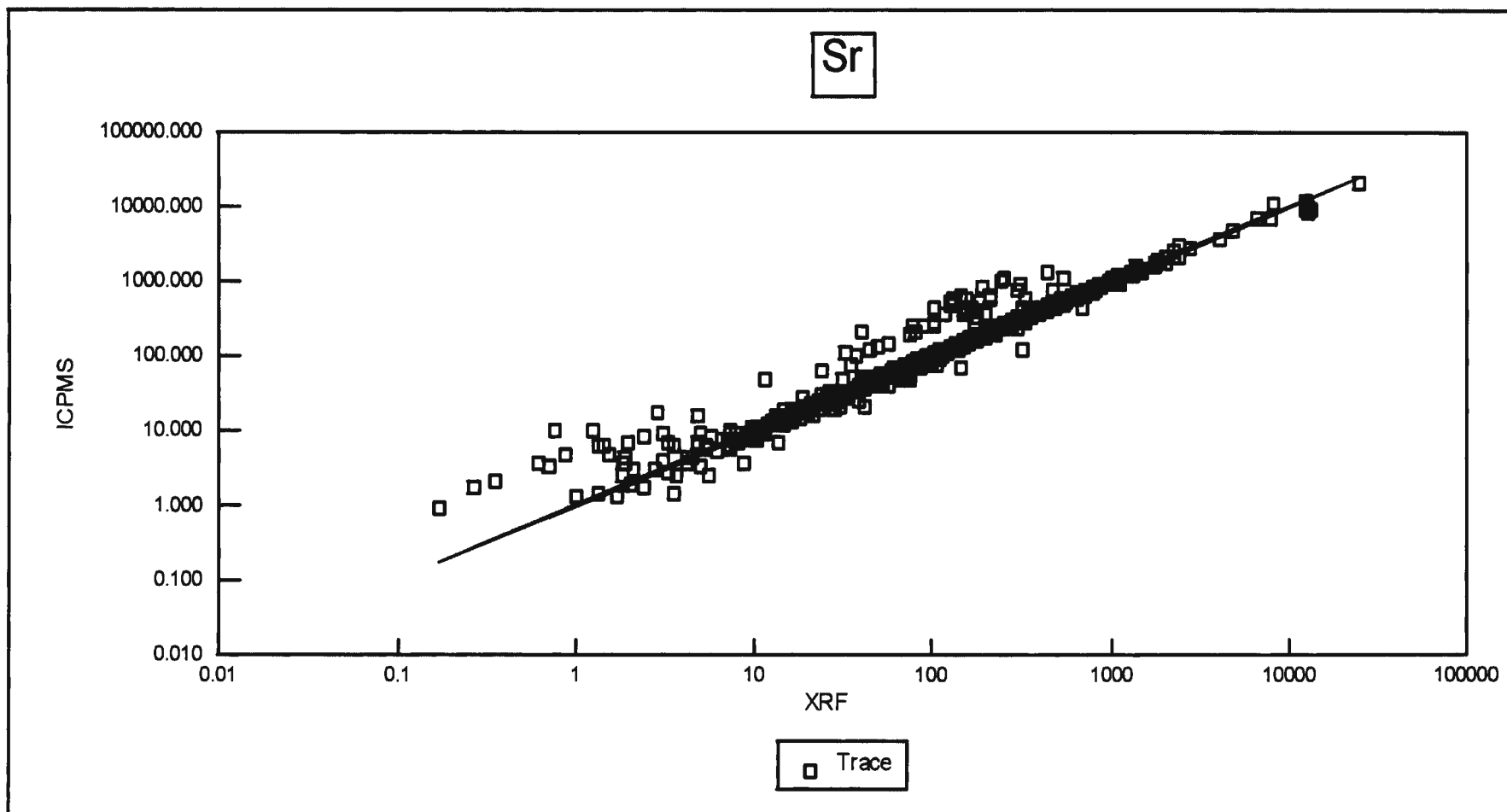


Figure 3.2 c: A comparison of the Sr determinations by XRF and solution nebulisation (acid digest) ICP-MS for a variety of geological samples analysed at Memorial University of Newfoundland, Canada. Detection limits for Sr XRF analyses are approximately 4 $\mu\text{g/g}$

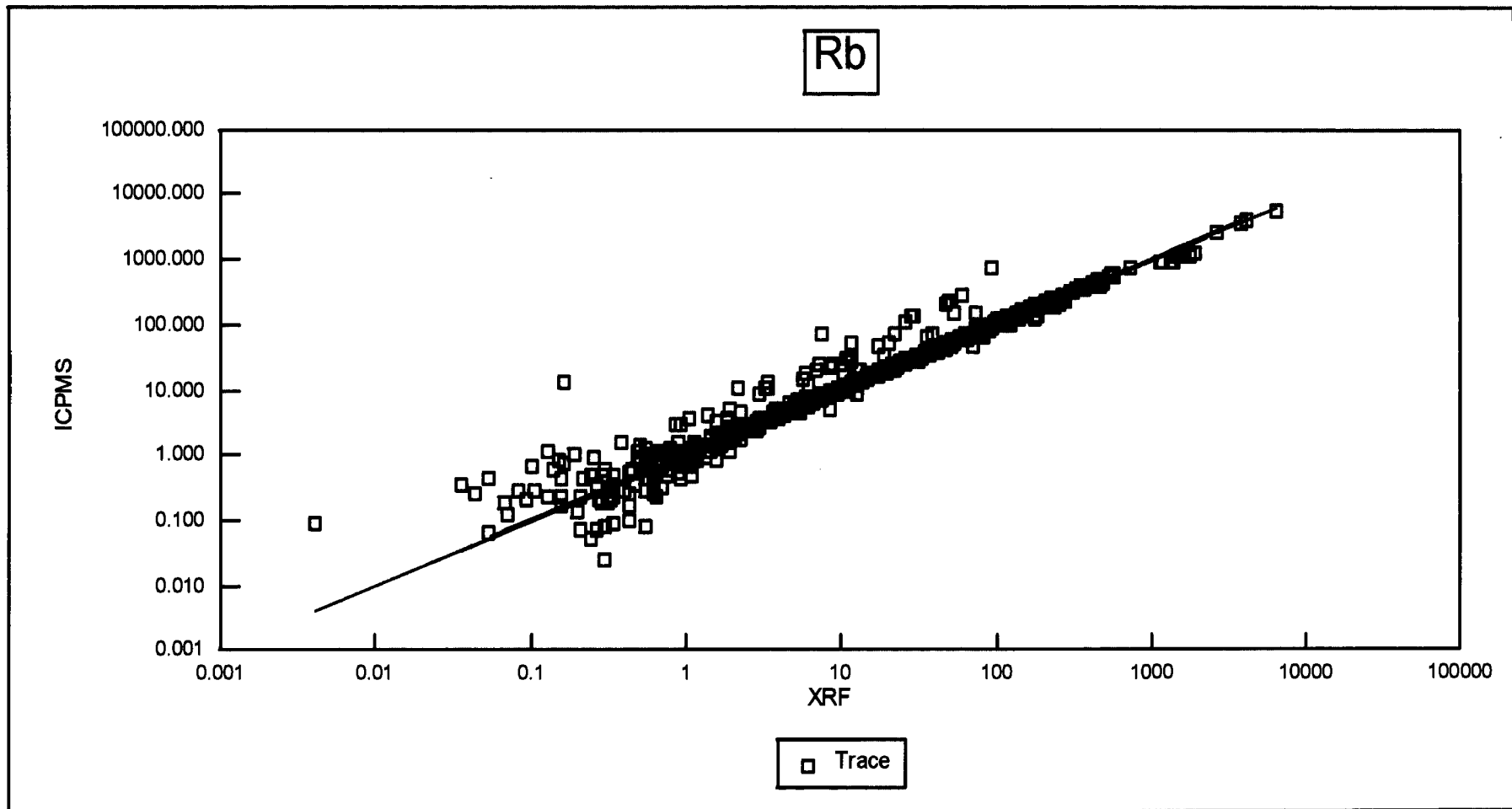


Figure 3.2 d: A comparison of the Rb determinations by XRF and solution nebulisation (acid digest) ICP-MS for a variety of geological samples analysed at Memorial University of Newfoundland, Canada. Detection limits for XRF Rb are approximately $0.6 \mu\text{g g}^{-1}$.

CHAPTER 4. WHOLE ROCK LA-ICP-MS AND AN INVESTIGATION INTO THE USE OF ISOTOPE DILUTION AS A MEANS TO IMPROVE THE PRECISION AND ACCURACY OF WHOLE ROCK LA-ICP-MS ANALYSIS

4.1 Strip heating as a rapid method of producing homogeneous glass beads

In order to determine reliable HFSE concentrations in rocks, the acid digestion method of sample preparation was avoided because of the instabilities of HFSE in solution and the difficulties of digesting resistant phases such as zircon (section 3.5). Instead, solid sampling LA-ICP-MS was used on synthetic glass beads made by fusing rock powder in an iridium strip heater.

The initial part of this project was to refine a method of sample preparation for whole rock LA-ICP-MS analysis involving the rapid, flux-free fusion of rock powder on a metal strip to form glass beads. In theory, this is a very simple task previously documented by Nicholls (1974), Fedorowich *et al* (1993) and Odling (1995) involving the set-up of a high current supply running through a thin metal strip of high melting point. A powdered sample is placed on the strip and fused. Turning the power off results in a rapid cooling. However, the following problems arose concerning the homogeneity of the final glass:

1. Small amounts of powdered sample (50 mg) lead to an inaccurate representation of the whole rock. This is especially pertinent to coarse grained, felsic rocks with a high percentage of accessory phases such as zircon, which concentrate the high field strength elements.

2. Inadequate homogenisation of the melt during fusion due to high viscosity. This also is more relevant to silica rich melts. The addition of sodium fluoride to the whole rock powder may overcome this viscosity problem as fluoride ions are depolymerising agents and sodium can act as a network modifier in a melt if it is not involved in a charge balancing role with Al^{3+} . However, the addition of a flux is compromising as it may impart impurities into the sample.
3. Refractory phases not melting in the heating time given, even for very fine-grained powders. This was the case for ultramafic rocks such as peridotites and a flux was required to produce a homogeneous glass.
4. Quench crystallisation of discrete mineral phases especially in the more mafic to ultramafic rocks. It was found that by shortening the heating strip, quench time was significantly decreased.

To overcome these problems, a sample preparation method was devised that varied somewhat with rock composition.

In order to improve the precision and accuracy of the analyses, isotope dilution was applied to the whole rock LA-ICP-MS technique. This technique, which has not been documented in the literature, was carried out as a preliminary investigation of seven geostandard reference materials with an emphasis on the determination of HFSE and to a lesser extent REE.

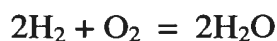
4.1 Strip heater set-up

The strip heater consisted of a steel box with insulated brass clamps that held a metal strip (usually iridium or tungsten) with dimensions 0.127 x 12.5 x 50 mm, or 0.127

x 12.5 x 25 mm with a clamp extension (Figure 4.1). A powdered sample, either dry or as a paste in an organic matrix (ethanol or glycerol) was placed onto the strip. A mixture of argon (150 ml/min) and hydrogen (5 ml/min) gas was passed through the steel box. A transformer controlled the power directed into the strip (and hence the temperature) and was calibrated with an optical pyrometer (Ircan, Illinois). The maximum temperature was constrained by the melting point of the strip (iridium at 2443°C and tungsten at 3410°C) and most runs were carried out at approximately 1600°C.

Both iridium and tungsten strips were used to fuse samples. Iridium was the preferred metal due to its malleability after heating and its chemical resistance. The high malleability aided sample removal as the strip could be bent and re-shaped. The disadvantage of iridium is the high cost of the pure metal foil (>US\$250 for one strip; Alfa Aesar). The price of the metal is US\$9.50/g (Goodfellow Cambridge Ltd, pers. comm. July 1997) and this rules out recycling the iridium scrap to gain back a reasonable percentage of the original cost. The metal strips typically break in the middle and so a clamp extension was made for the strip heater in order to utilise these pieces. This modification has the advantage of reducing the “quench” time of the melt subsequently reducing the risk of quench crystallisation. Tungsten was found to oxidise easily and, even after fusion under reducing conditions, was brittle. This made removal of the glass bead very difficult without breaking the strip. The advantage of tungsten is its low cost (~US \$4.00; Alfa Aesar).

To decrease the oxygen fugacity (f_{O_2}) in the strip heater cell a gas mixture of H_2 and Ar was used. The argon supply contains approximately $5 \mu\text{g g}^{-1}$ oxygen, which was then buffered by the addition of hydrogen to produce water:



Lowering the f_{O_2} in the strip heater cell lowers the melting point of the rock sample (Horn, 1995) and lengthens the life of the tungsten strip. The lower f_{O_2} conditions also reduced Fe^{3+} in the samples to produce greener coloured (Fe^{2+}), more transparent glasses (Figure 4.2a), which allowed heterogeneity to be seen using an optical transmission microscope.

The disadvantage of using hydrogen gas in the strip heater cell is the potential for creating an explosive gas mixture if the correct $O_2:H_2$ molar ratio is reached. This ratio is unlikely to be reached as long as the strip heater is sealed and flushed for approximately 2 minutes with argon and hydrogen before heating the strip.

4.2 Sample preparation

Sample preparation involved grinding approximately 0.5-1 g of powdered sample in an agate mortar and pestle (or in an alumina ceramic mill) for at least 10 minutes. For mafic to ultramafic compositions ($SiO_2 < 40 \text{ wt } \%$), sufficient $(NH_4)_2HPO_4$ was added before grinding to give approximately 10 wt % P_2O_5 in the sample. The powder was then divided roughly into three portions that were mixed into a paste with a small amount of ethanol or glycerol. The paste was placed onto the metal strip covering as small an area as possible to minimise interaction with the strip. Ethanol evaporated rapidly leaving a discrete pile of sample. This was fused at approximately 1600°C and the glass bead was

placed back into the mortar after quenching. When all the sample portions were fused, they were ground again into a powder and 30 mg of this was mixed with a small amount of glycerol to produce a pellet, which was then fused to produce the final glass.

The relatively large initial weight of powder (0.5-1g) was used to minimise sampling error. The ammonium orthophosphate monohydrate ((NH₄)₂HPO₄) breaks down at approximately 250°C to give:



The phosphorus acts as a flux and polymerising agent and, for mafic to ultramafic rock compositions, helps to produce a more homogeneous glass (Odling, 1995).

Two grinding and fusion steps are carried out in order to reduce the “grain” size to a minimum and to ensure that any crystals which have not fused or have formed on quench are homogenised with the rest of the glass. The precision of analysis of two geostandards prepared with only one grinding and fusion step are compared to that prepared with two fusions in Figure 4.3. The standard deviation of many elements is reduced with the additional grinding step.

Either glycerol or ethanol can be used to make a pellet of the sample powder before fusion. It was found that the precision for many elemental determinations in the glasses was increased when glycerol was used (Figure 4.3) and the number of volatile inclusions decreased in many samples (Figure 4.2b). This was probably due to the mixing effect produced by the volatiles released by the breakdown of glycerol during fusion and by the sample slowly collapsing into itself as the glycerol matrix disintegrated.

4.3 Homogeneity of synthetic glasses

To investigate the homogeneity of the major elements in a synthesised basaltic glass, 0.1g of BCR-2 powder was fused on the Ir-strip heater in three batches, which were then combined and ground in an agate mortar and pestle. The final powder (approximately 0.03 g) was introduced onto the strip heater as a glycerol paste and fused for 1.5 minutes at approximately 1600°C. The resulting glass was analysed by wavelength dispersive electron microprobe (Cameca SX50) for the elements Si, Al, Mg, Mn, Fe, Ca, K and Na (Table 4.1). There were no significant heterogeneities within the glass for the major elements analysed. The poor precision of Mn determinations is due to the low concentration of Mn (0.2 wt %) in the sample.

For trace elements determined by LA-ICP-MS, the more felsic material (*e.g.* geostandard SY-2) was more heterogeneous than basaltic material (*e.g.* geostandard MRG-1), probably due to the viscous nature of silica-rich melts. This can be seen in the better precision of geostandard MRG-1 analyses compared to SY-2 analyses (Figure 4.3). Ultramafic melts were homogenised with the use of $(\text{NH}_4)_2\text{HPO}_4$ flux but had a tendency to form quench crystallisation if not cooled rapidly using a short iridium (or tungsten) strip.

4.4 Strip cleaning between samples

There is often a small quantity of glass left on the strip after fusing and removal of a bead. This can be removed by either soaking the strip over-night in HF acid or by fusing powdered sodium carbonate for 60 seconds at approximately 900°C. The sodium carbonate can be removed quickly in a dilute mineral acid after fusion. For the iridium

strip, the sodium carbonate fusion is a rapid and successful method of cleaning. For the tungsten strip, the sodium carbonate fusion cleans the strip but also oxidises the tungsten, even under a reducing atmosphere. Therefore, the preferred method when using the tungsten strip is to use a new strip for each new sample and to soak the strips in HF overnight.

4.5 Impurities in the metal strip

Alpha Aesar specified the iridium strip as being 99.8% pure with a quantitative analysis of the strip yielding:

	Al	Si	B	Ag	Cu	Pt	Fe	Ru	Mo	Rh
$\mu\text{g g}^{-1}$	1	3	1	1	2	10	2	30	70	10
LD	1	3	1	1	1	1	1	1	3	3

LD = limit of detection of method of analysis used ($\mu\text{g/g}$)

LA-ICP-MS analyses of both a new and a well-used iridium strip were carried out using Mo as an internal standard ($70 \mu\text{g g}^{-1}$). It was found that the new strip contained an appreciable amount of Ru, Rh, Pt, (semi-quantitative) Ni ($3.53 \mu\text{g g}^{-1}$ in the used strip), Zr ($\sim 1 \mu\text{g g}^{-1}$), W ($5-6 \mu\text{g g}^{-1}$) and Cu ($\sim 25 \mu\text{g g}^{-1}$). The elemental abundances for all impurities were less in the used strip compared to the unused strip with the exception of Cu.

Analysis of the tungsten strip showed that it contained appreciable amounts of Mo, Cr and Nb with lesser amounts of Co and Ta (Figure 4.4). The Alpha Aesar specifications for the strip were $>99.95\%$ W, with all trace element abundances reported

as being below detection limits. To give an upper limit on the concentration of trace elements measured by LA-ICP-MS, the Alpha Aesar detection limit for Ca was used as an internal standard ($4 \mu\text{g g}^{-1}$). The well-used W strip contained a higher concentration of Mo, Nb and Ta and less amounts of Cr than the new strip, suggesting that these elements partitioned preferentially into the tungsten strip rather than the silicate melt. However, the degree of trace element movement between the strip and sample is thought to be negligible during the rapid fusion of one sample.

4.6 Analytical Procedure

The LA-ICP-MS system used for analyses in this thesis will be described in the four sub-sections, followed by the results of quality control analyses carried out on synthetic geostandard glasses. The application of isotope dilution to LA-ICP-MS is a new technique which is described in section 4.7.

4.6.1 ICP-MS

The ICP-MS was manufactured by Fisons (Winsford, UK) and is a PQII+"S" model instrument with a sensitivity of *ca.*500 million counts per second per $\mu\text{g g}^{-1}$ (cps/ $\mu\text{g g}^{-1}$) for both La and U when used with standard solution nebulisation sample introduction (Meinhard concentric nebuliser and a VG Scott type spray chamber cooled to 5°C) (Guenther *et al.* 1995). The ICP has been modified to improve limits of detection for selected elements (Horn *et al.*, 1996) and also to reduce the formation of some polyatomic background species in the low mass region by the use of a bonnet (Longerich *et al.*, 1997). Optimisation of the ICP-MS ion lens settings, gas flows and torch box position for dry plasma conditions was carried out using the signals from La^+ , Th^+ and

ThO⁺, from a continuous ablation of NIST SRM 612. This reduced oxide formation and optimised the sensitivity over the entire mass range. With the application of isotope dilution, Lu⁺, Th⁺ and ThO⁺ were used to reduce oxide formation and optimise the sensitivity for the high mass elements, Hf and REE. Zr, also measured by isotope dilution, had higher concentrations allowing for a lower sensitivity without compromising the precision of the analysis. All ICP-MS measurements were carried out using factory supplied "time resolved analysis" data acquisition software.

4.6.2 Laser ablation set-up

The laser ablation set-up is described by Jackson *et al.* (1992). In brief, it consists of a Q-switched Nd:YAG laser (Quantel YG-660, now Continuum, Santa Clara, CA) with a fundamental wavelength of 1064 nm in the infra red and a maximum pulse energy of *ca.* 400 mJ (9 ns pulse width at FWHM). Using non-linear optics, the beam frequency has been quadrupled, to produce a wavelength of 266 nm in the ultra-violet, and can also be quintupled to produce a beam of 213 nm wavelength in the ultra-violet. The beam is steered optically (using mirrors and prisms) through the phototube of a petrographic microscope and focused with an objective onto the sample. The sample lies behind a fused quartz window in a sample cell. A continuous flow of argon through the cell transports ablated material to the ICP torch where it is ionised and subsequently detected.

4.6.3 Data collection and reduction

Lamtrace[®] (Jackson) interactive software was used for data reduction of the raw counts-per-second data files. This reduction process allows for the integration of selected time slices from a time resolved analysis plot (Figure 4.5) avoiding the integration, into

the final result, of unwanted elemental concentrations from inclusions and some contaminants.

4.6.4 Interferences

There are polyatomic species formed in the plasma of the ICP that result in mass interferences on several isotopes, predominantly in the low-mass region. Expected polyatomic species arise due to the combination of elements or ions with argon (the plasma gas) as well as other gaseous impurities including oxygen, nitrogen, hydrogen, carbon, rare gases and some metals (Sn, Na, Pb). For example, oxides, argides (MAr^+) and nitrides will form (ArO^+ , ArN^+ , ArC^+ , CO^+ , NO^+ , CO_2^+ , O_2^+ etc). All these species form the background spectrum in the low-mass region (<80) and decrease the ability to detect many low-mass elements. During analysis, many metals, especially the first row transition metals, bond with argon and/or oxygen to form interfering polyatomic species. The formation of these interferences especially limits the ability to detect monoisotopic elements and those elements whose choice of isotope is limited by isobaric interferences with other isotopes. For this study, it was important to quantify the CrAr^+ (53+40) interference on Nb (93), which is monoisotopic. Five Cr-spiked glasses were produced (approximately 500, 1000, 2000, 5000 and 10000 $\mu\text{g g}^{-1}$ Cr) with the geostandard powder BCR-2 and a chrome standard solution. As shown in Figure 4.6, approximately 3000 $\mu\text{g g}^{-1}$ of Cr are required to produce an interference of 1 $\mu\text{g g}^{-1}$ on Nb. This interference, therefore, becomes significant for Cr-rich, Nb-poor minerals and some ultramafic rocks *e.g.* chromitites.

An unexpected interference on Nb was discovered after evaluation of the solution -ICP-MS database at Memorial University of Newfoundland. For rocks with >50 wt % Al_2O_3 there was a marked overestimation of Nb values by ICP-MS compared to XRF (Figure 4.7). This is assumed to be an ICP-MS overestimation of concentration rather than an underestimation by XRF. The cause of the interference is suspected to be a polyatomic species involving aluminium and argon. However, the exact nature of this species is not known.

4.6.5 Results of whole rock - LA-ICP-MS on selected standard reference materials

To investigate the accuracy and precision of the whole rock LA-ICP-MS technique the following geological reference materials were analysed; G-2, NBS688, MRG-1, SY-2, SY-3, AGV-1 (Table 4.2). It was found that on average, compared to literature values (Govindaraju, 1994), the REE were within 11% and HFSE (V, Ti, Zr, Nb, Ta, Hf) were within 7% accuracy. The average precision for analyses of the glasses (5 analyses from each glass) was within 5% for REE and within 4% for HFSE. The results suggest that this technique is an accurate and precise method of whole rock analysis. Because there is no sample dissolution required, the issues of solution instability and incomplete digestion of mineral phases makes this method of analysis particularly useful for the determination of HFSE.

4.7 Isotope dilution - LA-ICP-MS: A new technique

It is theoretically possible to improve the precision and accuracy of analysed glasses even further with the application of isotope dilution analysis (Moore *et al.*, 1973). Isotope dilution is a method of standard addition where the added standard (spike) is the

same element as that being measured. The difference between the added spike and the sample lies in their isotopic ratios; the spike is enriched in one of the isotopes, whereas it is assumed that the sample has a natural isotopic ratio. It follows that the element of interest must have more than one isotope to be analysed by isotope dilution and that the isotopes be free of (or corrected for) interference. By determining the isotopic composition of the spike, sample (natural ratio) and equilibrated mixture of spike and sample, the concentration of the analyte in the sample may be calculated as shown in equation 1:

$$C = \frac{(R_e - R_b) \Sigma(R_n A_n) W}{(R_b - R_n) \Sigma(R_e A_e) V} \quad (1)$$

Where, C = the original concentration of the analyte in the sample

R_e, R_n, R_b = isotope ratios for the enriched isotope spike, the unspiked sample and the mixed sample and spike, respectively.

$\Sigma R_n, \Sigma R_e$ = sum of ratios of every isotopic abundance to the chosen reference isotope abundance for the unspiked sample and the enriched isotope spike, respectively.

A_n, A_e = relative atomic masses of the unspiked sample and the enriched isotope spike, respectively.

W = amount of enriched spike added.

V = volume or weight of sample.

The benefit of isotope dilution lies in the fact that because the spike and sample are the same element, matrix effects and machine drift are corrected. Also, once the spike is added, there is no need to quantify the weights or volumes measured because the ratio is not affected by sample loss. The effect of mass discrimination (differences in the sensitivity as a function of mass), produces inaccuracy in measured isotope ratios and must be corrected for in most cases. The effect is usually 1-2% for quadrupole ICP-MS

analysis in the high-mass range using typical set-up conditions (this study). Longerich (1989) showed that if the ratios of the sample, spike and mix are all measured by the same instrument under the same operating conditions then the mass bias correction is not needed as it cancels out of the isotope dilution equation. Precision is typically better than 0.005% when isotope dilution is used with multi-collection, thermal ionisation mass spectrometry (Longerich, 1989, Fassett and Paulsen, 1989). With solution-ICP-MS, precision of this level has also been achieved with some elements (Zr in BCR-2, 184 $\mu\text{g g}^{-1}$, 0.005 %, Xie and Kerrich, 1995) but is more commonly in the range of 0.3-2.0 % (Longerich, 1989). Owing to the lower precision of ICP-MS, in comparison with TIMS, there is a smaller degree of under-spiking and over-spiking possible while maintaining acceptable precision. It is therefore important to pre-measure a sample of unknown concentration to ensure the correct spike concentration is added. This makes ID-ICP-MS a time consuming and expensive method of analysis.

Laser-ablation is a relatively new technique of sample introduction into the ICP-MS. External calibration with an internal standard is often used with a synthesised glass standard of well-documented composition; the accuracy of measurement is a function of how well the external standard material is known. Most external calibration uses Ca as the internal standard, a major element in most rocks that can be easily measured by the electron microprobe and which has six isotopes. However, Ca is not an ideal internal standard as the background counts are high (*e.g.* 2000-10000 cps/ $\mu\text{g g}^{-1}$ Memorial University). With the use of isotope dilution, drift and matrix affects are corrected. External calibration is not needed and the accuracy of analysis is therefore not

limited by how well the standard reference material is known (for example, NIST SRM 612, Pearce *et al.*, 1997). In this study, a precision of 1% was sought for the analysis of Zr, Hf, Nd, Eu, Dy and Yb by isotope dilution-LA-ICP-MS. It is not possible to measure monoisotopic elements, such as Nb, by isotope dilution, unless radiogenic isotopes (with a reasonably long half-life) are available. Also, the low abundance isotope ^{180}Ta (0.01%) and its isobaric interferences by Hf and W makes the determination of this element by isotope dilution expensive and more complicated. However, by using internal calibration with well-constrained (isotope dilution) Zr values, better accuracy can be obtained for Nb and Ta, although accuracy is still limited by poorly known standard reference materials.

4.7.1 Application of isotope dilution to whole rock LA-ICP-MS

In this study the natural isotopic abundance of all elements of interest are known and assumed accurate. A small amount of accurately known spike solution (0.1 g) was added to the powdered rock sample (0.075 g). The spike was added in the appropriate concentration to produce a mixture of spike and sample that had an isotopic ratio that was the geometrical average of the ratios in the spike and in the sample, which should be between 1 and 4 (Jochum *et al.*, 1988). This was then altered to give a slightly over-spiked mixture (section 5.4.1).

When there is a large difference in the natural abundances of a pair of isotopes and when the naturally rarer isotope is abundant in the spike, there is a large working range (Reeves and Brooks, 1978). When the natural ratio is close to unity, the working range is smaller. This criterion was used when choosing the enriched isotopes for each element so that the working range was maximised.

The isotope dilution equation utilised for this study was taken from Longrich (1989); the following example uses Zr:

⁹¹ Zr spike: Isotopes	Atomic %*	Precision (RSD) %*
90	6.51	0.05
91	88.5	0.1
92	3.21	0.05
94	1.61	0.05
96	0.17	0.03

	⁹⁰ Zr %	⁹¹ Zr %	90/91	AMU
Natural	51.4	11.2	4.60	91.22
Spike	6.51*	88.5*	0.07	91.02

* Values from Oak Ridge National Laboratory, USA.

It can be shown (Reeves and Brooks, 1978) that:

$$C_{jk} = \frac{(xa_j / M + yb_j / M')}{(xa_k / M + yb_k / M')} \quad (2)$$

Where

C_{jk} = the ratio of the number of moles (or atoms) of j and k in the equilibrated mixture of spike and sample.

a_j and a_k = the abundance of isotopes j and k in the sample.

b_j and b_k = the abundance of isotopes j and k in the spike.

x = weight of natural element (g).

y = weight of enriched element (g).

M = Relative atomic mass of the natural element.

M' = Relative atomic mass of the enriched element.

Therefore,

$$x = y \frac{b_k M (C_{jk} - B_{jk})}{a_k M' (A_{jk} - C_{jk})} \quad (3)$$

Where, A_{jk} = the ratio of the number of moles (or atoms) of j and k in sample, and B_{jk} = the ratio of the number of moles (or atoms) of j and k in the spike.

Using Case 2 from Longerich (1989):

$$C_{jk} = \sqrt{(A_{jk}B_{jk})} \quad (4)$$

C_{jk} is therefore the geometrical average of A_{jk} and B_{jk} , minimising error propagation due to over- and under-spiking.

In the case of Zr,

$$\begin{aligned} C_{jk} &= \sqrt{(4.60 \times 0.07)} \\ &= 0.58 \end{aligned}$$

From equation (3) it can be seen that

$$x/y = 1.00$$

If 0.05g of rock powder containing $146 \mu\text{g g}^{-1}$ Zr is used, then the sample contains $7.3 \mu\text{g}$ Zr.

Therefore, $y = 7.3/1.00 = 7.3 \mu\text{g}$ Zr spike needed.

The spikes were added to the sample powder from a stock solution containing all of the spikes in their correct concentrations. The desired quantity of each spike was added in one aliquot of stock solution. The spike concentrations in the stock solution were based on the average concentrations of the elements of interest in six basaltic-andesitic reference materials (Table 4.3),

The stock solution was added to 0.05g of sample powder in a small SPEX[®] quartz mill vessel. This was then allowed to dry in an oven at a temperature of approximately

40°C and ground in the SPEX[®] mill for 30 minutes. This powder was then fused in the manner outlined in section 5.1.2 to give a final spiked glass for LA-ICP-MS analysis.

4.7.1.1 Spike calibration:

For errors to be minimised, accurate measurement of the weight of the sample and spike must be carried out along with accurate and precise measurement of the isotopic ratios in both the spike and the mixture of spike and sample. Weighing errors are minimised by the use of accurate scales and are thought to be <0.1%. Using thermal ionisation mass spectrometry and multicollector ICP-MS, accurate measurement of isotopic ratios can be carried out. The enriched isotopes were calibrated using the following method of analysis:

- Nd: Thermal ionisation mass spectrometry (TIMS) at Memorial University of Newfoundland.
- Zr, Hf, Eu, Dy, Yb: VG PQII+"S"quadrupole ICP-MS at Memorial University of Newfoundland. 1 µg g⁻¹ solutions of each enriched element were prepared along with 1 µg g⁻¹ Ventron[®] standard solutions of the same element. The standard solutions were used to determine the mass discrimination of the ICP-MS (the mass discrimination correction is calculated from the difference in the accepted natural abundance of the isotopes of an element and the abundance derived from the analytical instrument). This correction factor is a mass dependant function of the sensitivity instability and varies slightly on a daily basis.

The concentration of the final, multi-element spike solution was determined using the MUN quadrupole ICP-MS. This minimised the weighing error that was high due to the dilution (by several orders of magnitude) of concentrated solution (*e.g.* 400 $\mu\text{g g}^{-1}$ Zr) before calibration in the ICP-MS.

4.7.2 Results of ID-LA-ICP-MS on selected standard reference materials

4.7.2.1 Precision

The main factors limiting the precision of isotope ratio determinations using ICP-MS are the instability of the plasma, Poisson counting statistics and background standard deviation, depending on analyte concentration. In this study, Poisson counting statistics limited the precision of the analyses of all isotope ratios (it should be noted that the Poisson counting statistics could be improved by increasing the volume of material ablated and/or sensitivity).

Poisson counting statistics were calculated for the background corrected ratios of $^{90}\text{Zr}/^{91}\text{Zr}$, $^{178}\text{Hf}/^{179}\text{Hf}$, $^{145}\text{Nd}/^{146}\text{Nd}$, $^{151}\text{Eu}/^{153}\text{Eu}$, $^{161}\text{Dy}/^{163}\text{Dy}$, and $^{171}\text{Yb}/^{172}\text{Yb}$ and compared to the observed precision of the ratios (Table 4.4). The contribution of the background (< 5 cps) to the precision was found to be negligible at the count rates observed. Table 4.4 shows that the main source of error (>50%) limiting the precision of the analyses was based on counting statistics and that it is not possible to increase significantly the precision of Hf, Eu, Dy or Yb analyses using isotope dilution (2.7% average RSD) compared to internal standardisation with an external calibration using NIST SRM 612 (5% RSD). This is true for all elements at low concentrations analysed by LA-ICP-MS

with the sensitivity presently available. Other sources of error are sample heterogeneity and drift in mass discrimination. Due to higher concentrations in the analysed materials, it is possible to improve the precision of Zr and, to a lesser extent, Nd determinations from approximately 5% (external calibration with major element (e.g. Ca) internal standard) to 1% using isotope dilution making the procedure viable in terms of cost and time. It was decided to use the Zr (ID) results as internal standardisation for the analyses of Nb, Ta and REE in this study.

To illustrate the reproducibility of the sample preparation, the basaltic rock powder BCR-2 has been prepared twice using the procedure described above. Each of these two glasses were then analysed 5 times. The individual spot analyses are shown in Table 4.5 illustrating that the procedure is reproducible. However, to obtain a higher confidence requires a greater number of glasses to be prepared and analysed.

4.7.2.2 Accuracy

A preliminary investigation into the effects of under- and over-spiking brought to light an unexpected variation in accuracy. Geostandard BCR-2 powder was spiked to different levels; for each level, three glasses were made. In each glass, 0.1 g spike solution was added and only the sample weight changed.

- Level 1) 0.1 g sample powder. According to the laws of error propagation this was under-spiked by doubling the sample weight.
- Level 2) 0.075 g rock powder.

- Level 3) 0.05 g rock powder. According to the laws of error propagation this was correctly spiked.
- Level 4) 0.0375 g rock powder.
- Level 5) 0.025 g rock powder. According to the laws of error propagation this was over-spiked by halving the weight of rock powder.

The results for Zr, Hf, Nd, Eu, Dy and Yb show a trend of degree of over-spiking is roughly proportional to the degree of over-estimation of concentration (based on literature values, Figure 4.8). For all elements, the degree of spiking that gave results closest to literature values was level 2. Zr, Yb and Nd showed very slight improvement from level 2 to level 1 (Figure 4.8).

The reason for this variation in accuracy with the degree of spiking is poorly understood. In theory, as long as the weights of spike and sample are known and accounted for in the final calculation, accuracy should not alter. The precision would change proportionally with increase of error propagation due to both over-spiking and under-spiking.

The most reasonable explanation for this variation in accuracy is that with decreasing amounts of powder, there is a decrease in the amount of spike that can be adsorbed onto the surface of the powder prior to fusion. For the over-spiked samples, therefore, there will be an overestimation of the amount of spike in the calculation. It was found that by lowering the weight of spike solution in the final calculation by up to 5%, extremely accurate results were obtained for the over-spiked glasses.

Due to the limitations of precision on most of the elements used in this study, it was decided that only Zr and Hf would be analysed by isotope dilution and the results of the ID Zr determinations would be used as an internal standard for the determination of Nb, Ta and selected REE (La, Ce, Pr, Sm, Gd, Ho, Tm, Lu). The results obtained by isotope dilution LA-ICP-MS (Zr, Hf) and by external calibration (NIST SRM 612) with internal standardisation (Zr ID values) are shown in Table 4.6. The accuracy of the results for Zr and Hf determinations of the reference materials BHVO-1, AGV-1, MRG-1 and BCR-2 (if given the values of BCR-1, which was derived from the same sample location) are within 4% of the literature values (Figure 4.9) (Govindaraju, 1994). The accuracy of Zr and Hf determinations for the Japanese geostandards is within 10% for Zr and 8% for Hf. The results for Nb and Ta, for BHVO-1, AGV-1, MRG-1 and BCR-2 determined from external calibration with internal standard (Zr, ID values), show an accuracy within 3% for Nb and 6% for Ta compared to literature values (Govindaraju, 1994). The accuracy of Nb and Ta determinations for the Japanese geostandards Jb-1a and Jb-2 is 22% and 30% respectively, which along with the less accurate Zr and Hf values, probably reflects the poorly known concentrations of these geostandards cited in the literature. For all the Japanese geostandards analyzed, the values determined by Jochum and Jenner (1994) are in better agreement to the values determined in this study.

For the analysis of BHVO-1, MRG-1 and BCR-2 the average accuracy of REE determinations (external calibration with NIST SRM 612 and with ID Zr as

internal standard) is within 8% of literature values (Table 4.6). For AGV-1 and the Japanese geostandards this average accuracy is within 22% and 15% respectively. The values for REE determined in this study are consistently low for AGV-1 compared to literature values.

4.7.3 Conclusion

The results obtained for Zr and Hf by ID-LA-ICP-MS of the 7 reference materials agree well with the literature values, illustrating the accuracy of the technique. Results for external calibration also agree well with the exception of the Japanese Geological Survey SRM Jb-2 and Jb-3, the REE contents of which are poorly known in the literature. Analyses by Jochum and Jenner (1994) by spark source mass spectrometry and solution nebulisation ICP-MS show a better correspondence with the values found in this study. Chondrite normalised REE plots support the accuracy of the values determined in this study as they form more convincing trends than those typically found in the literature (Figure 4.10) since their abundance in rocks reflect only their change in ionic radii (Coryell *et al.*, 1963).

4.8 Summary

The use of a strip heater to fuse rock powder provides an effective alternative method of whole rock sample introduction into an ICP-MS with the use of laser ablation on synthetic glass beads. This technique avoids the problems currently inherent in acid digestion ICP-MS where solution instability and incomplete digestion result in relatively poor precision for HFSE determinations. The use of isotope dilution is an effective method of improving the precision and accuracy of whole rock LA-ICP-MS analyses for

elements of sufficiently high concentration. Although the use of isotope dilution does not improve the precision of LA-ICP-MS to the same degree as with solution nebulisation ICP-MS, the ease of sample preparation and the absence of an acid digestion procedure makes this technique worthwhile in terms of cost and time.

Table 4.1: Major element homogeneity in a synthetic BCR-2 glass analysed by wavelength dispersive electron microprobe (Cameca, SX 50)

	wt%	stdev	RSD%
SiO ₂	55.1	0.54	1.0
FeO	12.0	0.32	2.7
TiO ₂	2.3	0.06	2.6
Na ₂ O	3.6	0.07	2.0
MgO	3.7	0.06	1.6
Al ₂ O ₃	13.8	0.11	0.79
K ₂ O	1.6	0.05	2.9
CaO	7.2	0.10	1.4
MnO	0.2	0.03	16.6

Table 4.2: Results of geological standard synthetic glass analyses by whole rock - LA-ICP-MS. Oxides in weight %. Traces in $\mu\text{g g}^{-1}$

	MRG-1	Literature	SY-2	Literature	SY-3	Literature
SiO ₂	36	39.12	57	60.11	48.2	59.68
Sc	69	55	8.8	7	7.4	6.8
TiO ₂	3.2	3.77	0.11	0.15	0.16	0.15
V	473	526	45	50	42.5	50
MnO	0.13	0.17	0.28	0.32	0.29	0.32
Sr	275	266	275	271	293	302
Y	12	14	124	128	758	718
Zr	101	108	119	280	211	320
Nb	20	20	30	29	194	148
Ba	53	61	489	460	409	450
La	9.7	9.8	70	75	1344	1340
Ce	26	26	158	175	2315	2230
Pr	4.0	3.4	20	18.8	240	223
Nd	20	19.2	80	73	790	670
Sm	5.1	4.5	17.1	16.1	138	109
Eu	1.6	1.39	2.5	2.42	18.8	17
Gd	4.2	4	16.8	17	124	105
Tb	0.63	0.51	3.1	2.5	22	18
Dy	3.2	2.76	22	18	147	118
Ho	0.57	0.49	4.9	3.8	32	29.5
Er	1.35	1.12	16.3	12.4	96	76.8
Tm	0.18	0.11	2.6	2.1	13.5	11.6
Yb	0.91	0.6	19.0	17	78	62
Lu	0.14	0.13	3.2	2.7	9.5	7.9
Hf	4.7	3.76	4.6	7.7	6.0	9.7
Ta	0.88	0.8	1.9	2.01	22	30
Th	0.89	0.93	330	379	874	1003
U	0.26	0.24	225	284	486	650

Table 4.2 continued:

	G-2	Literature	NBS688	Literature	AGV-1	Literature
SiO ₂	74	69.0	48	49.0	61	59.3
Sc	4.1	3.5	38	37	13.2	12.1
TiO ₂	0.49	0.49	1.17	1.17	1.07	1.06
V	35	36	242	241	107	123
MnO	0.04	0.034	0.17	0.15	0.09	0.10
Sr	478	487	169	166	647	662
Y	9.8	11.4	17.0	18.1	19.2	21.0
Zr	301	300	61	52	241	225
Nb	12.6	13.0	5.0	3.7	13.8	15.0
Ba	1861	1880	200	164	1158	1221
La	94	86	5.3	5.2	42	38
Ce	171	159	13.0	11.8	66	66
Pr	16.4	19.0	2.4	1.7	8.2	6.5
Nd	56	53	9.6	8.7	34	34
Sm	7.6	7.2	2.5	2.5	6.3	5.9
Eu	1.45	1.41	1.01	1.04	1.77	1.66
Gd	3.9	4.1	3.2	2.7	4.8	5.2
Tb	0.48	0.48	0.52	0.47	0.66	0.71
Dy	2.4	2.5	3.4	3.1	3.8	3.8
Ho	0.39	0.37	0.81	0.73	0.72	0.73
Er	0.95	1.20	2.1	2.0	1.89	1.61
Tm	0.12	0.17	0.29	0.27	0.26	0.32
Yb	0.86	0.78	2.1	2.0	1.83	1.67
Lu	0.12	0.11	0.35	0.33	0.27	0.28
Hf	7.5	7.9	1.55	1.36	5.6	5.1
Ta	0.82	0.88	0.31	0.31	0.82	0.92
Th	26	25	0.33	0.35	7.1	6.5
U	3.0	2.0	0.31	0.29	1.84	1.89

Table 4.3: Calculated concentrations of spike solutions and stock solution.

Concentrations are in micrograms per gram ($\mu\text{g g}^{-1}$)

Form of enriched element	average $\mu\text{g/g}$ in basalts to be analyzed	μg of spike needed for ID analysis of 0.05mg basalt	Concentration of enriched element in stock solution	μg spike added in 0.1g of stock
Zr	146.2	7.28	70.10	7.01
HfO ₂	3.652	0.17	1.73	0.17
Pb(NO ₃) ₂	12.2	0.57	5.15	0.51
Nd ₂ O ₃	22.94	0.65	6.44	0.64
Eu ₂ O ₃	1.552	0.17	1.55	0.15
Dy ₂ O ₃	4.46	0.28	2.79	0.28
Yb ₂ O ₃	2.298	0.11	1.06	0.11

Table 4.4: Precision (RSD) of background corrected ratios of duplicate BCR-2 analyses and NIST SRM 612 glass compared to Poisson counting statistics.

	Observed%	Poisson%	Observed%	Poisson%
	Glass 1	Glass 1	Glass 2	Glass 2
Zr	0.87	0.35	0.57	0.27
Hf	3.39	2.10	2.39	1.62
Nd	1.35	0.98	2.14	0.75
Eu	4.15	2.01	2.97	1.57
Dy	3.25	1.77	3.87	1.33
Yb	2.07	2.67	3.13	2.06
Pb	16.60	4.98	14.82	7.20

Table 4.5: Duplicate analyses of SRM BCR-2					
glass 1	Zr	Hf	glass 2	Zr	Hf
analysis	$\mu\text{g g}^{-1}$	$\mu\text{g g}^{-1}$	analysis	$\mu\text{g g}^{-1}$	$\mu\text{g g}^{-1}$
BCR-2	178	4.7	BCR-2	174	5.0
BCR-2	174	4.5	BCR-2	178	4.8
BCR-2	178	4.9	BCR-2	176	4.3
BCR-2	174	5.0	BCR-2	175	5.0
BCR-2	176	5.0	BCR-2	175	5.0
Average	176	4.8	Average	176	4.8
Stdev	2	0.2	Stdev	1.4	0.3
RSD%	1	4.8	RSD%	0.8	5.7
Overall average Zr		$\mu\text{g g}^{-1}$	176		
RSD% Zr			1.0		
Overall average Hf		$\mu\text{g g}^{-1}$	4.8		
RSD% Hf			5.0		

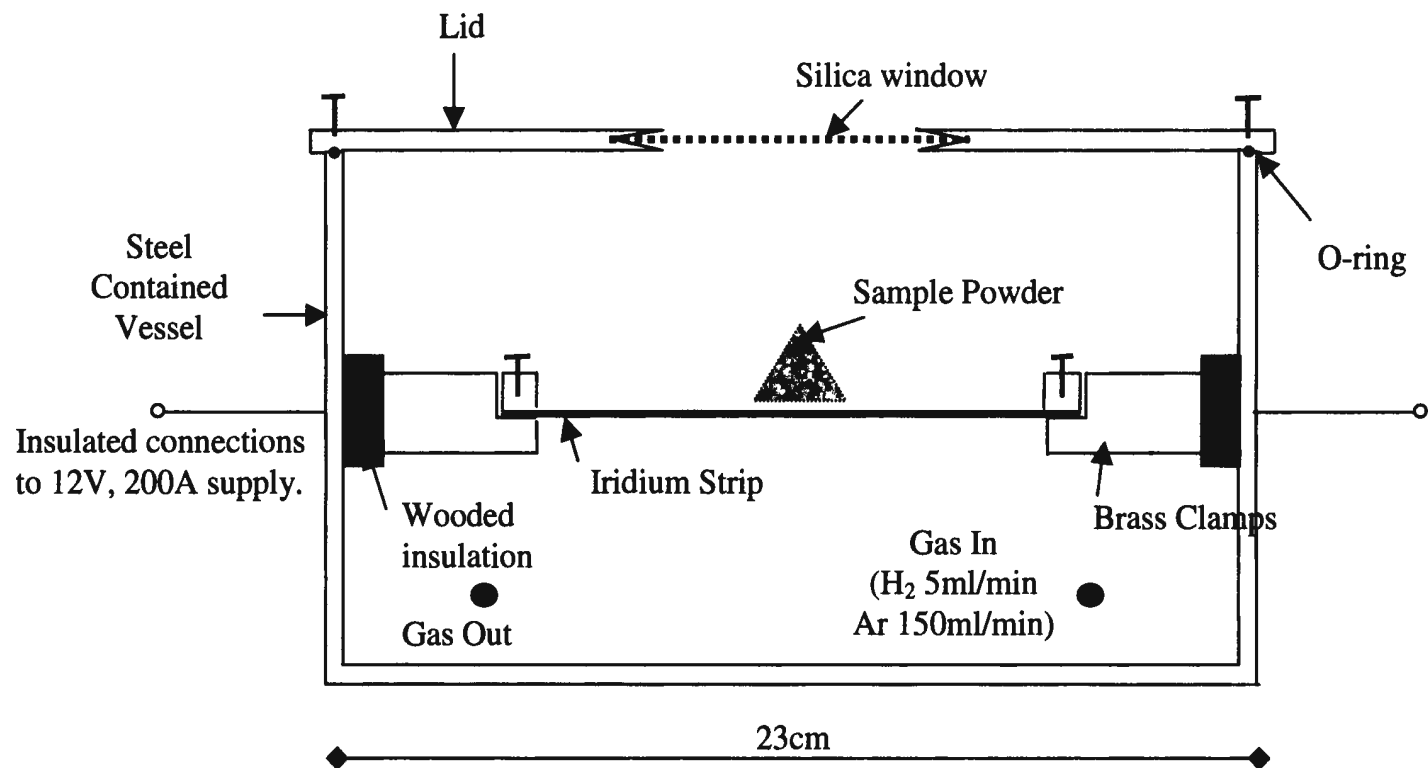


Figure 4.1: Schematic sketch of strip-heater and sample



a

3mm



b



Figure 4.2: Photographs taken of synthetic glasses under a petrographic microscope using plane polarized light. (a) shows the pale transparent basaltic glasses fused in a reduced atmosphere, (b) shows a glass (USGS SRM SY-2) fused with (right) and without (left) glycerol. The glass fused with glycerol contains considerably less volatile inclusions resulting in a more homogeneous glass.

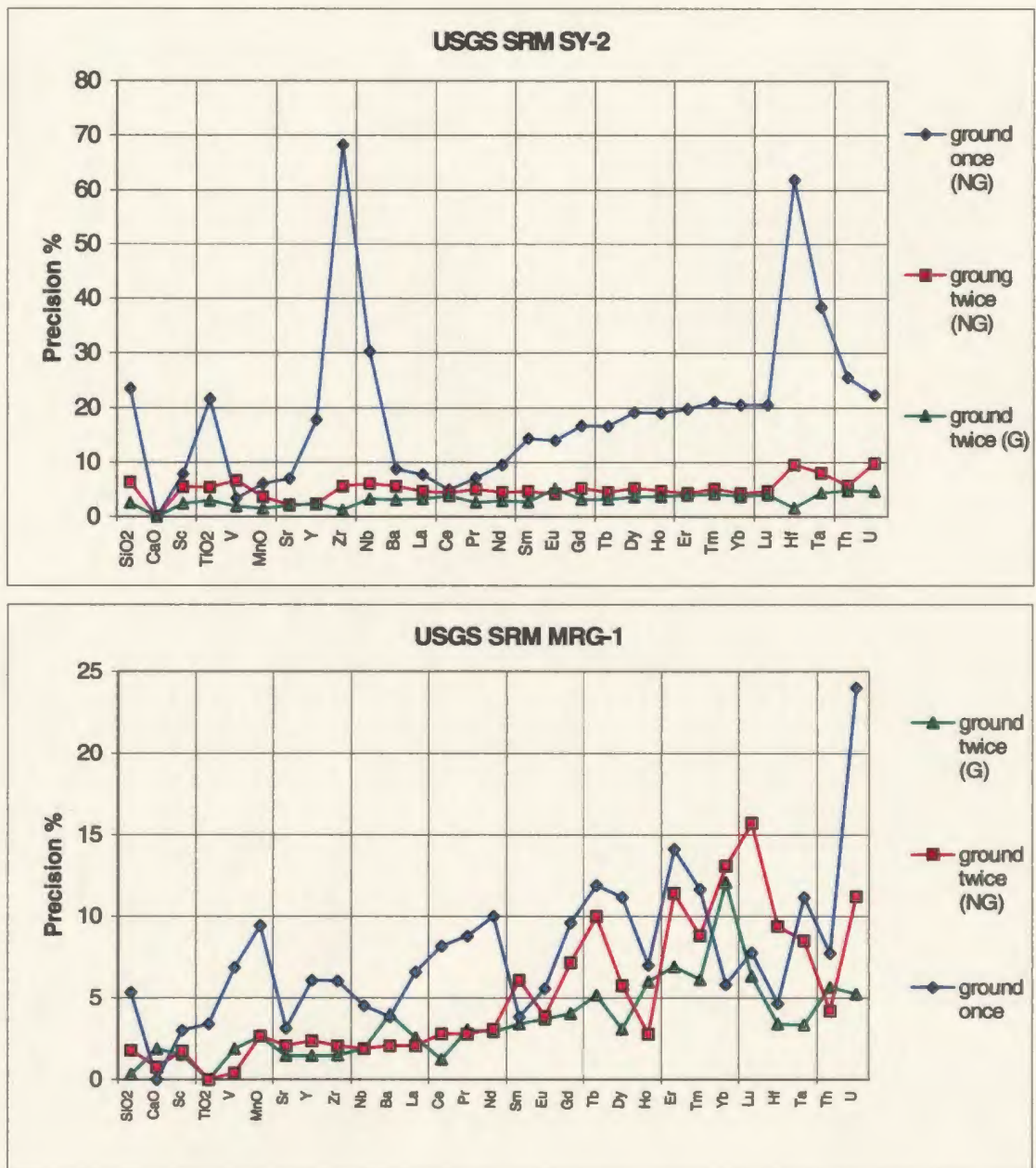
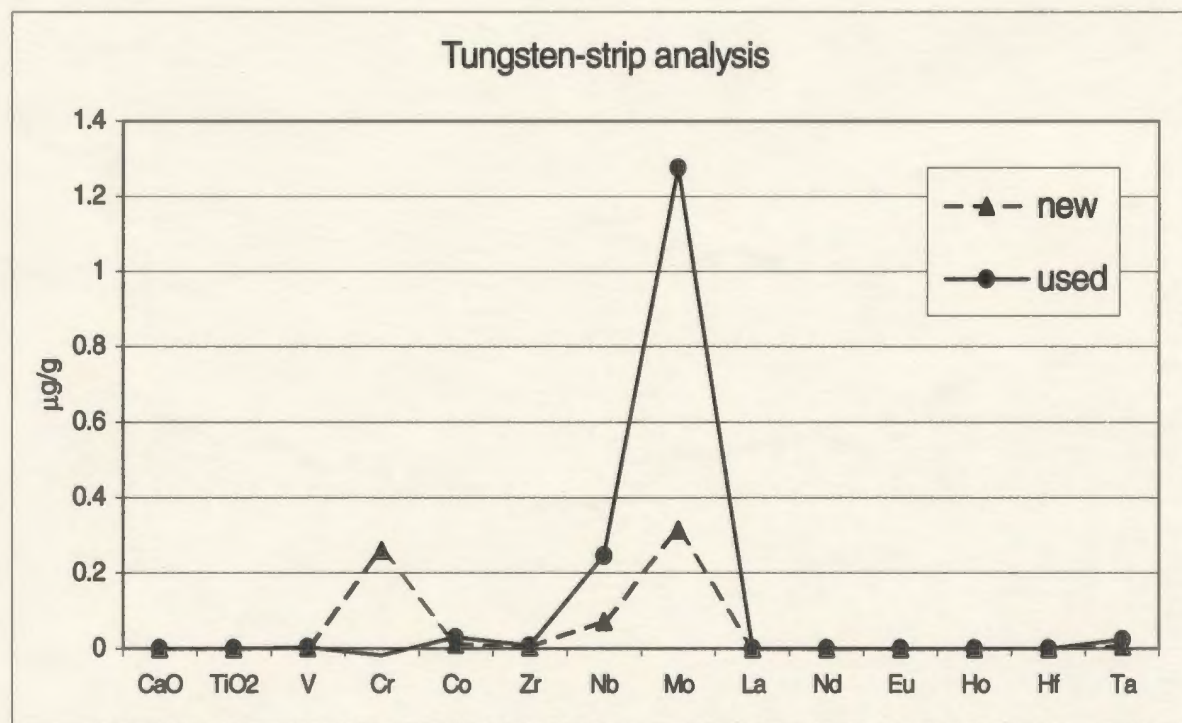


Figure 4.3: The precision of the analyses of two synthetic geostandard glasses analysed using LA-ICP-MS. "G" refers to samples prepared using glycerol, "NG" refers to samples prepared without glycerol.

Figure 4.4: Semi-quantitative impurity concentrations in a >99.95% (Alpha Aesar[®]) tungsten-strip.

The internal standard, for external calibration with NIST SRM 612, was taken from the

Ca detection limits for the analytical results derived from Alpha Aesar[®].



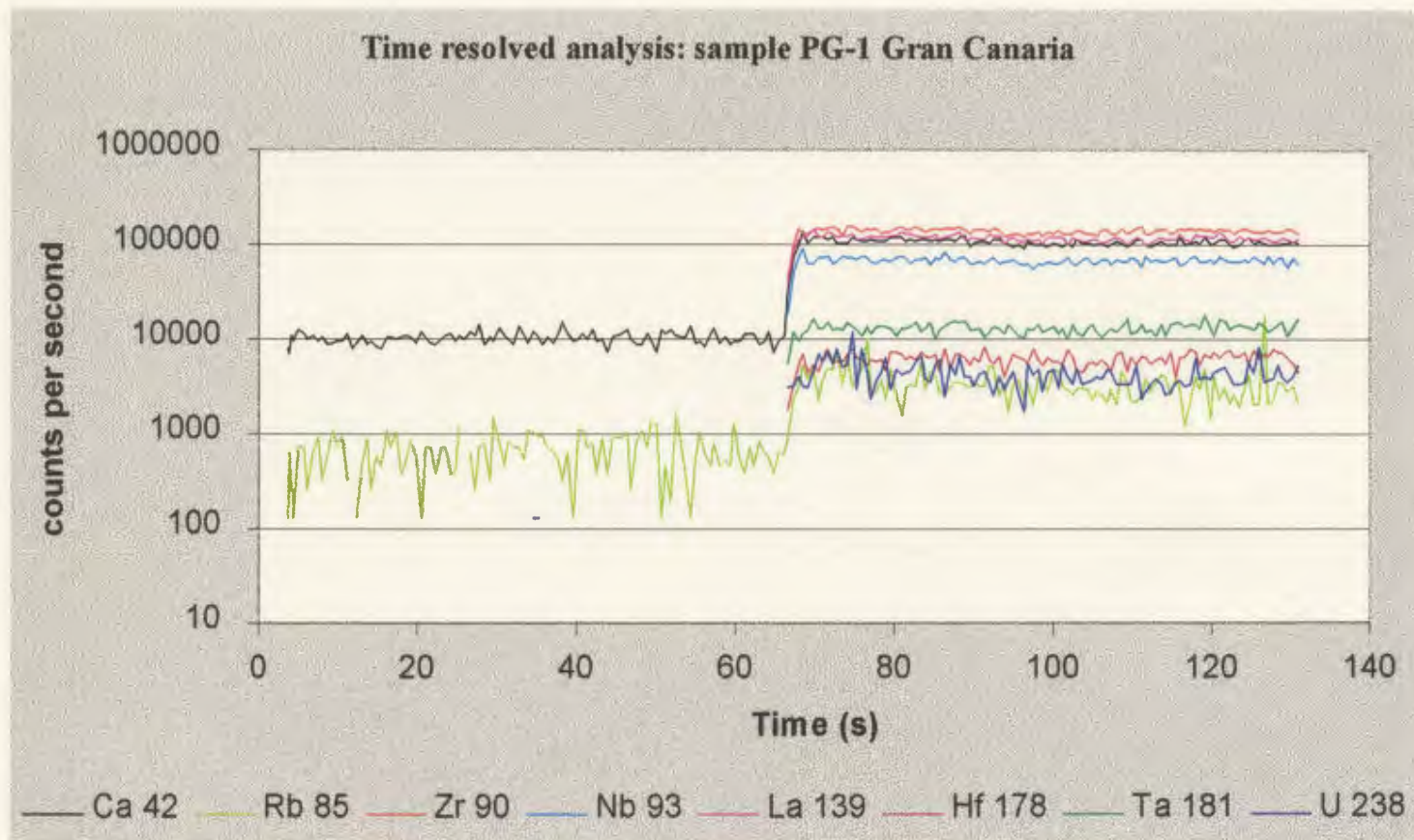


Figure 4.5: Time resolved LA-ICP-MS analysis of Gran Canaria synthetic glass. Analysis carried out at Harvard University LA-ICP-MS laboratory, for set-up and operating conditions see Reid *et al.*, (submitted 1998).

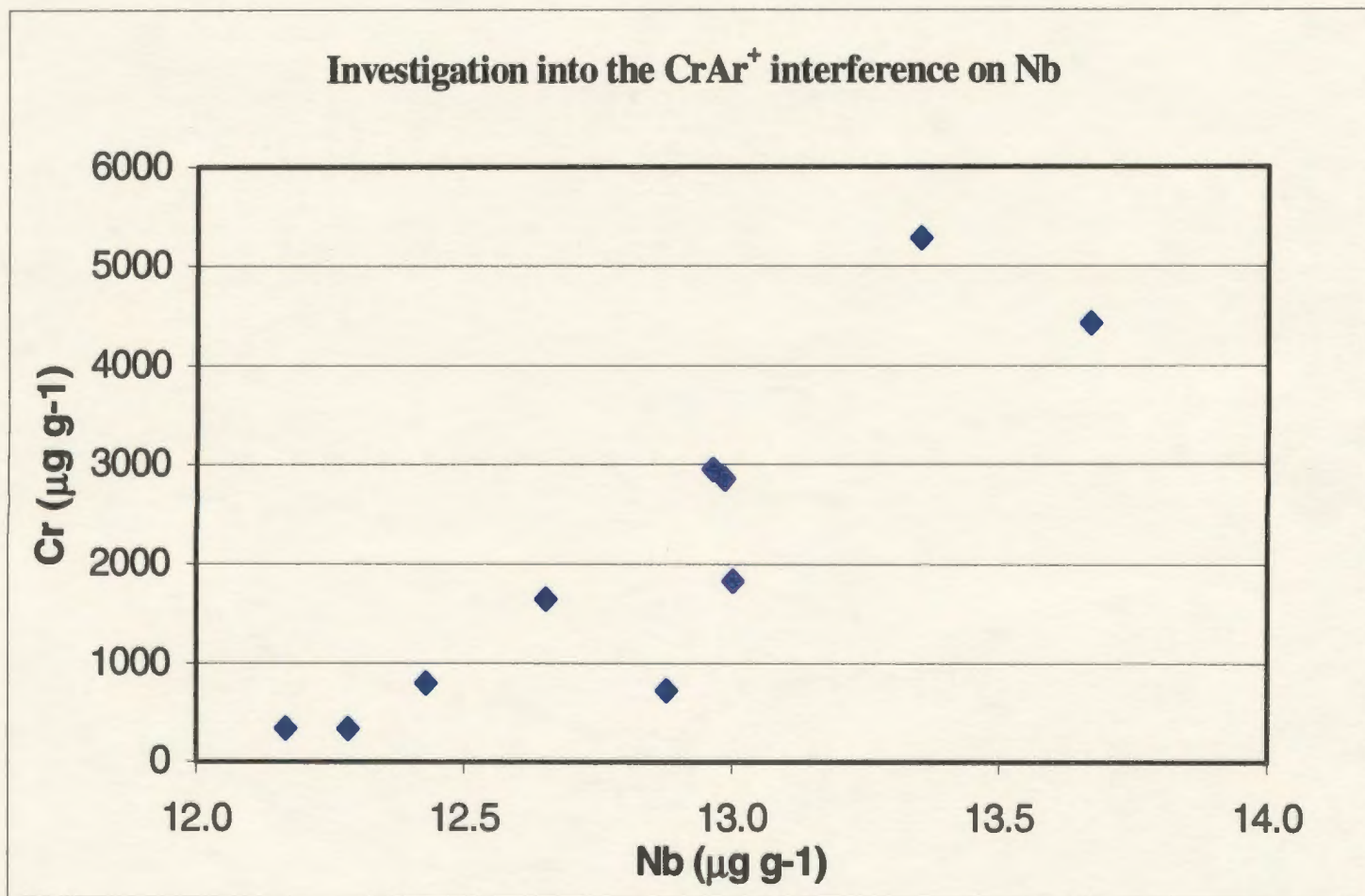


Figure 4.6: CrAr^+ interference on Nb.

Results include both the value of the interference and the Nb concentration in BCR-2 (14 μ g/g).

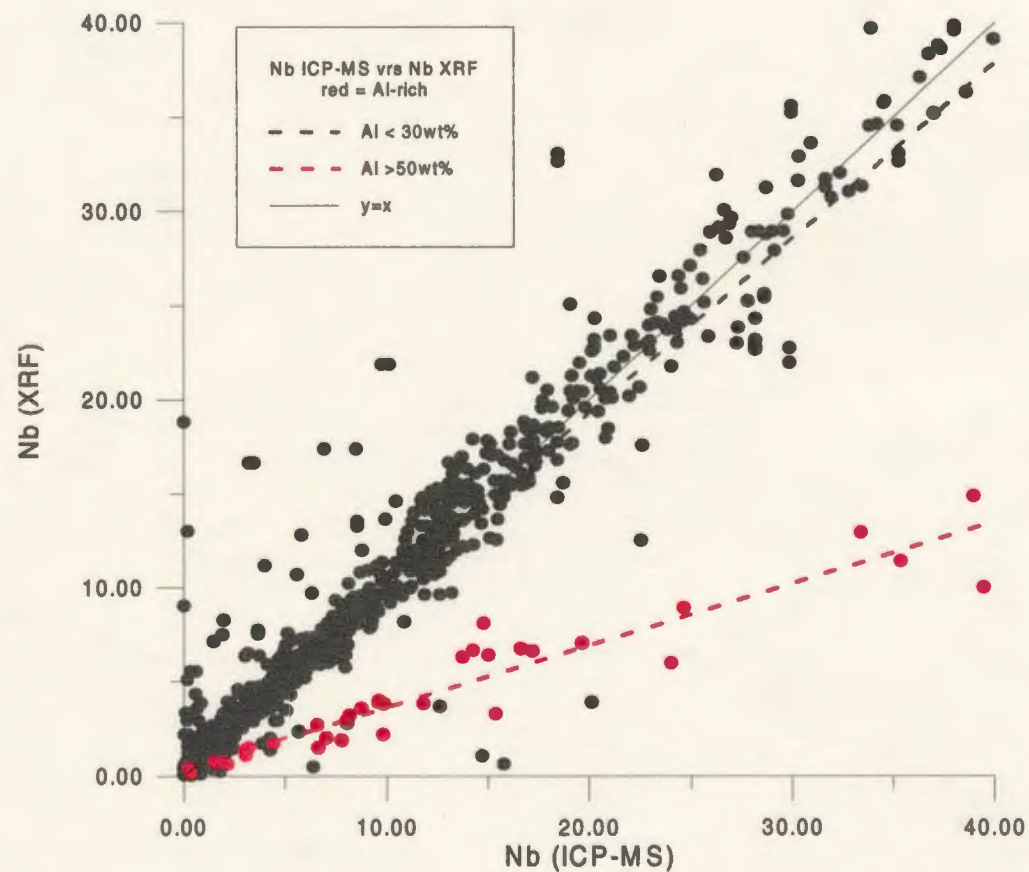


Figure 4.7: Suspected interference on Nb in Al-rich rocks analyzed by solution nebulisation ICP-MS. This can be seen in the trend of red sample points which show overestimated Nb concentrations compared to XRF. Data taken from the data bases of Memorial University of Newfoundland. Concentrations in μ g/g.

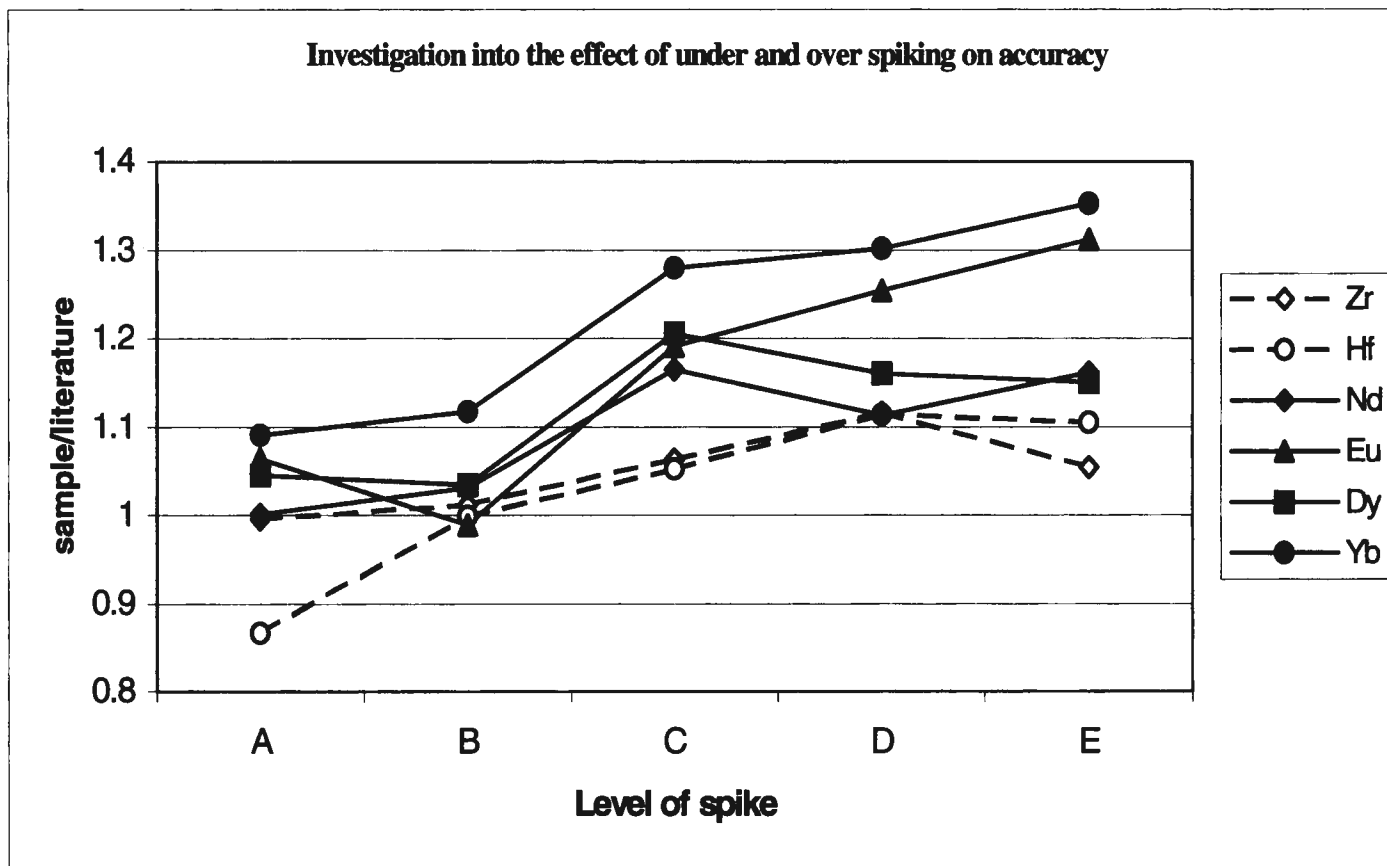
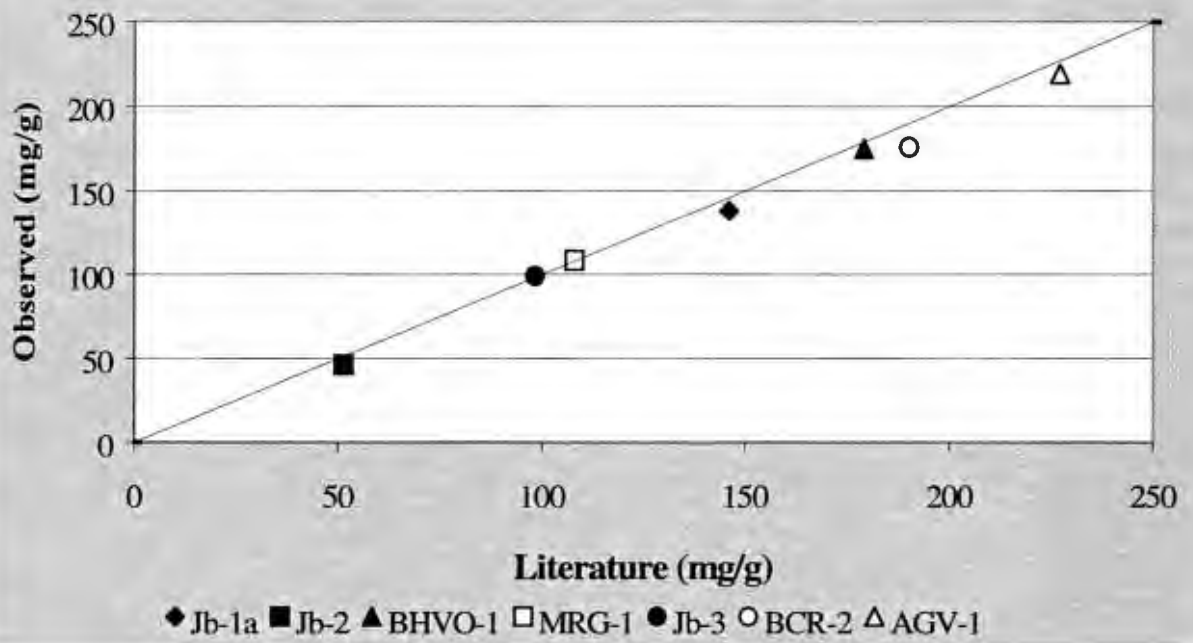


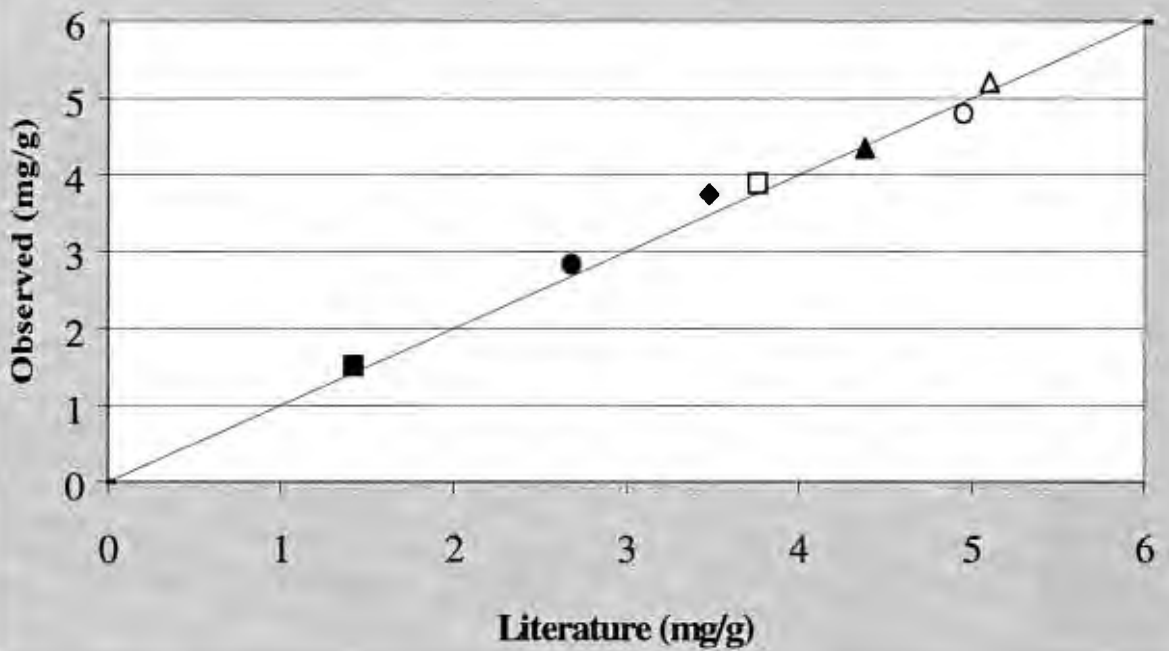
Figure 4.8: The effect of over- and under-spiking on the resulting accuracy of a BCR-2 analysis by ID-LA-ICP-MS.

According to the rules of error propagation, A is the most under-spiked sample shown, C is correctly spiked and E is the most over-spiked sample shown (see text for details).

Figure 4.9: Accuracy of Zr ID-LA-ICP-MS determinations



Accuracy of Hf ID-LA-ICP-MS determinations



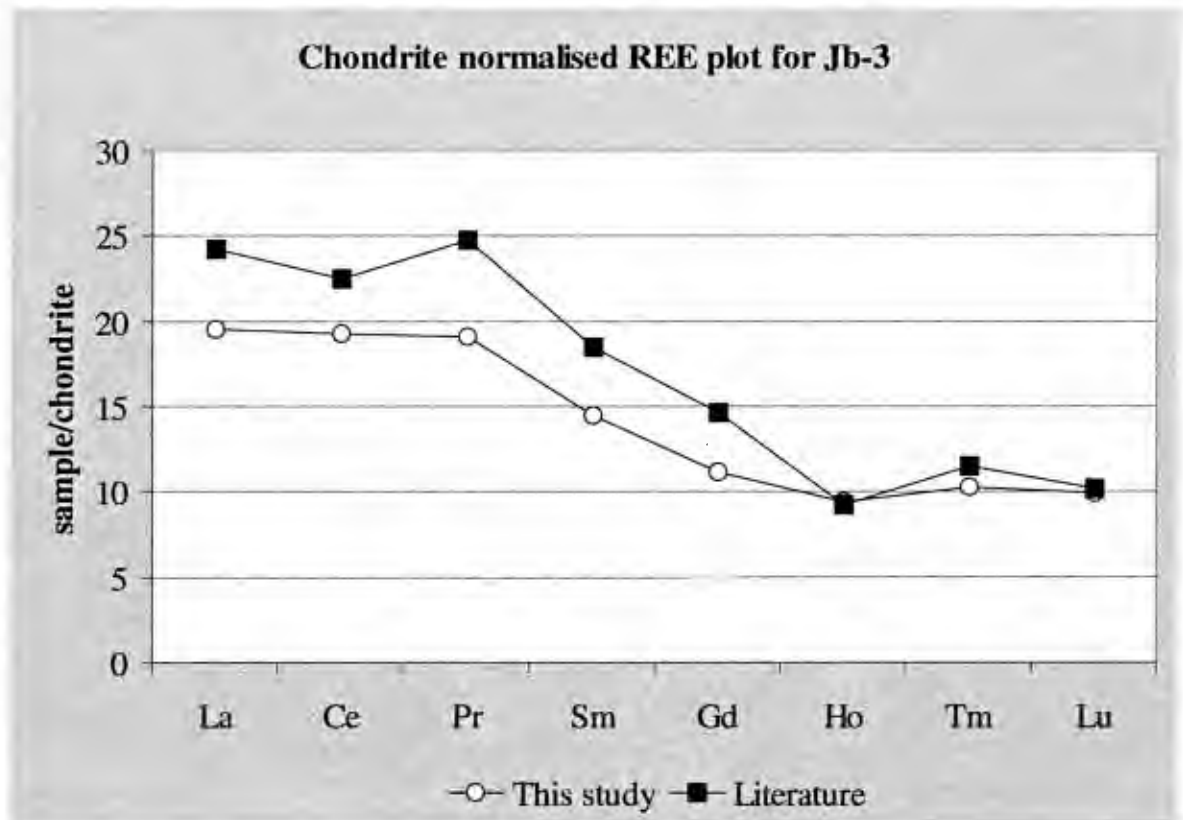
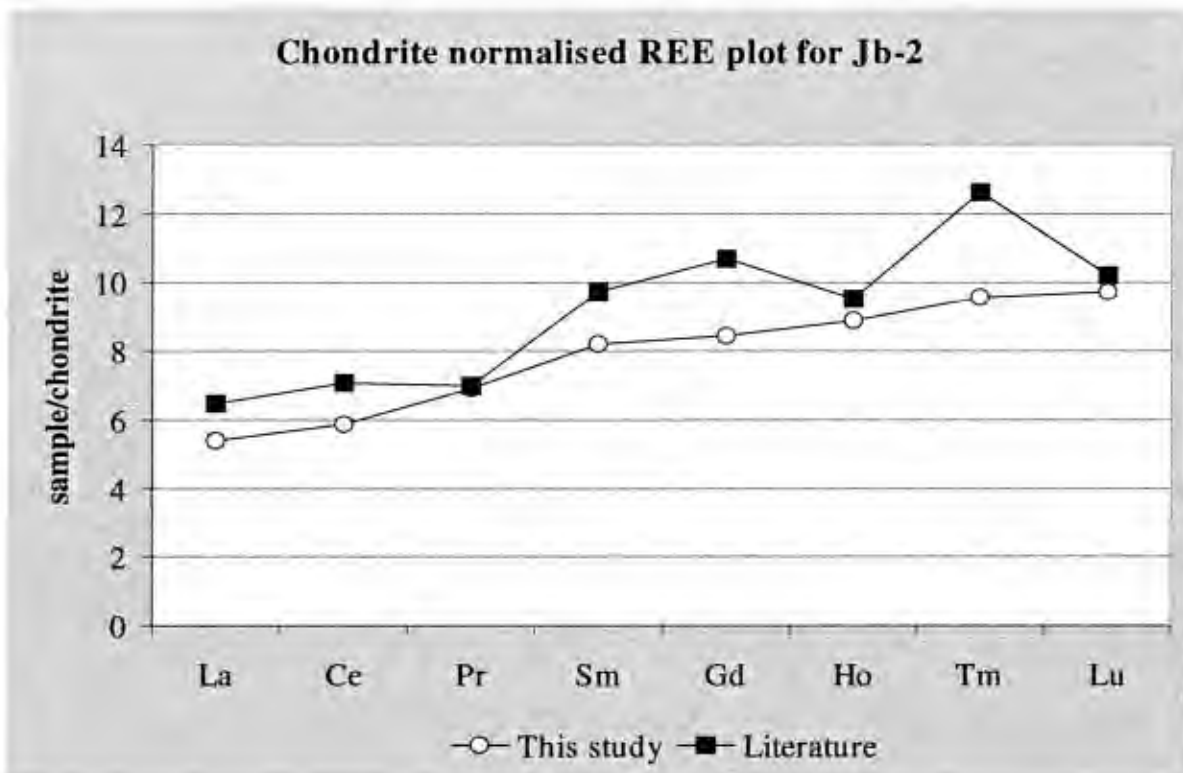


Figure 4.10: Chondrite normalised REE plots for Japanese geostandards Jb-2 and Jb-3 as determined by ID-LA-ICP-MS and from literature values. 4-39

CHAPTER 5. HIGH FIELD STRENGTH ELEMENT BEHAVIOUR: EVIDENCE FROM A VARIETY OF ROCK SUITES ANALYSED BY WHOLE ROCK - LA-ICP-MS

One hundred and eight samples of igneous, sedimentary and metamorphic rocks were chosen from a broad range of tectonic settings in order to investigate the level of HFSE variation with particular emphasis on Nb/Ta and Zr/HF ratios. Synthetic glasses were prepared (as described in section 4.3) from pre-ground samples for trace element analysis by LA-ICP-MS. Natural glasses were also analysed from Macquarie Island, Lau Basin and the Azores (Leg 82). The sample suite includes the following:

- Mid-ocean ridge basalts (E-MORB) (Macquarie Island, Leg-82)
- Ocean island basalts (OIB) (Gran Canaria)
- Destructive plate margin volcanics (Vanuatu, Tonga, Flores, Lombok, Sumbawa, Java)
- Back arc basin basalts (Lau Basin)
- Boninites and related rocks (Newfoundland, Bonin Island, Papua New Guinea, Japan)
- Ultramafic xenoliths and peridotites (Cyprus ophiolite, Italian ophiolite, xenoliths)
- Continental representative (Labrador Shield).

Descriptions of tectonic environment and geographical location for each sample group are given in Appendix I. All elemental concentrations determined are shown in Appendix II. Elemental normalising values for C1-chondrite, N-MORB, E-MORB and primitive mantle have been taken from Sun and McDonough (1989).

5.1. Nb/Ta and Zr/Hf variation in each tectonic environment investigated: Results

The results will be described in relation to their deviation from the chondritic value ($\text{Nb/Ta} = 17.5$, $\text{Zr/Hf} = 36.3$, Sun and McDonough, 1989). Each HFSE determination has a precision of approximately 5% and, accordingly, the ratios have a precision of approximately 7%. Therefore, all ratio determinations within the range of chondritic error or slightly outside of this range (up to 7% RSD of the extreme values) will not be regarded as being significantly different from the chondritic value. The mean Nb/Ta and Zr/Hf values for each environment with the standard deviation of the ratios and the range of concentrations are given in Table 5.1. Figure 5.1 illustrates how Nb/Ta varies with Nb concentration and Figure 5.2 illustrates the level of Zr/Hf variation with Zr concentration for arc-related and non-arc-related samples. A brief description of the results will be given for each tectonic environment, followed by a discussion on how this data set corresponds with HFSE ratios in the literature.

5.1.1 MORB

The majority of the MORB samples analysed are E-MORB, with characteristic enrichments (compared to N-MORB) in LILE, HFSE and LREE and negative Sr anomalies on primitive mantle normalised extended plots (Figure 5.3). Nb/Ta and Zr/Hf ratios are chondritic within error (Table 5.1) with the exception of sample 56-A from Macquarie Island, which had a sub-chondritic Nb/Ta value of 11 and Zr/Hf value of 22.

5.1.2 Ocean Island Volcanic Rocks

The Nb/Ta ratios of this study were within the chondritic margin of error although a trend of increasing Nb/Ta ratio with decreasing Nb concentration is discernible can be

seen (Figure 5.1). All samples analysed are primitive ($\text{MgO} > 6 \text{ wt}\%$) with the exception of RN-2, which shows highly enriched trace element concentrations ($246 \mu\text{g g}^{-1} \text{ Nb}$). The Zr/Hf ratios exhibit a greater range of values than Nb/Ta and have a tendency to be super-chondritic (Figure 5.2). The most evolved sample has a sub-chondritic ratio suggesting that zircon may have precipitated, leaving the melt relatively enriched in hafnium (based on a zircon analysis by Su and Pan (1973), $\text{ZrO}_2 = 64.03 \text{ wt}\%$ and $\text{HfO}_2 = 1.18 \text{ wt}\%$).

5.1.3 Continental Crust

The Nb/Ta ratios of continental rocks (Gagnon Terrane, Labrador) are sub-chondritic, supporting work carried out on continental rocks analysed by Barth *et al.* (1998) and those compiled by Green (1995). The spread of Nb/Ta ratios follows a trend of increasing Nb/Ta ratio with increasing Nb concentration. The low Nb/Ta anomalies of those samples are due to a process that resulted in a negative Nb anomaly with no negative Ta anomaly. The Zr/Hf ratios are consistently low, falling slightly below the chondritic margin of error. There is no apparent correlation between Zr concentration and Zr/Hf ratio.

5.1.4 Destructive Margin Volcanic Rocks

Samples in this group all exhibit negative Nb and Ta anomalies on primitive mantle normalised plots (Figure 5.4), a characteristic feature of volcanic arc magmatism. For most of the samples analysed there is very little spread of Nb/Ta ratios outside of the chondritic range (Figure 5.1). The sample from Rindjani (Indonesia) has a super-chondritic ratio (24) and Tanna (Vanuatu) samples have both super-chondritic (21,25,26)

and sub-chondritic (11) ratios. The variation of Zr/Hf ratios shows a tendency towards sub-chondritic ratios for most island arc volcanics (Figure 5.2).

5.1.3 Back-arc Basin and Related Volcanic Rocks

The majority of Lau Basin glasses (synthetic and natural) exhibit a large range of Nb concentrations ($0.03 \mu\text{g g}^{-1}$, Ata Island, to $15 \mu\text{g g}^{-1}$, central Lau Basin) and Zr concentrations ($21 \mu\text{g g}^{-1}$ Ata Island, to $121 \mu\text{g g}^{-1}$, south Lau Basin). Nb/Ta ratios are chondritic to sub-chondritic with some extremely low outliers within the samples from south Lau Basin natural glasses (Figure 5.1). It should be noted that the south Lau Basin natural glasses contained both volatile and crystalline inclusions, the former having high Nb and Ta concentrations ($\text{Nb} > 30 \mu\text{g g}^{-1}$) and low Nb/Ta ratios ($\text{Nb/Ta} = 6$). Incorporation of these inclusions during the analysis of the glass may explain the low Nb/Ta ratios of samples SLB54 and SLB127. Zr/Hf ratios show a spread extending from within the chondritic range (south and central Lau Basin natural glasses) at higher Zr concentrations, to sub-chondritic values (Ata Island, Valu Fa Ridge) at lower Zr concentrations (Figure 5.2). South Lau Basin samples show pronounced negative HFSE anomalies on an N-MORB normalised plot (Figure 5.5). Central Lau Basin natural glasses exhibit less pronounced Nb, Ta, Zr and Hf depletions and have relatively high Ti concentrations (Figure 5.6). Sample CLB10 shows E-MORB characteristics with enriched LILE, LREE and HFSE concentrations.

5.1.4 Boninites and Related Rocks

The boninites are perhaps the most unusual group of rocks analysed in this study and they have Nb/Ta ratios that reflect this exotic character (Figure 5.1). Despite the fact

that contamination, through grinding in tungsten carbide vessels (section 3.6), undoubtedly contributed to the low Nb/Ta ratios of the Newfoundland boninites, it is apparent from the other boninitic samples that this feature is real, if amplified. All the other boninites and related rocks show sub-chondritic ratios which, in the case of the sanukitoid, the Pacquet Harbour Group samples and the Dabi Volcanics, was due to relatively depleted concentrations of Nb and slightly enriched concentrations of Ta, compared to other elements of similar compatibility normalised to primitive mantle values. The Zr/Hf ratios show no correlation with the Nb/Ta ratios and are within or slightly below the chondritic range (Figure 5.2).

A more detailed description of the boninites (and related rocks) geochemistry is given below.

5.1.4.1 Dabi Tholeiites

All samples have flat primitive-mantle normalised REE patterns ($\text{La/Yb} < 2$, 10 x chondritic, Sun and McDonough, 1989) as illustrated in Figure 5.7. The HFSE (with the exception of Ta) and REE are depleted with respect to MORB in all samples, whereas LILE are enriched. All samples show negative Nb anomalies (with the exception of LB86) with no Ta, Zr or Hf anomalies (Figure 5.8). It can be seen from Figure 5.9 that the Nb/Ta ratio variation from 2.2 to 13.3 is a result of an increase in Nb with a relatively constant Ta concentration ($0.24\text{-}0.33 \mu\text{g g}^{-1}$). The most evolved rocks have the lowest Nb/Ta ratios and the least evolved rock has the highest ratio. There is a positive correlation between Nb concentration (and hence Nb/Ta ratio) and all the LREE (especially Ce), Sr, Zr,

Ti, and Hf. The Nb/Ta ratios are markedly sub-chondritic and the Zr/Hf ratios vary from 27 to 32 and are slightly sub-chondritic (Table 5.1). There is a positive correlation between Eu/Yb and Ti/Eu and between Nb/Yb and La/Yb, which is not apparent in the plot between Zr/Sm and Sm/Yb or between Ta/Yb and La/Yb .

5.1.4.2 Paquet Harbour Group, Newfoundland

These boninites exhibit characteristic U-shaped primitive mantle normalised REE plots (Figure 5.7) and high Zr/Sm ratios. The samples analysed were, unfortunately, ground in tungsten carbide and seem to have been contaminated by Ta, giving them exceptionally low Nb/Ta ratios of near unity. However, similar to the tholeiites of the Cape Vogel (ground in agate, section 5.1.4.1) there is a negative Nb anomaly seen in the primitive-mantle normalised extended plot (Figure 5.8). There is also thought to be a genuine Ta positive anomaly, which has been amplified by the grinding contamination. In contrast to the Cape Vogel tholeiites, variation in the Nb/Ta ratios seem to be controlled by variations in Ta concentrations with relatively constant Nb (Figure 5.10). Nb, Ta and Nb/Ta values show positive correlations with the concentrations of all incompatible elements analysed and also with Ca, Al and Mn. There is no apparent correlation between the plotted ratios of Nb/Yb (or Ta/Yb) against La/Yb or between the ratios of Ti/Yb against Eu/Yb. The Zr/Hf ratios of the samples analysed from this area have a chondritic value, within margin of error.

5.1.5 Ultramafic Rocks

The xenoliths from Sangeang Api, Indonesia, show sub-chondritic Nb/Ta ratios (11 and 5) and very sub-chondritic Zr/Hf ratios (19 and 20). The Nb concentration is typical of that of island arc volcanics ($1-2 \mu\text{g g}^{-1}$). Sample B10-C is far more enriched in incompatible elements (Zr, $54 \mu\text{g g}^{-1}$) than sample B10-A (Zr, $13 \mu\text{g g}^{-1}$) and shows LREE enrichment on a primitive mantle normalised plot. Both samples show characteristic Nb, Hf, Zr and Ti negative anomalies on primitive mantle normalised plots, however as the Nb/Ta ratios suggest, sample B10-C shows a negative Ta anomaly which is absent in sample B10-A.

5.2 Discussion

As discussed in section 2.2.3, Nb and Ta can be decoupled from each other by a number of processes, for example: small degrees of partial melting from a source containing a phase that has very different compatibilities for Nb and Ta (garnet, rutile); metasomatism by a fluid or melt into which Nb preferentially partitions over Ta or *vice versa*; fractional crystallisation of a phase such as rutile or sphene; and evolution of a melt with changing alkalinity that variably affects the activity of Nb and Ta in the melt.

In most cases, the small variations in Nb/Ta ratios could be attributed to analytical error. Any variations caused by fractional crystallisation would, in most cases, be smaller than those caused by analytical error as the major fractionating phases (pyroxenes, amphiboles, plagioclase, olivine) do not partition Nb and Ta to a significant degree. The possible extent of Nb and Ta decoupling by fluid or melt metasomatism is as yet unclear. All experimental studies in the literature-to-date suggest that HFSE are not compatible in

aqueous fluids (Brenan *et al.*, 1993; Keppler, 1996) and only moderately compatible in siliceous melts (Pearce and Peate, 1995). However, detailed work on the effects of fluid/melt composition and oxygen fugacity on trace element partitioning under mantle conditions of pressure and temperature has yet to be published. Work by Rudnick *et al.* (1991) showed that Zr/Hf ratios in Tanzanian xenoliths are increased by carbonatitic metasomatism. However, experimental studies by Sweeney *et al.* (1992) show that Nb and Ta are not decoupled between carbonatite melt and major mantle phases. Recent work by Petibon (pers comm, 1998) shows that decoupling of Nb and Ta between silicate and carbonatite melts can occur during liquid immiscibility and that Nb is more compatible in the carbonatite melt, possibly due to a change of valence to the trivalent state. The role of oxygen fugacity on the partitioning of Nb and Ta has not been investigated but may cause decoupling of this element pair due to the greater electronegativity of Nb. This property allows Nb to enter into lower valence states more easily than Ta and so reducing conditions may result in a change in the partitioning behaviour of Nb.

5.2.1 Nb/Ta variation within the samples analysed

The Nb/Ta ratio variation with Nb content for all localities investigated can be seen in Figure 5.1. The chondritic Nb/Ta value is 17.5 ± 2 (Sun and McDonough, 1989), which encompasses the vast majority of determinations given the analytical error of LA-ICP-MS analyses (5%) and that of the ratio of two such analyses (7%). However, there are marked exceptions in the following sample groups:

- Boninites and related groups show sub-chondritic ratios;

- continental crust samples show sub-chondritic ratios; and
- several samples from Tanna volcano (Vanuatu) and Rindjani volcano (Lombok, Indonesia) show super-chondritic ratios.

The sub-chondritic values of boninites and rocks with related petrogenesis, such as sanukitoids and tholeiites, have not been noted in the literature due to the difficulty of measuring the low concentrations of incompatible elements in these rocks ($\text{Nb} = 0.4 - 6.8 \mu\text{g g}^{-1}$). The data suggest that the low Nb/Ta ratios are due to Ta enrichment rather than Nb depletion. It has been noted by Brenan *et al.* (1993) that, when aqueous fluids are in equilibrium with rutile, Ta is more compatible in the fluid than Nb. This has also been observed for paragenetic amphiboles when in equilibrium with alkaline melts at approximately 20Kbars pressure (Adam *et al.*, 1993). It is theoretically possible, therefore, to transport a fluid or melt from a source containing rutile and/or amphibole to the site of boninite genesis causing a relative enrichment in Ta superimposed on a previously depleted source. This would result in the relatively depleted Nb concentrations and enriched Ta concentrations observed. To explain the decoupling of Sm and Zr in boninite petrogenesis, Murton *et al.* (1992) proposed that amphibole was present in the source. This phase may also influence the Nb/Ta ratio of the derivative melts although there are no supporting experimental data.

The Nb/Ta ratios of the samples representing continental crust analysed in this study have sub-chondritic values and relatively depleted Nb concentrations (Table 5.1) consistent with those reported in the literature (Green, 1995; Linnen and Keppler, 1997; Barth *et al.*, 1998; Taylor and McLennan, 1985). Relative enrichment of Ta (rather than

depletion in Nb) causing the low Nb/Ta ratios has also been observed by Taylor and McLennan (1985). The similar relative Nb depletions of continental crust and arc rocks provide strong evidence that the continental crust was formed at subduction zones (Thirlwall *et al.*, 1994). However, two models can be used to explain the relationship between continental crust and island arc magmatism.

The first model proposes that the negative Nb anomalies of the continental crust were produced early in the Earth's history and that this elemental depletion has influenced the trace element systematics of arc magmatism via the subduction of continental derived material. The second model proposes that the Nb and Ta anomalies reflect the composition of the mantle source for arc magmatism before subduction commenced, or that they were produced by subduction related processes, and have imposed their trace element systematics on the continental crust as it formed. The first model seems unlikely as the estimated contribution of subducted sediment to arc magmatism (*i.e.* recycled continental crust) is very small, on the order of 2-3% (Rea and Ruff, 1996; von Huene and Scholl, 1991; Hawkesworth *et al.*, 1991). Insufficient recycling of the continental crust would not allow for the ongoing production of arc magma with a negative HFSE anomaly. There is also inconsistency in the first model, in that island arc magmatism typically has chondritic Nb/Ta ratios and both Nb and Ta depletions (this work). The second model, which calls upon a source effect for the anomalies, has been fairly extensively explored in the literature especially with respect to processes that could cause a depletion of HFSE in subduction related magmatism.

Linnen and Keppler (1997) provide evidence that the solubilities of Nb and Ta are a function of the alkali content of a silicate melt and that the Nb/Ta ratio is systematically decreased with increasing fractionation of peraluminous granites and rhyolites. To balance the low Nb/Ta ratio of the crust, requires a deep-seated reservoir containing a high Nb/Ta ratio component related to the genesis of the continental crust. Although evidence for this reservoir has yet to be found, the proposal of a rutile-bearing refractory eclogitic reservoir deep within the mantle (McDonough, 1991) could provide complimentary, super-chondritic Nb/Ta ratios to the crust.

The analysis of Nb and Ta in island arc volcanics has been inhibited by the analytical uncertainty resulting from their low concentrations in these rocks. In an assessment of the significance of Nb/Ta as an indicator of geochemical processes, Green (1995) chose literature values where Nb was $>5 \mu\text{g g}^{-1}$ and Ta was $> 0.1 \mu\text{g g}^{-1}$ in order to minimise the effects of analytical uncertainty. Nevertheless, it has been shown that there is consistent, relative depletion of HFSE (particularly Nb and Ta) and a variation of island arc volcanic Nb/Ta ratios that extends outside of the chondritic error and analytical error (Green, 1995; Stolz *et al.*, 1994; Eggins *et al.*, 1997; Münker, 1998), consistent with findings in this study.

Much speculation on the behaviour of HFSE in subduction zone settings hinges on elemental partition coefficient data derived from experimental results and from mass balance calculations from phenocryst-matrix pair concentrations in rock assemblages. It has been shown that the HFSE are highly incompatible in most upper mantle phases (Green and Pearson, 1987, Green *et al.*, 1989, Sweeney *et al.*, 1992, Hart and Dunn, 1993,

Adam *et al.*, 1993), which suggests that the HFSE depletion in arc rocks is an inherent characteristic of the source region. This theory is supported by the fact that many intra-oceanic arc rocks seem to be depleted in HFSE with respect to MORB, which have a depleted mantle source (Pearce and Peate, 1995). Further complexity is added by the fact that incompatible elements other than the HFSE are not depleted in arc related magmas, namely large ion lithophile elements (LILE) which are enriched relative to HFSE. Kelemen *et al.* (1990) observed that the HFSE are more compatible in harzburgitic residue than La and K, and interaction between percolating melt and this residue could result in significant HFSE anomalies. However, there would have to be depleted harzburgite above lherzolite in every mantle wedge and every melt package would have to interact with a large proportion of this harzburgite to achieve the LILE/HFSE characteristics (Ionov and Hofmann, 1995). These prerequisites are theoretically possible, but not thought probable based on the available data.

The most frequently cited models in the literature, that attempt to explain the apparent HFSE anomalies, involve processes related to melt production and transport and often state the need for a phase in the mantle which could preferentially retain the HFSE (*e.g.* rutile). It is often assumed that the factor controlling the level of Nb and Ta depletion is similar to that controlling the level of Zr and Hf depletion. However, this study shows that HFSE depletions in different arc settings do not necessarily correlate with one another and that not only does Zr fractionate from Nb and Ta but that it also fractionates from Hf. This is also true for Nb and Ta although they fractionate from each other to a lesser extent compared to Zr and Hf.

In this study, the majority of Nb/Ta ratios from arc environments are within chondritic error but some also show sub-chondritic and super-chondritic outliers (Figure 5.1). The island of Tanna (Vanuatu) is an example of a volcano that shows a range of Nb/Ta ratios over a very limited geographical area and concentration range (6 of the 7 samples have MgO > 6 wt%). This suggests either a variable source composition or processes affected the melt as it migrated from the melt region to the surface. Stolz *et al.* (1996) found that low K-tholeiites from the Sunda arc had essentially chondritic Nb/Ta ratios and that more potassic rocks from this arc had substantially higher Nb/Ta ratios (up to 33). The high Nb/Ta values are thought to be due to hybridisation of the source region of the potassic volcanics by silicic melts derived from the subducting slab. However, it is not made clear what process led to the high Nb/Ta ratios of the hybridising silicic melt. It is possible that a phase such as rutile or amphibole preferentially held onto Ta, allowing for an increase in Nb/Ta in the segregating silicic melt, although experimental studies between amphibole and silicic melt do not support this theory (Adam *et al.*, 1993). However, a study by Ionov and Hofmann (1995) brought to light unusually enriched samples of amphiboles and micas separated from mantle xenoliths in alkali basalts from southern Siberia and Mongolia. These vein amphiboles and micas showed a 50-200-fold enrichment in Nb and Ta, highly variable Nb/Ta ratios and very high Nb-Ta partition coefficients between amphibole and clinopyroxene. The samples are thought to have a subduction-related metasomatic origin where fluids generated in the subducted slab ascend through the mantle wedge and precipitate amphiboles enriched in Nb and Ta. As the now-depleted fluid continues, it may either induce partial melting in a sufficiently hot

part of the mantle wedge, or precipitate non-enriched amphiboles (Ionov and Hofmann, 1995). A study by Eggins *et al.* (1998) on the composition of peridotites also suggested that Nb and Ta partition strongly into amphibole at upper-mantle conditions. No “exotic” accessory phases hosted these elements and the mass balance was achieved only by including data from precursor amphibole, which had broken down into glassy pockets containing olivine, pyroxene and spinel. The apparent inconsistency between experimental data (Adam *et al.*, 1993) and these enriched samples may be explained by unusual fluid and/or amphibole compositions effecting the partitioning behaviour of HFSE between the two phases in the mantle.

In a study of HFSE behaviour, Eggins *et al.* (1997) measured a number of samples from subduction zone environments. It was observed that Nb-poor samples tended to have sub-chondritic values whereas Nb-rich samples tended to have super-chondritic values. This observation was also made by Münker (1998) when analysing Cambrian arc and back arc samples. Münker concluded that rutile/fluid interaction was the cause of sub-chondritic Nb/Ta ratios and that interaction between rutile and siliceous melt, produced by low degrees of melting of the slab, resulted in high Nb/Ta ratios. This model is supported by experimental data (Green and Pearson, 1987; Brenan *et al.*, 1993) although the presence of rutile in the mantle is questionable. Rutile has a low solubility in basic melt compositions (Green and Pearson, 1986), however, Foley and Wheller (1990) and Ayres and Watson (1993) emphasise that it can be stabilised in a subduction zone under certain unusual conditions of high pressure, low temperature and oxygen fugacity (fO_2). According to Foley and Wheller (1990) the role of pressure and fO_2 on the stability

of rutile has been understated. Small volume, siliceous, hydrous melts are thought to segregate in the hybridised zone above a subducting slab at about 1000°C (Pearce and Peate, 1995). In this zone, rutile is thought to be able to precipitate due to its low solubility in more felsic melts. With rutile stabilised, Nb and Ta will be preferentially withdrawn from the melt (Ta more than Nb), which can then migrate upwards through “cross-fed” mantle to the base of the melting column. The experiments of Green and Ringwood (1967) showed that rutile and olivine are not stable in the same assemblage but react to form ilmenite. However, subsequent work (Taylor and Green, 1988, Wallace and Green, 1988) showed that certain conditions of oxygen fugacity and volatile content will allow ilmenite, rutile and olivine to co-exist in peridotite at subsolidus temperatures. Collinear Zr/Nb and Sm/Nb versus Nb, and TiO₂/Zr versus Zr plots for island arc basalts and mid-ocean ridge basalts provide evidence that rutile did not control the HFSE depletion in these rocks (McCulloch and Gamble, 1991). It has also been seen that rutile fractionates Nb from Ta ($D_{\text{Nb}} = 26.5$, $D_{\text{Ta}} = 44.0$, Green and Pearson, 1987) and that approximately 1wt% rutile in the residue of a melt would cause an increase in the Nb/Ta ratio of 25% (Sen and Dunn, 1994). From this present study alone it can be seen that an increase in the Nb/Ta ratio of island arc basalts is not necessarily coincident with depletion in HFSE concentrations. This would argue against the control of rutile in depleting HFSE.

The data derived from island arc volcanics in this study do not support the evidence that Nb/Ta ratios are a function of Nb concentration. Instead, a scatter of Nb/Ta values can be seen over limited Nb concentrations. Explanations of the data are hindered by the

lack of partition coefficient data for HFSE between mantle phases and fluids, especially under varying conditions of fluid concentration and oxygen fugacity. It is possible that the only factor significantly affecting Nb-Ta fractionation is a low oxygen fugacity, which may force Nb into a lower valence state than Ta. The redox conditions of the mantle are poorly constrained but thought to be at the quartz-magnetite-fayalite buffer at temperatures of approximately 1300°C. Lower in the mantle the conditions may be more reducing, allowing for deep seated metasomatic melts to infiltrate the more oxidised upper mantle.

5.2.2 Zr/Hf variation within the samples analysed

There is a more broad-ranging spread of Zr/Hf ratios compared to Nb/Ta ratios for the samples analysed in this study. It is apparent that Zr and Hf fractionate more easily than Nb/Ta and that Zr is more compatible in many phases (compared to Hf) resulting in a tendency for sub-chondritic ratios in derivative melts. No correlation between Nb/Ta and Zr/Hf ratios in volcanic arc magmas is apparent from the data derived in this study, as was suggested by Eggins *et al.* (1997). However, there is a correlation between the ratios for samples representing the continental crust where in both cases the ratios increase with increasing Nb and Zr concentrations.

5.2 Conclusion

It can be seen from the whole rock LA-ICP-MS results that there is little variation in Nb/Ta ratios outside of analytical error over a broad spectrum of tectonic environments. However, the variation that occurs is significant and probably reflects unusual processes that, if better understood, may shed light on the petrogenesis of the

rock types involved *e.g.* boninites, continental crust, and island arc volcanics. There seems to be a far greater variation of Zr/Hf ratios compared to Nb/Ta ratios with no apparent correlation between the two.

Table 5.1: A review of the samples analysed by whole rock LA-ICP-MS; number of samples analysed, tectonic setting and geographical location, and HFSE ratio characteristics.

Tectonic setting	# samples	Location	Nb/Ta average \pm standard deviation	Nb/Ta range	Zr/Hf average \pm standard deviation	Zr/Hf range
Chondrite		Sun and McDonough, 1989	17.5 ± 2		36.3 ± 4	
MORB	12	Macquarie Island	17 ± 2	11.0 - 19.2	34 ± 5	22.4 - 41.8
	8	Leg 82	16 ± 1	14.7 - 16.7	30 ± 2	26.6 - 31.2
	5	Eclogites	16 ± 1	15.1 - 17.0	33 ± 2	30.5 - 35.7
OIB	6	Gran Canaria	18 ± 1	15.9 - 19.1	40 ± 5	31.9 - 45.3
IAB	7	Sunda arc	16 ± 5	15.0 - 24.0	34 ± 4	29.7 - 40.2
	9	Vanuatu	18 ± 5	11.3 - 26.0	29 ± 3	22.7 - 32.4
	2	Tonga	16 ± 3	13.9 - 18.7	25.9 ± 0.1	25.8 - 26.0
BAB	28	Lau Basin	14 ± 3	6.2 - 18.2	30 ± 4	20.7 - 38.3
Boninites and related rocks	2	Bonin Island boninites	11 ± 2	9.1 - 12.4	31 ± 5	27.3 - 34.4
	4	Dabi tholeiites	6 ± 5	2.2 - 13.3	30 ± 7	27.1 - 31.9
	6	Pacquet Harbour Group boninites	1.5 ± 0.5	1.0 - 2.2	35 ± 1	28.5 - 39.5
	1	Japanese sanukitoid	6.9	-	29.3	-
Island arc xenoliths	2	Sangeang Api, Indonesia	8 ± 4	4.8 - 11.0	19 ± 1	19.1 - 20.1
	2	Cyprus Ophiolite	19 ± 5	15.7 - 22.1	26 ± 1	25.6 - 26.8
Continental Crust	7	Labrador sediments	7 ± 2	4.1 - 9.4	30 ± 2	27.9 - 32.5

Figure 5.1: Nb/Ta vs Nb for all island arc related samples

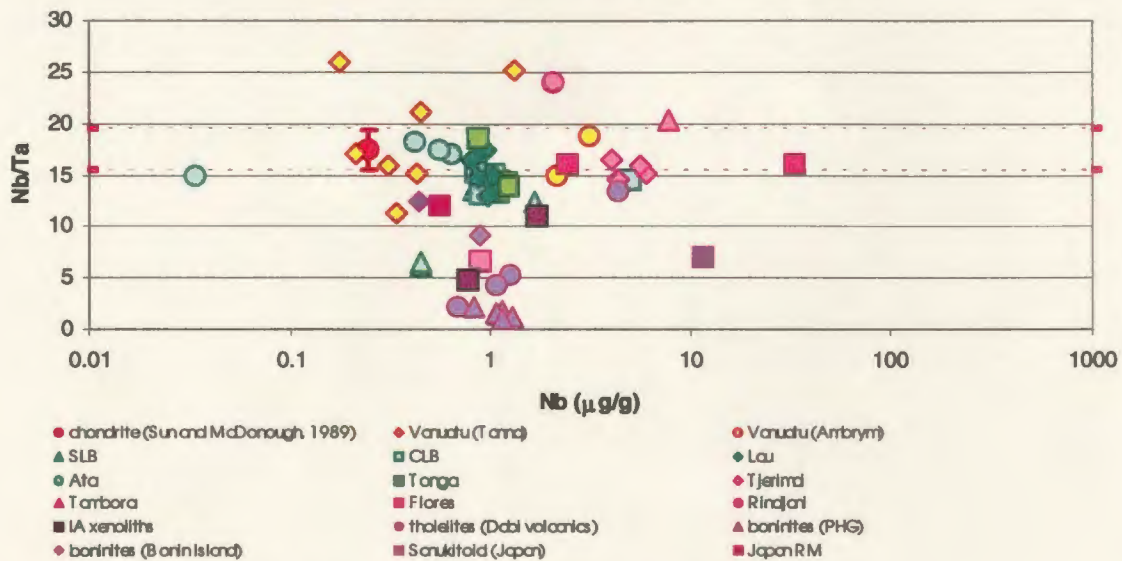


Figure 5.1: Nb/Ta vs Nb for non-arc related samples

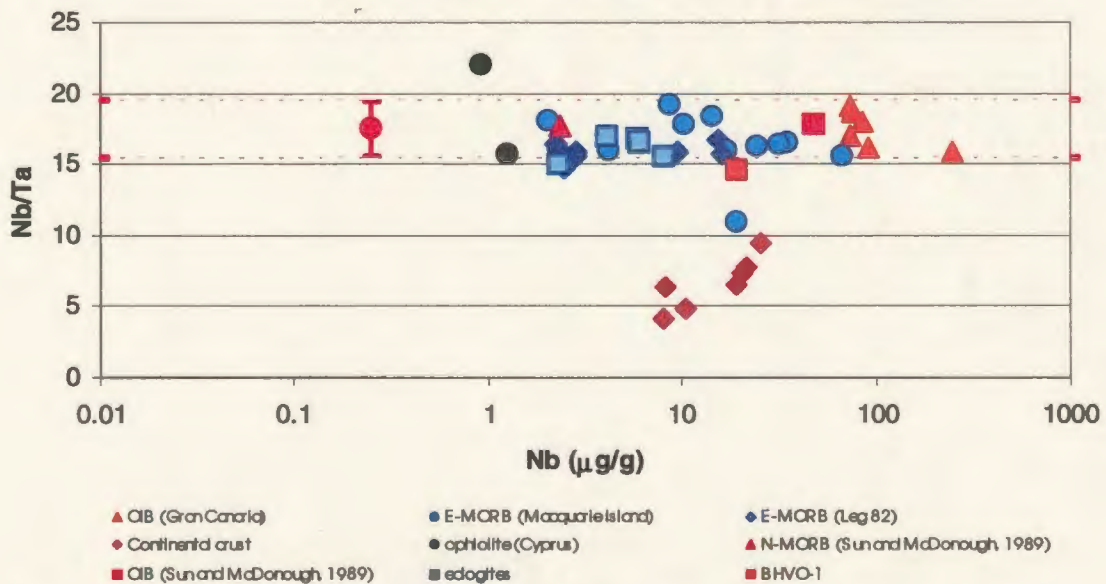


Figure 5.1: The variation of Nb/Ta with Nb for arc-related rock suites and non-arc related rock suites. Explanation of key: SLB (south Lau Basin) and CLB (central Lau Basin) are natural glasses; Lau are synthetic Lau Basin glasses; Ata is derived from Ata Island; Japan RM refers to Japanese geostandards Jb-1, Jb-2 and Jb-3; Bonin refers to Bonin Island boninites and PHG refers to Pacquet Harbour Group boninites; BHVO-1 is a geostandard from Hawaii; Leg 82 refers to E-MORB samples derived from the Azores Triple Junction; Chondrite, N-MORB and OIB references are the values given for each by Sun and McDonough (1989).

Figure 5.2: Zr/Hf vs Zr for island arc related samples

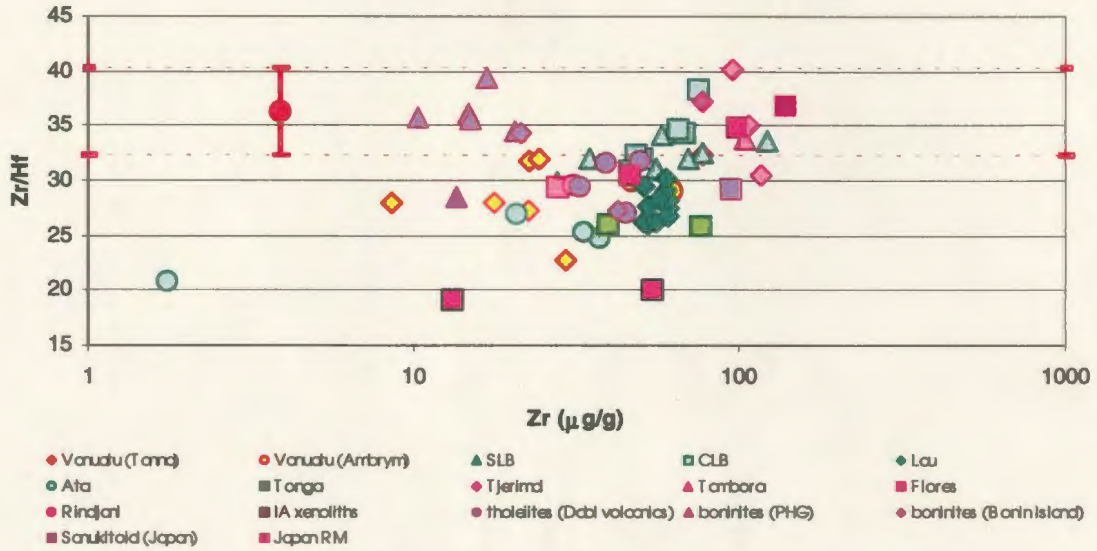


Figure 5.2: Zr/Hf vs Zr for non-arc related samples

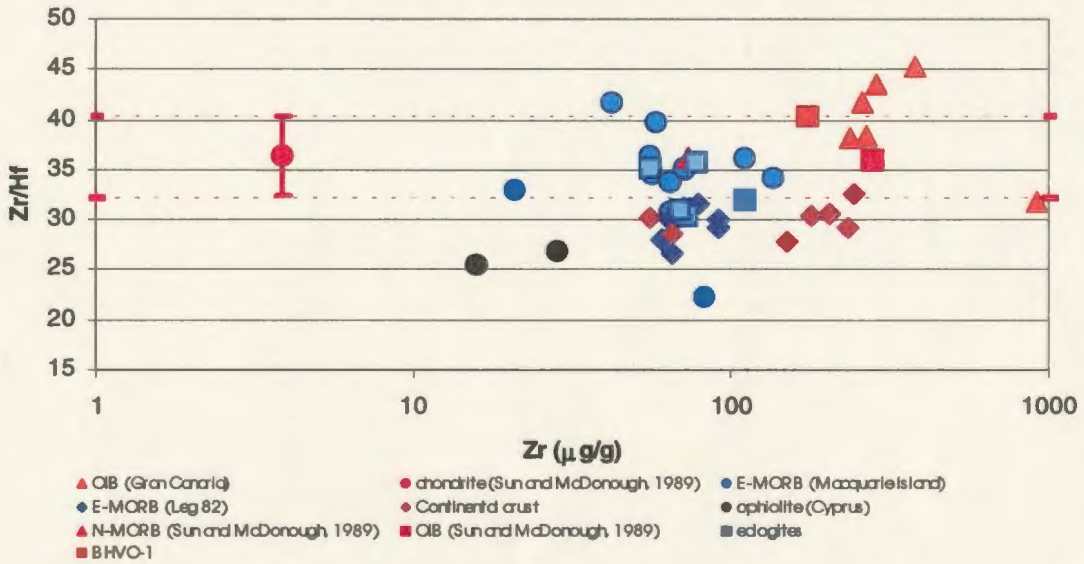


Figure 5.2: The variation of Zr/Hf with Zr for arc-related rock suites and non-arc related rock suites. Explanation of key: see Figure 5.1.

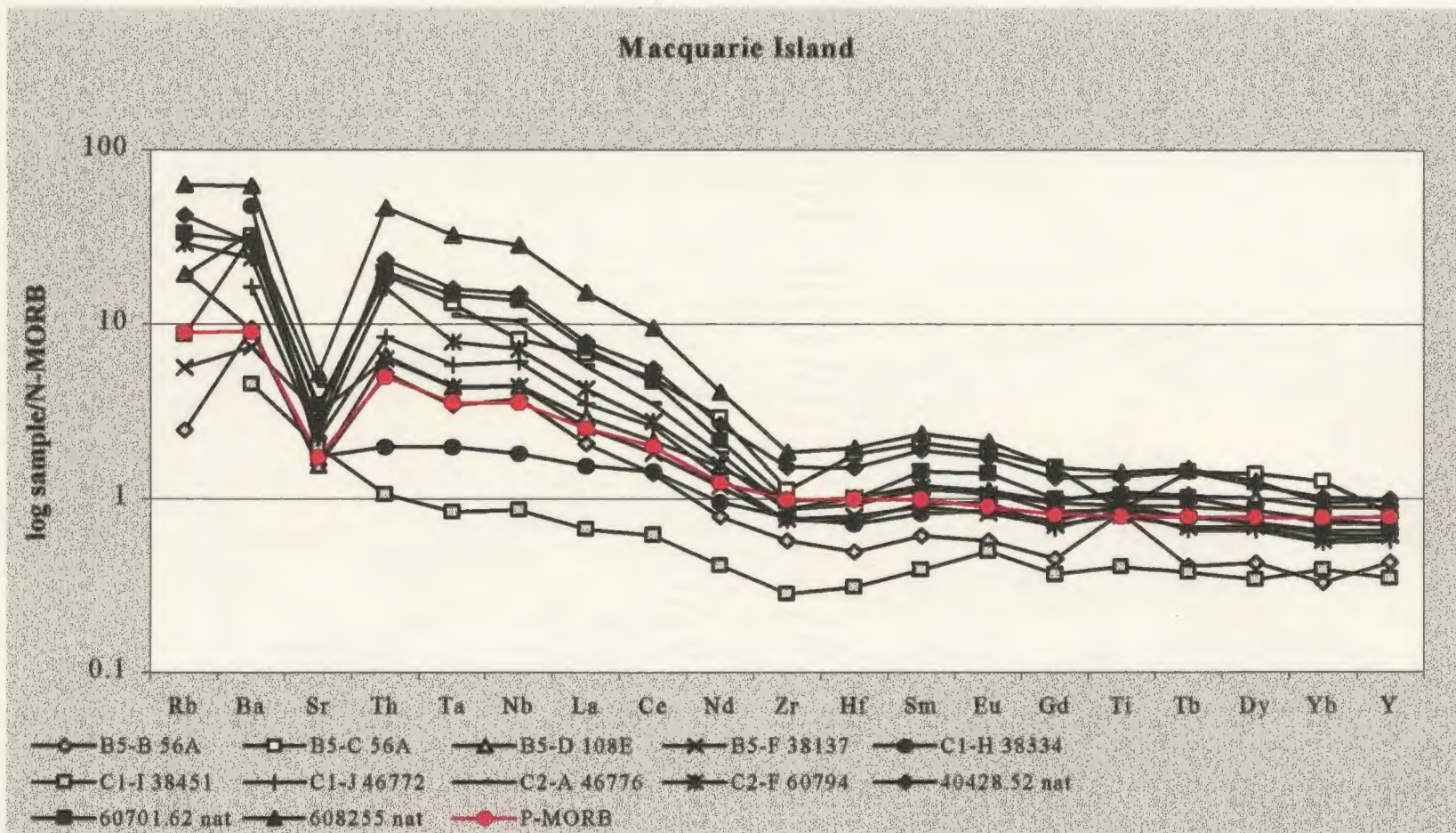


Figure 5.3: N-MORB normalised extended plot for E-MORB samples from Macquarie Island. The E-MORB values given by Sun and McDonough (1989) are given in red for comparison. The sample names followed by "nat" refer to natural glasses.

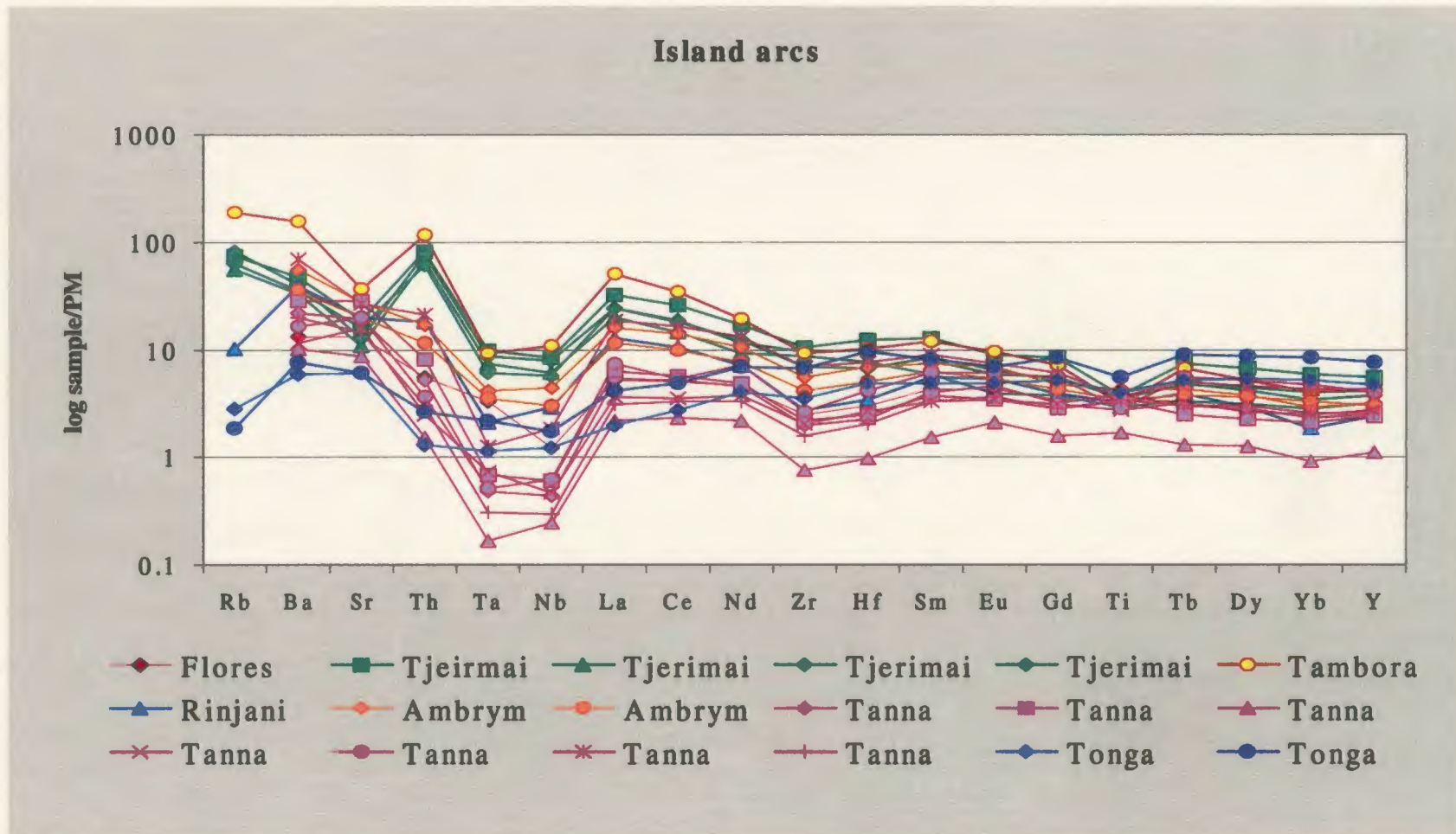


Figure 5.4: Primitive mantle normalised extended plot for all island arc samples. Ambrym and Tanna are IAB from Vanuatu, Tjerimai, Rinjani, Tambora and Flores are Indonesian samples from the Sunda arc.

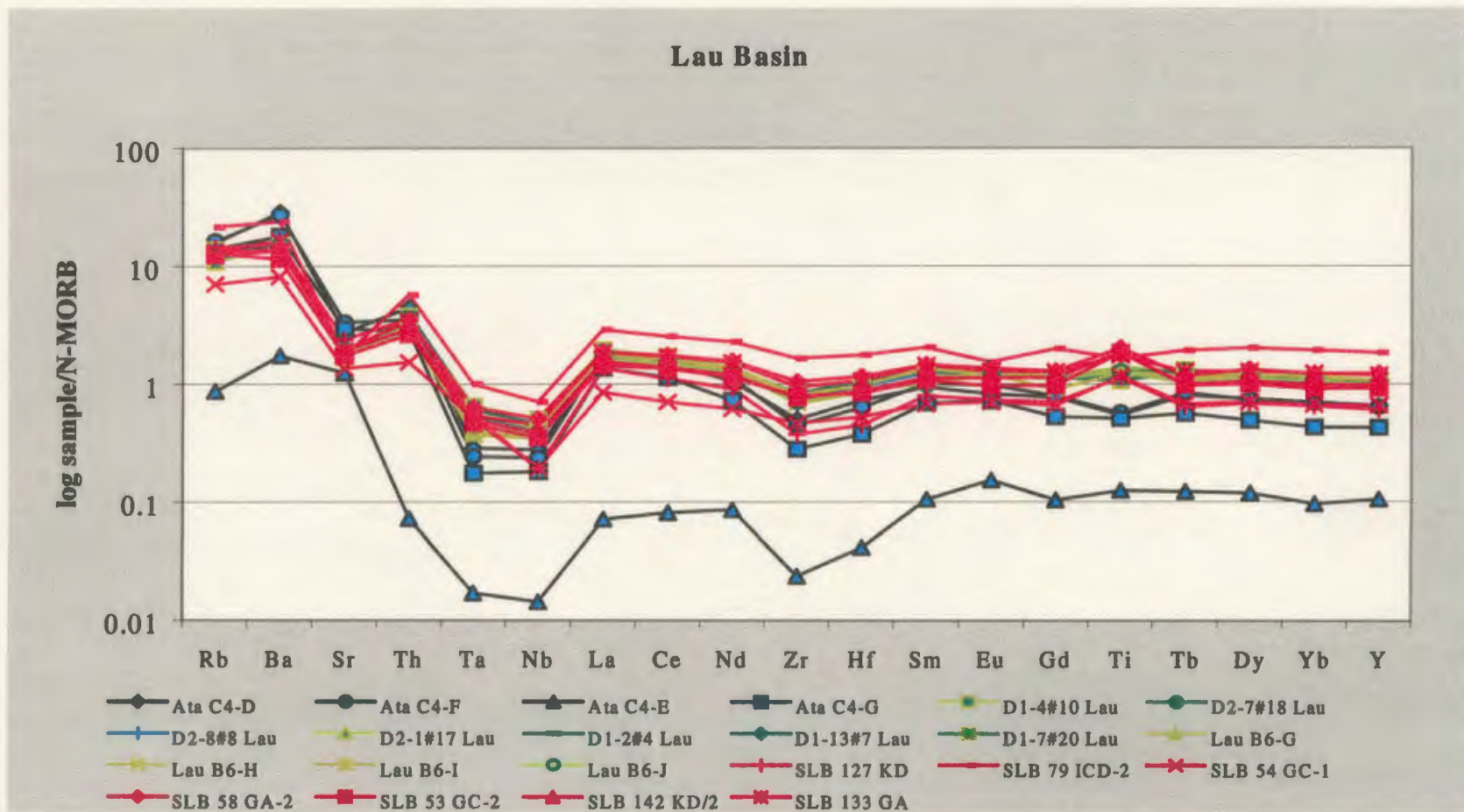


Figure 5.5: Extended N-MORB normalised plot for synthetic and natural glasses from southern Lau Basin. SLB refers to natural glass samples. Ata refers to Ata Island. Lau and D* samples are synthetic glasses from Valu Fa.

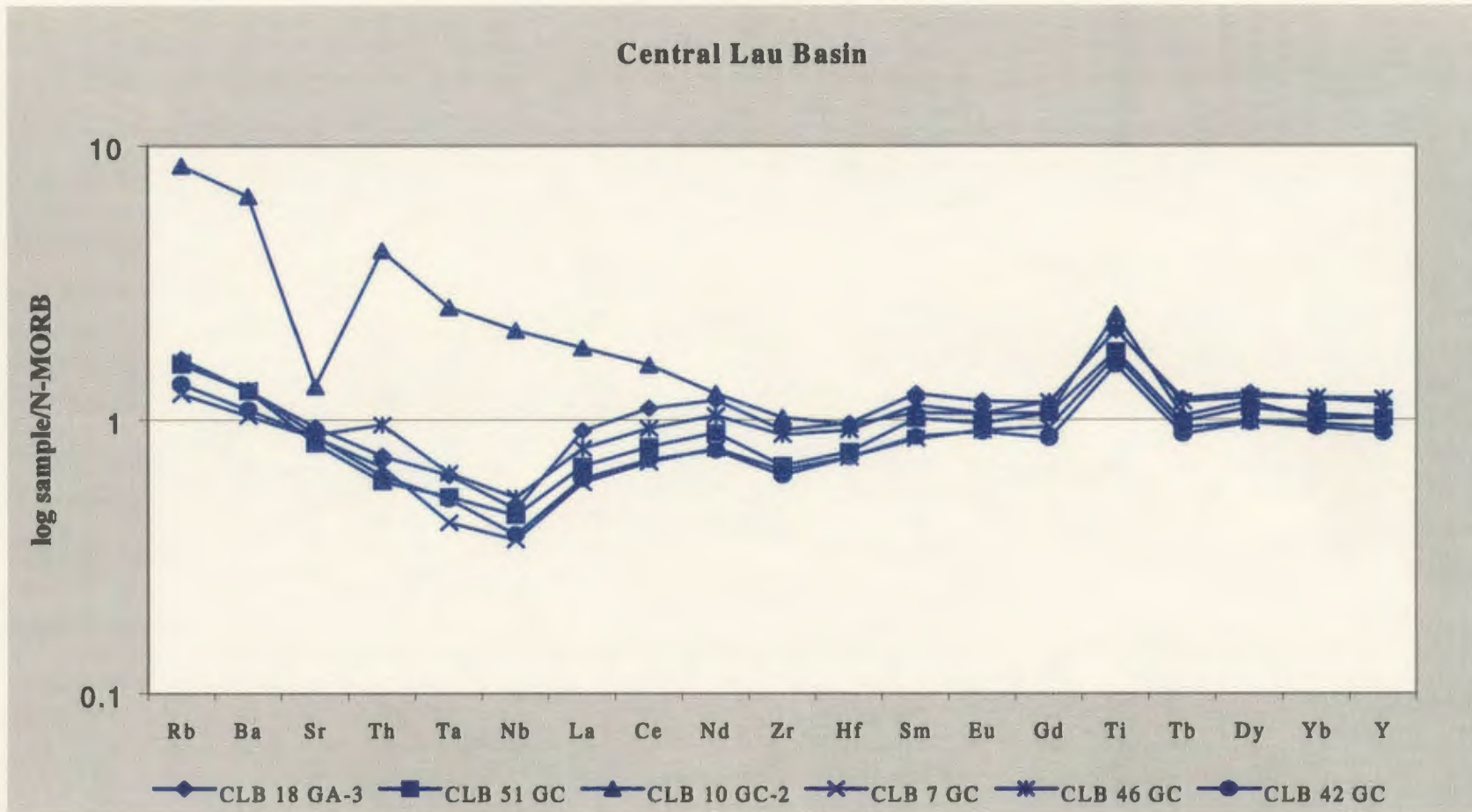


Figure 5.6: Extended N-MORB normalised plot for natural glasses from Central Lau Basin.

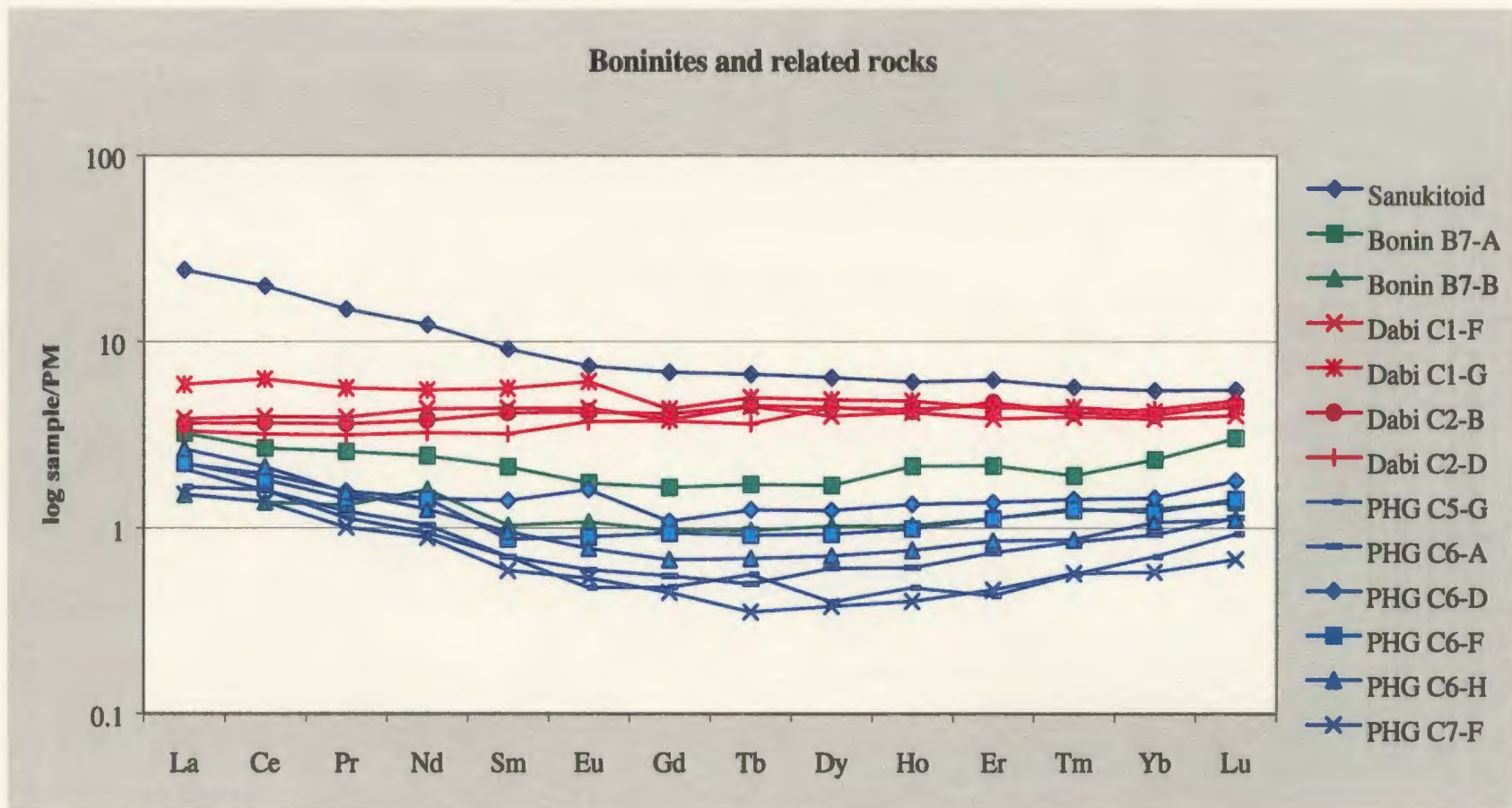


Figure 5.7: Primitive-mantle normalised REE plot for all boninites and related rocks from Bonin Island (Bonin), Japan (sanukitoid), Dabi Volcanics (Dabi) and the Pacquet Harbour Group, Newfoundland (PHG).

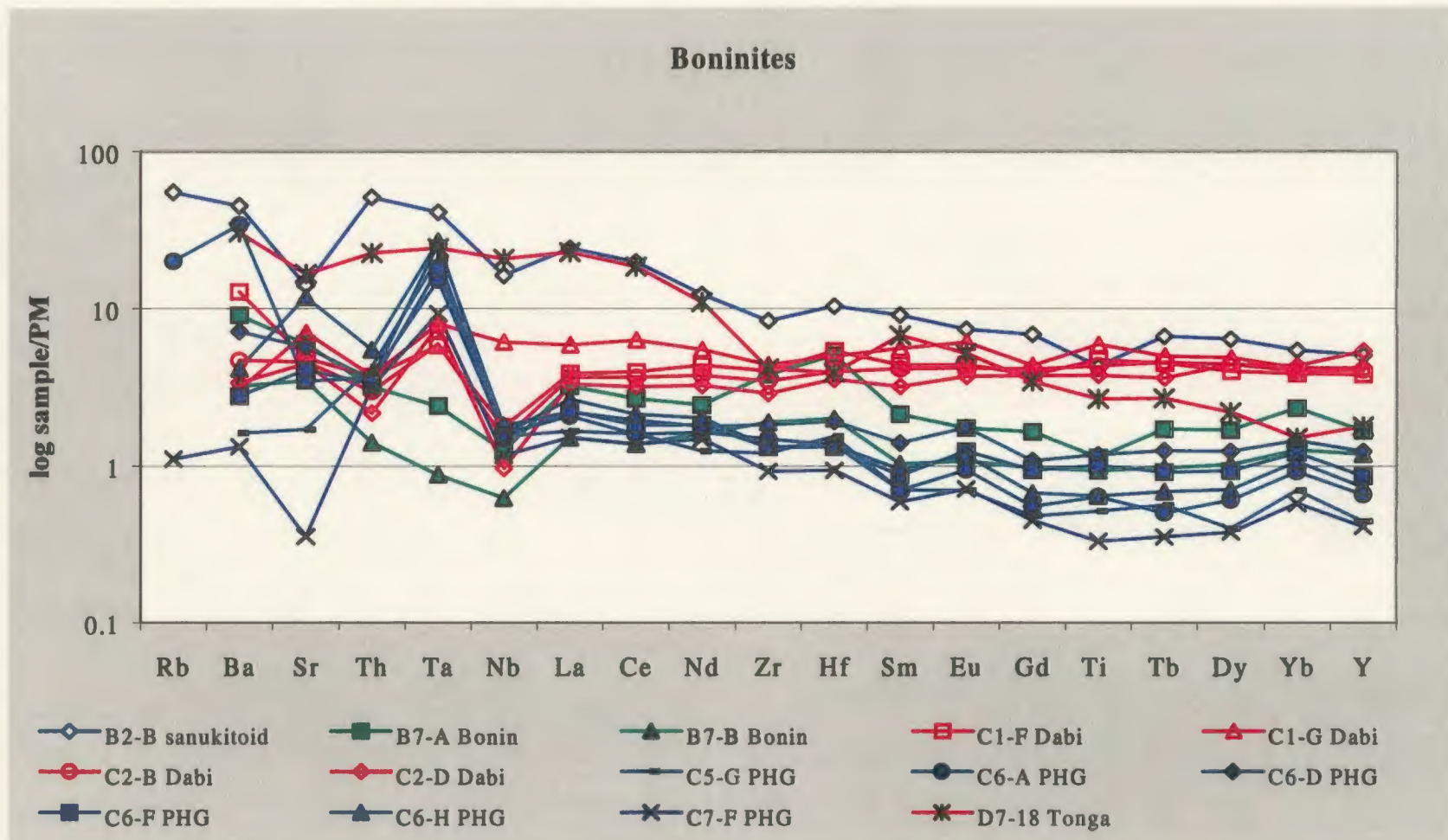


Figure 5.8: Primitive-mantle normalised extended plot for all boninites and related rocks from Bonin Island (Bonin), Japan (sanukitoid), Dabi Volcanics (Dabi) and the Pacquet Harbour Group, Newfoundland (PHG).

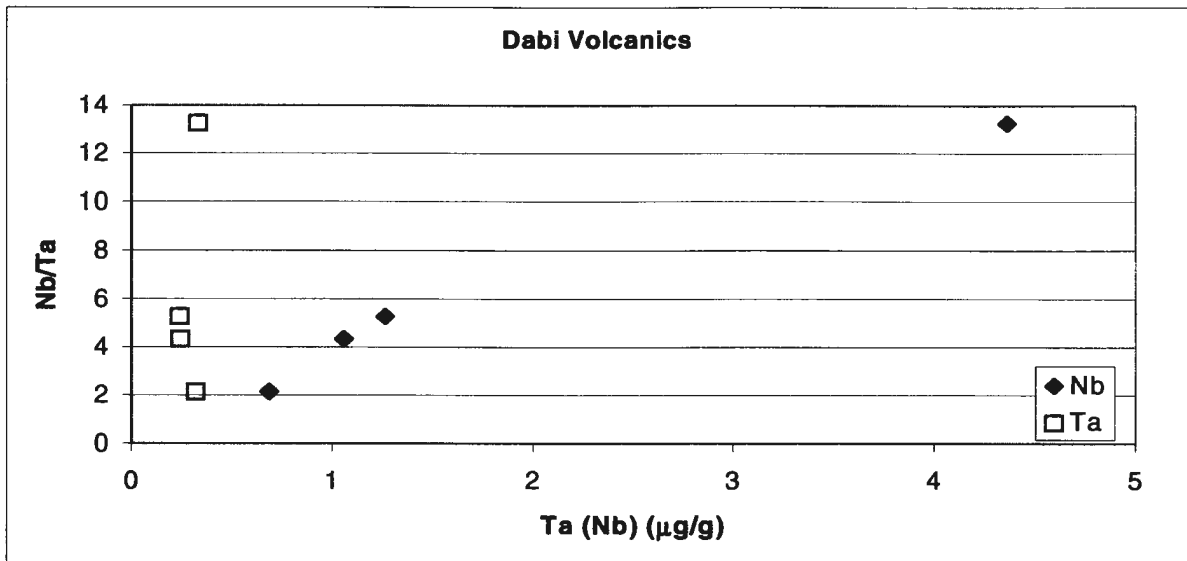


Figure 5.9: Nb/Ta variation with Nb and Ta for the Dabi tholeiites, Cape Vogel. It can be seen that the increase Nb/Ta is due to increase in Nb with a relatively constant Ta concentration.

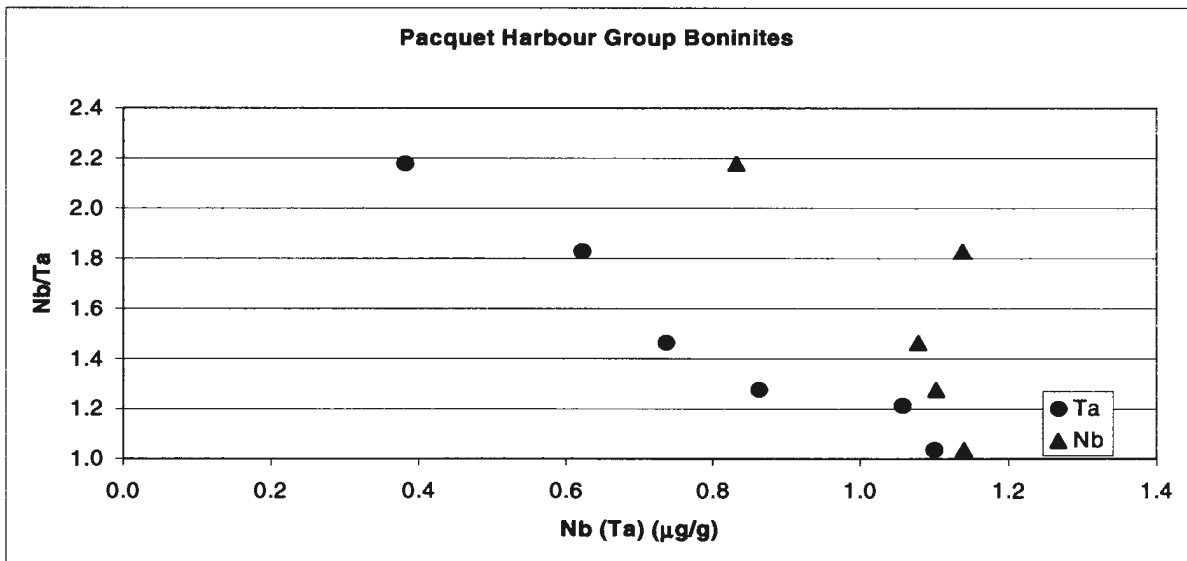


Figure 5.10: Nb/Ta variation with Nb and Ta for the Pacquet Harbour Group boninites. It can be seen that the increase Nb/Ta is due to decrease in Ta with a relatively constant Nb concentration.

APPENDIX I. TECTONIC SETTINGS AND GEOGRAPHICAL LOCATIONS

A.1 MORB

A.1.1 Macquarie Island

Macquarie Island consists of a cross section of the oceanic crust located approximately 1100 km SSW of the southern tip of New Zealand, which is the nearest continental landmass crust (Griffin and Varne, 1980, Duncan and Varne, 1988). It is a narrow ridge running south from New Zealand to join the Indian-Pacific ridge system and is thought to be the boundary that separates the Indo-Australian plate from the Pacific plate (Griffin and Varne, 1980). The island consists of a series of tilted blocks exposing mafic, coarse-grained intrusives to the north and volcanics with related sea floor sediments to the south (Figure A.1). Doleritic dyke swarms are also prevalent.

According to a study carried out by Griffin and Varne (1980) the Macquarie Island rocks that plot within the ocean-floor basalt (OFB) field typically have relatively high Ti/Zr ratios, $Na/(Na+K) > 0.9$, low K contents, $K/Rb > 360$ and relatively low Nb values. The rocks that are not characteristic of ocean floor basalts tend to be relatively enriched in Nb ($20-60 \mu\text{g g}^{-1}$), K and Sr, to have low Zr/Nb, Y/Nb, Ti/Zr and K/Rb ratios, and to be nepheline normative. These properties are similar to those of other so-called “anomalous” ridge segments. Fractional crystallisation is thought to be the cause of the major element variation on Macquarie Island (Griffin and Varne, 1980).

In this study nine samples were analysed from Macquarie Island, three of which are natural glasses (40428, 60701, 608255). All samples with the exception of 38451 and 38334 show LREE and LILE enrichments with strong negative Sr anomalies relative to

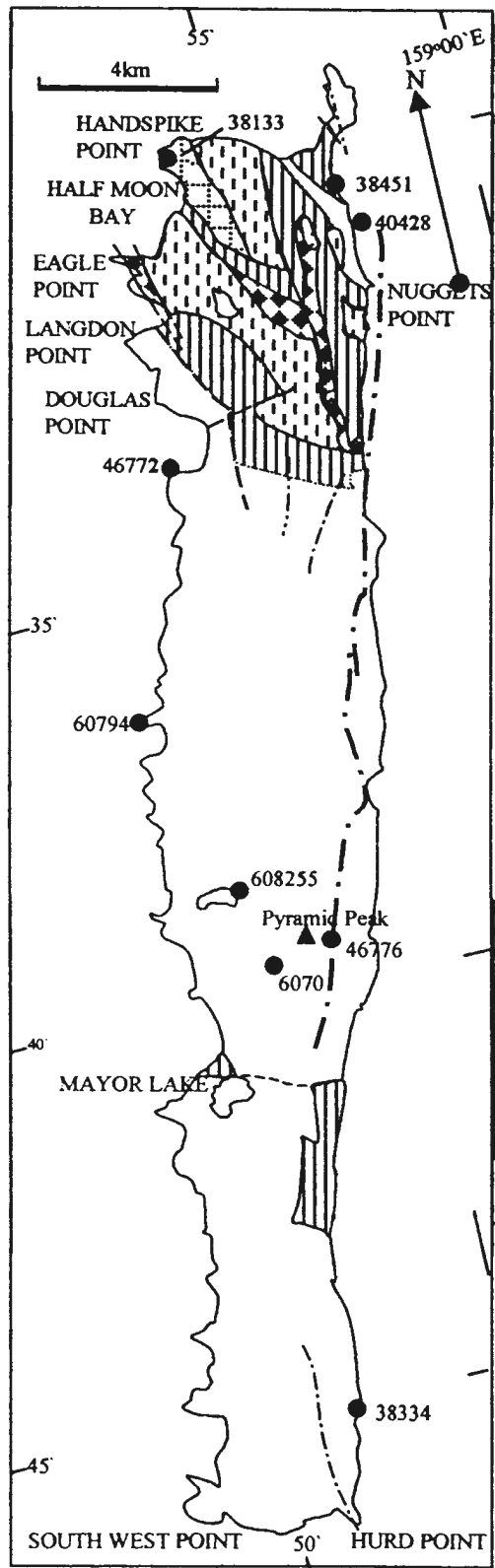


Figure A1 Macquarie Island modified from Duncan and Varne (1988)

The location of all samples analyzed from this area are shown as filled circles with reference numbers.

-  serpentinitised peridotite
-  layered gabbro
-  dolerite dyke swarms
-  gabbro
-  extrusive volcanics and associated sedimentary rocks
-  structural lineament
-  fault

N-MORB, which is a pattern typical of enriched (E)-MORB (Sun and McDonough, 1989).

A.1.2 ODP Leg 82 - MORB

These MORB samples were derived from drilling project sites 556-559 and 561-564 of the deep sea drilling project (Hertogen *et al.*, 1985). The *Glomar Challenger* drilled at 9 sites south-west of the Azores during leg 82 in an effort to relate regional variations in basaltic geochemistry to dynamic processes in an anomalous segment of the Mid Atlantic Ridge, the Azores Triple Junction. The recovered basalts span a wide range of age (14-37 Ma) and trace element composition (Hertogen *et al.*, 1985).

In this study eight basaltic natural glasses from Leg 82 have been analysed. All glasses were homogeneous, free of both crystalline and volatile inclusions. The samples exhibit varying degrees of LILE and LREE enrichments relative to N-MORB. Samples 10, 85 and 91 are particularly typical of E-MORB and have marked negative Sr anomalies.

A.2 Destructive Margin Volcanic Rocks

The samples covered in this section are destructive margin volcanics from the Sunda arc (the islands of Java, Lombok, Sumbawa and Flores), Vanuatu (the islands of Tanna and Ambrym), and Tonga. Four calc-alkaline basalts have been analysed from Tjerimai on Java, and only one sample has been analysed from each of the other Sunda islands mentioned above. Six primitive basalts and one andesite from Tanna and two primitive basalts from Ambrym have been analysed. Two tholeiitic basalts have been

analysed from Tonga. All samples exhibit the negative HFSE anomalies characteristic of island arc magmatism (Figure 5.4).

A.2.1 Sunda arc volcanics (Indonesia)

The Sunda arc, Indonesia, extends from the north of Sumatra approximately 4000km to the east of the Banda Islands. There are a variety of tectonic environments represented, from Sumatra (30km thick crust with a shallow Benioff Zone; 200-250km deep) to the Banda Sea (15km thick crust with a near-oceanic velocity structure and a Benioff Zone extending to 500-600km depth).

The samples taken from this volcanic arc were collected from the islands of Java (Tjerimai volcano), Lombok (Rinjani), Sumbawa (Tambora) and Flores (Figure A.2). Samples from Tjerimai are calc-alkaline andesites, the sample from Rinjani volcano is a primitive, tholeiitic basalt, and those from Tambora and Flores are calc-alkaline basalts (Irvine and Baranger, 1971; Pearce and Cann, 1973). It is interesting to note that Tambora is one of the few mafic volcanoes to have produced ignimbrite eruptions (Robin *et al.*, 1994). Petrographic details can be found in Barberi *et al.* (1987) and Whitford (1975).

A.2.2 Vanuatu Island arc (New Hebrides Anglo-French condominium)

Vanuatu forms one sector of a Cretaceous to recent island arc system extending from New Britain through to Solomon Islands to Vanuatu, Fiji, Tonga and the Kermadec Islands (Figure A.3). It is a persistently active arc resulting from the subduction of oceanic lithosphere (the Loyalties Plateau) under an oceanic plate (the Fiji Plateau) (Briqueu *et al.*, 1984). Vanuatu is considered to be a typical intra-oceanic arc,

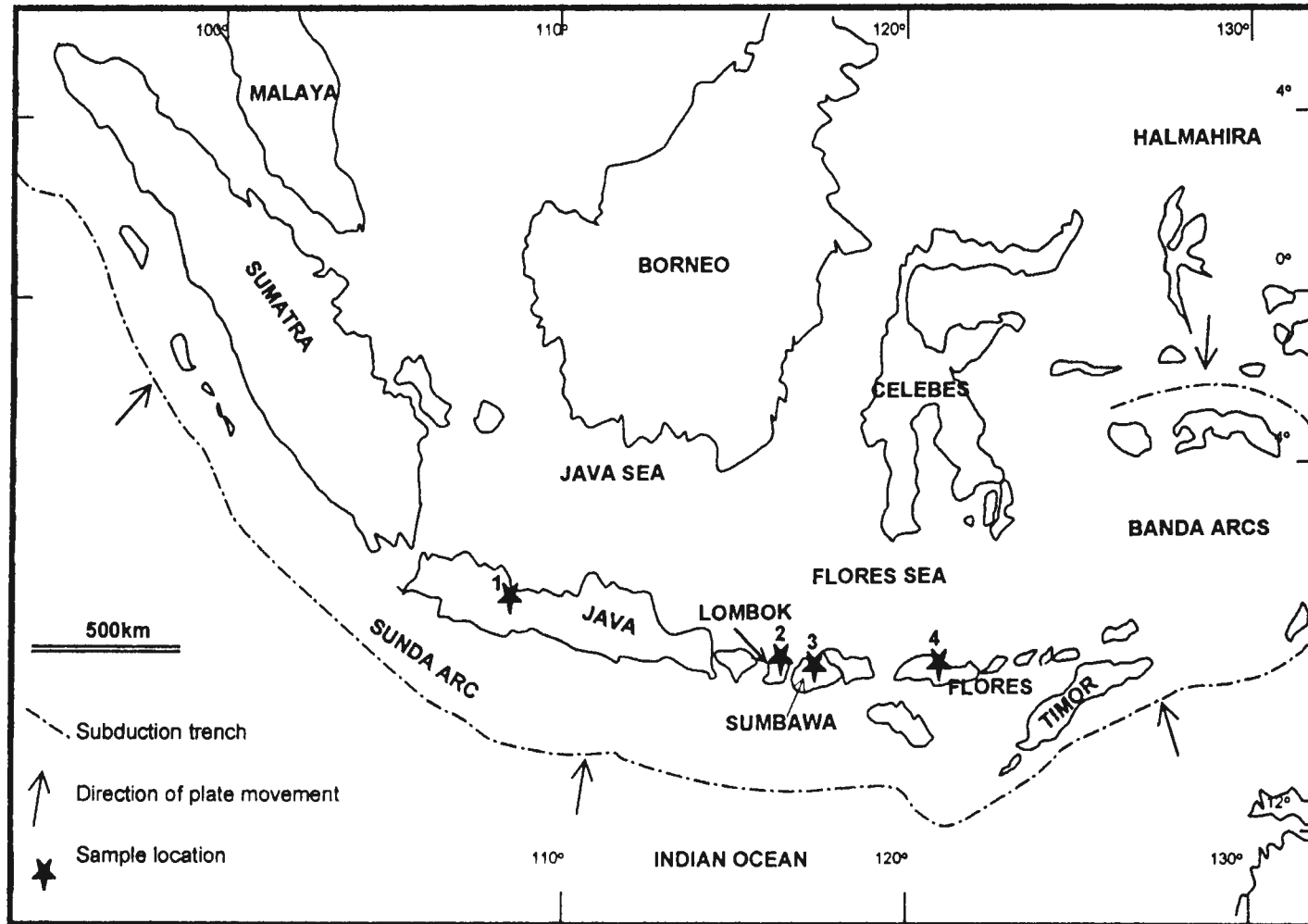


Figure A2: The Sunda and Banda arcs of Indonesia. Sample localities are shown by stars: (1) Tjerimai volcano, Java; (2) Rinjani volcano, Lombok; (3) Tambora volcano, Sumbawa; and (5) Flores.

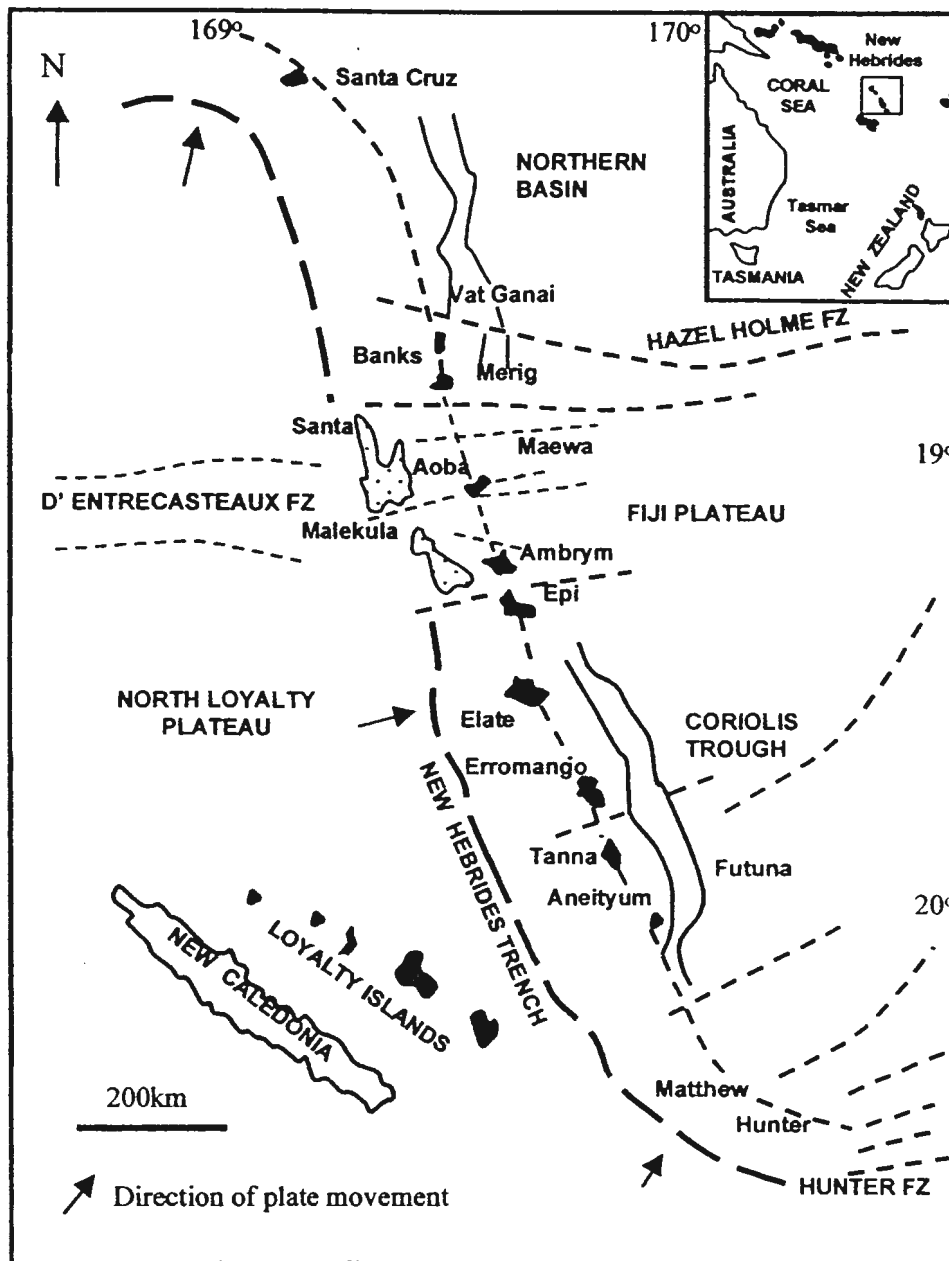


Figure A3: Vanuatu island arc. Modified from Briquet *et al.* (1984)

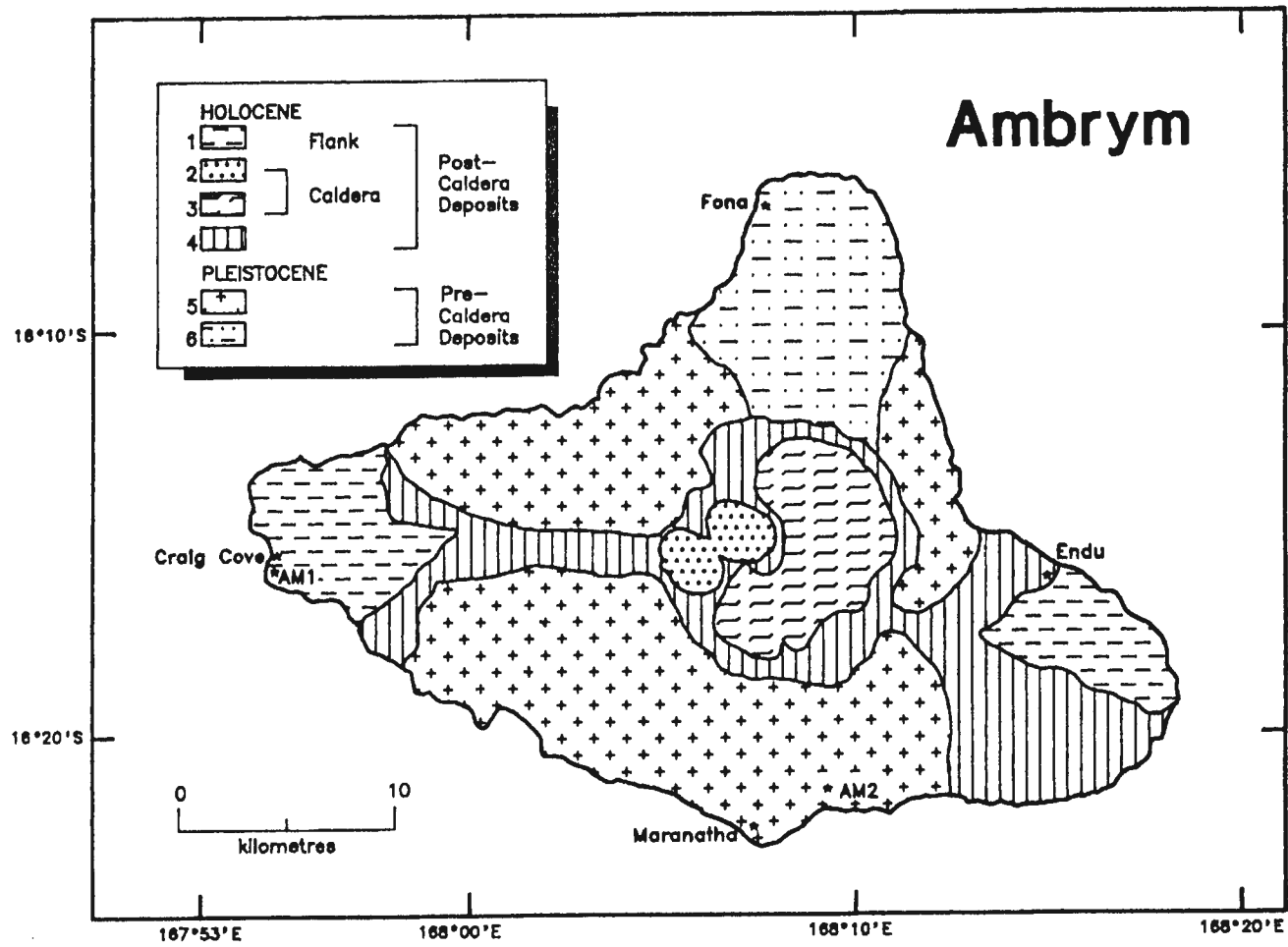
complicated only by a topographic high in front of the arc (D'Entrecasteaux zone), which has an oceanic character and complicates the structure of the arc in its middle portion (Briqueu *et al.*, 1984). The compositional transition observed in this area, is thought to be due to either the collision-subduction in this area or the invasion of DUPAL-type enriched mantle (Monzier *et al.*, 1997).

The samples analysed in this study are from the islands of Ambrym (Figure A.4) and Tanna (Figure A.5). Ambrym is an effusive basaltic volcano located in the area where the D'Entrecasteaux Zone collides with the arc. Tanna volcano is located in the Marginal Provinces unaffected by the D'Entrecasteaux Zone (Robin *et al.*, 1994). Both volcanics represent rare but well known, mafic (basaltic and basaltic andesite) ignimbrite eruption centers (also including Tambora, Indonesia).

All the samples analysed from Tanna volcano have MgO > 6wt% with the exception of V-8 which has a MgO of 2.7wt%. All samples can be considered primitive and are classified as sub-alkaline basalts and andesites (Winchester and Floyd, 1977). The samples from Ambrym volcano show very similar characteristics to those from Tanna, with slightly less negative HFSE anomalies.

A.2.3 Tonga Ridge

The Tonga Ridge is an active island arc volcanic ridge that extends for more than 1100km in the south-west Pacific (Figure A.6). It is made up of two belts of seamounts, shoals, atoll reefs and islands that separate the 2-3km deep Lau Basin from the 10.5km deep Tonga trench (Hawkins Jr, 1995). The predominant lithologies of the arc belong to a tholeiitic series ranging in composition from basalt to low-potassium rhyolite (Bryan *et*



FigureA4: Ambrym Island, Vanuatu. Sample locations are shown as stars.

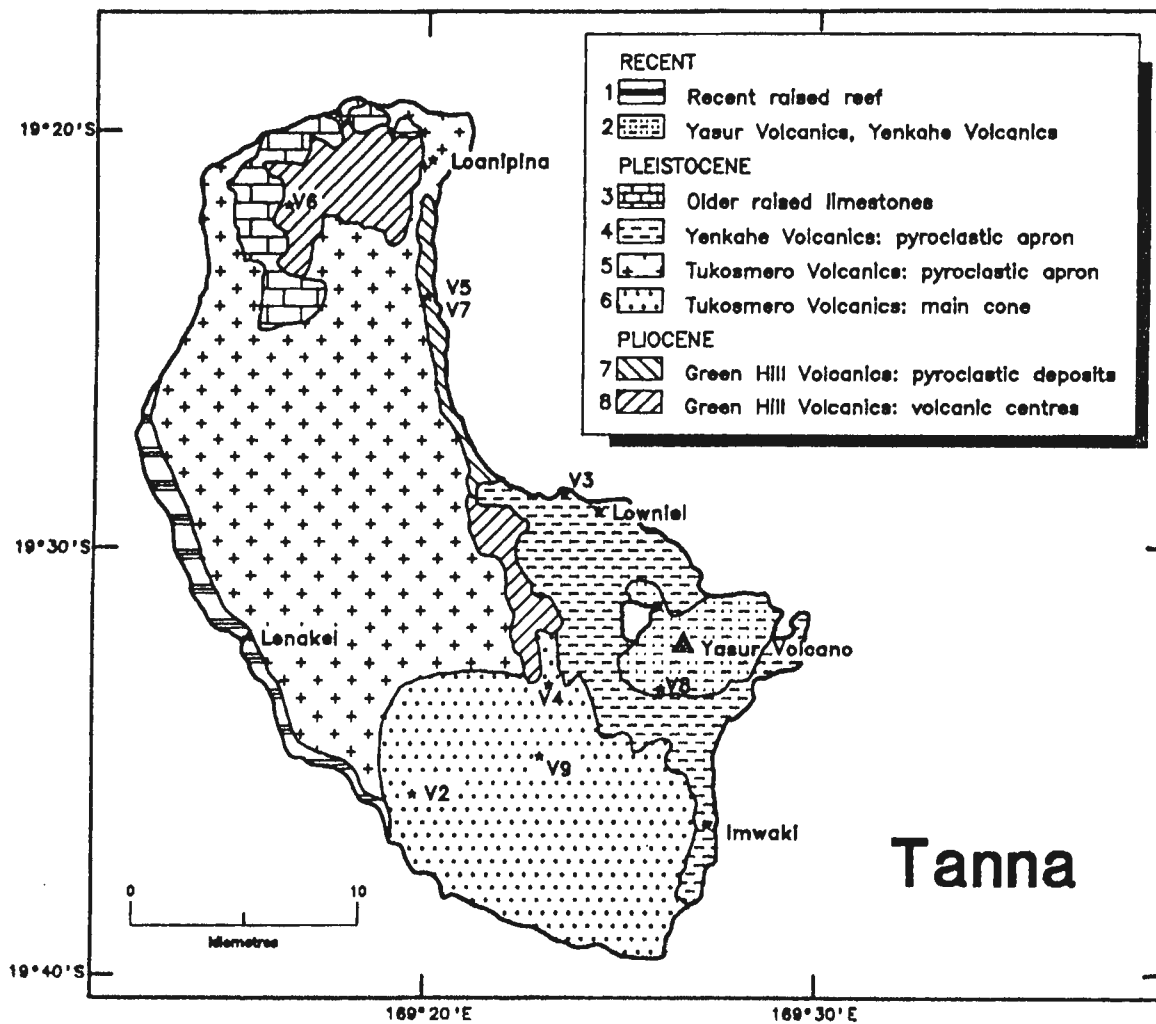


Figure A5: Tanna Island, Vanuatu. Sample locations are shown as stars.

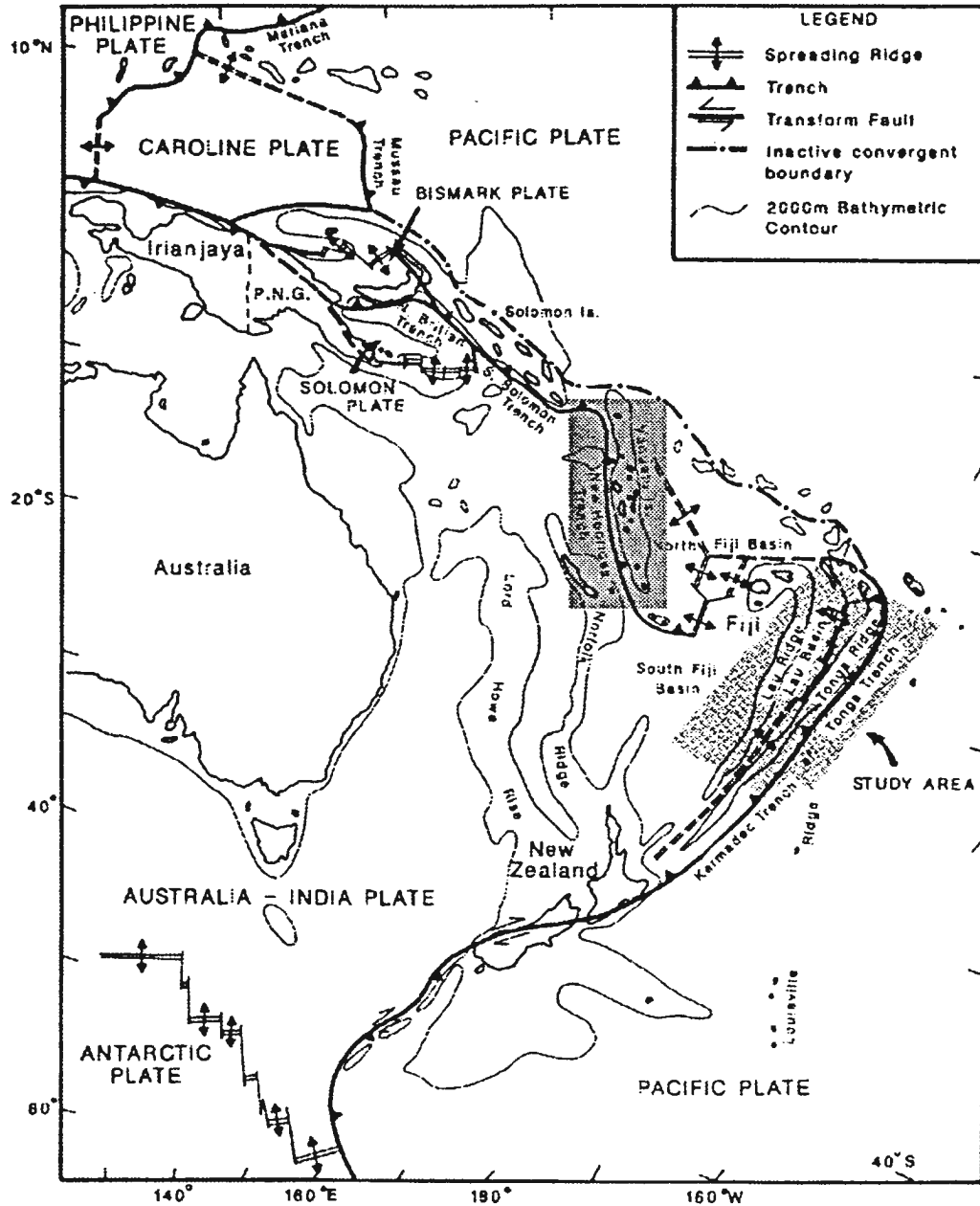


Figure A6: Map showing the location of, and spatial relationship between, Vanuatu, Tonga and Lau Basin (shaded areas). Taken from Jenner *et al.* (1987).

al., 1972). The main magma types are basalts and basaltic andesites (Bryan *et al.*, 1972), which are similar in composition to those found in the Lau Basin (section 6.3.1) (Ewart and Hawkesworth, 1987).

A.3 Back-Arc Basin Volcanic Rocks

A.3.1 Lau Basin, SW Pacific

A back-arc basin is a relatively shallow (<3km deep) region of the oceanic crust that is situated in between inactive, remnant volcanic arcs and the active volcanic arcs that result from the subduction of oceanic lithosphere (Hawkins Jr, 1995). The Lau Basin is a well-studied classic example of a back-arc basin, which separates the remnant Lau Ridge volcanic arc from the active Tonga arc (Figure A.7 (a)). It overlies the west dipping seismic zone of the Tonga Trench subduction complex but has a predominantly MORB-like composition despite its close proximity to a subduction zone. However, there are older parts of the basin with a more transitional composition between that typical of MORB and that typical of island arc volcanics (Hawkins Jr., 1995).

The samples analysed from this area are mainly from southern Lau Basin (Valu Fa Ridge and Ata Island) and comprise both natural glasses and synthetic (ground in ceramic). Six natural glasses from Central Lau Basin were also analysed. It should be noted that southern Lau Basin glasses are highly vesicular and heterogeneous, containing crystalline inclusions. The vesicles were probed by LA-ICP-MS and were found to contain appreciable amounts of Nb and Ta (>30µg/g), perhaps due to an enriched phase or fluid associated with the vesicles. This may account for any spurious Nb and Ta concentrations associated with the natural glasses.

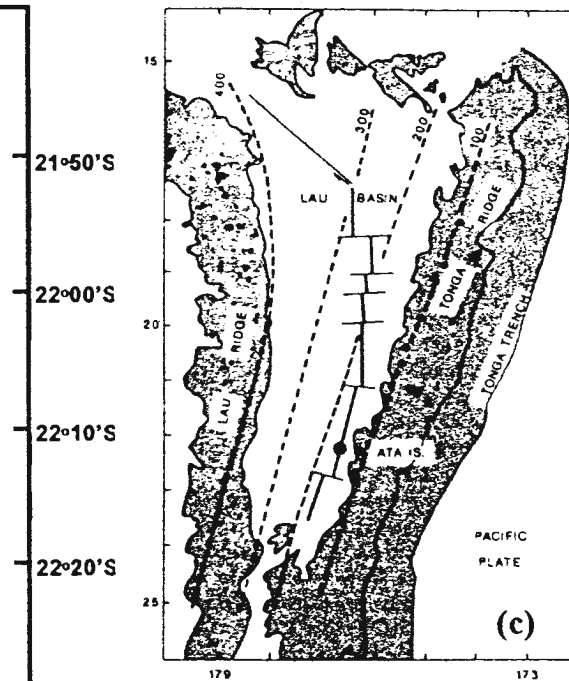
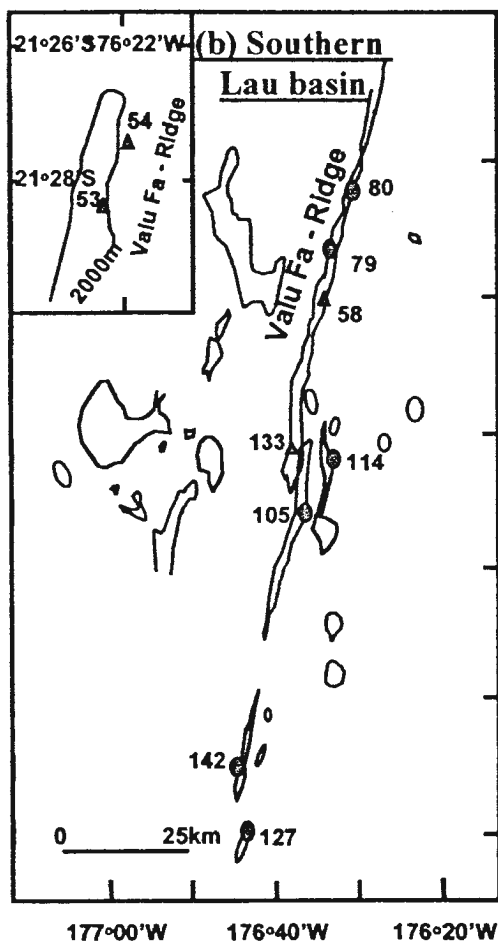
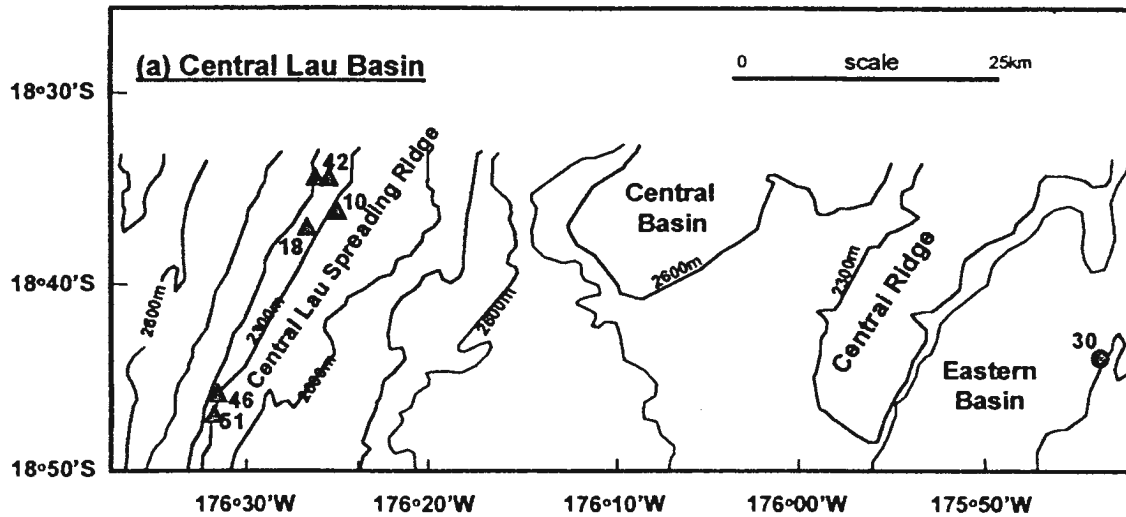


Figure A7: Tonga Ridge and Lau Basin. (a) Sample locations in Central Lau Basin, taken from Look (1992), (b) sample locations in southern Lau Basin taken from Look (1992), (c) map of Lau Basin showing the location of Ata Island, taken Jenner *et al.* (1987).

The Lau Basin samples are thought to have been derived from different mantle source compositions depending on tectonic and geographic location (Loock *et al.*, 1992). From the data collected in this study, it can be seen that southern Lau Basin samples have a more pronounced island arc signature seen in marked HFSE negative anomalies and relative LILE and LREE enrichments (Figure 5.5) compared to Central Lau Basin samples (Figure 5.6).

A.3.2 Valu Fa Ridge

Valu Fa Ridge is an active spreading centre in the Lau Basin, located at the southern end of the Eastern Lau Spreading Centre (Figure A.7(b)). This spreading centre is propagating southward into older crust, which is thought to have a more arc-like signature (Hawkins Jr., 1995). It has been shown that ratios of LILE to LREE (*e.g.* K/La) for Valu Fa rocks are enriched and resemble ratios for island arc volcanics (Jenner *et al.*, 1987) suggesting that there has been assimilation of the older crust into the newly forming crust. However, isotopic data show a similarity of Valu Fa Nd-Sm isotope ratios with Lau Basin axial ridge samples, and a Pb-isotopic similarity to Tonga arc lavas, suggesting either mixing of sources or mixing of magmas between MORB end-member and arc end-member compositions (Hawkins Jr., 1995).

Jenner *et al.*(1987) described the petrography of Valu Fa samples as follows: Samples from this area are typically highly vesicular lava fragments of andesitic composition. Variations between the samples are small within and in between the two dredge sites. All have a similar petrography and mineralogy; rare euhedral phenocrysts (An₇₅₋₈₈) in a hyalopilitic mesostasis of plagioclase microlites (An₅₂₋₆₈) with interstitial

brown glass and rare subhedral augite and pigeonite. There is no olivine observed. Minute magnetite inclusions have been identified within the glass. However, there are variations between the two dredge sites that cannot be explained in terms of low-pressure crystal fractionation from a common magma source. The exact nature of the Valu Fa andesites is unknown. It would require approximately 50% fractional crystallisation from a basaltic parent to derive these andesites (Jenner *et al.*, 1987).

A.3.3 Ata Island

Ata Island lies to the east of the Valu Fa Ridge at the edge of the Lau Basin (approximate location is 22°S/176°W; Figure A.7 (c)).

There are marked similarities in isotopic composition of Ata volcanics and those from the Valu Fa Ridge, although it is thought that the source for the Valu Fa volcanics is more enriched in HREE, TiO₂ and P₂O₅ compared to the source of Ata volcanics (Jenner *et al.*, 1987). Approximately 400 ka ago Ata Island occupied the same position as Valu Fa (with respect to the mantle reference frame) (Hawkins Jr., 1995). It is possible therefore, that those remnant subduction components are causing an effect on Valu Fa's signature.

A.4 Boninites and Related Rocks

By definition a *boninite* is a magnesium and silica rich (11-20% MgO and 57-58wt% SiO₂, Jenner, 1981) rock named after the type locality, Bonin Island, Izu-Bonin arc, south Japan. The geochemical characteristics defining boninites are high Zr/Sm, Zr/Ti, Zr/Y and Zr/MREE ratios, both LREE and HREE greater than MREE (resulting in a U-shaped REE plot), and LILE and LREE enrichment (Jenner, 1981; Coish, 1989). The

genesis of boninites is somewhat controversial. However, there seems to be agreement in the literature that they are derived from a depleted, supra-subduction zone harzburgite which has been fluxed by slab-derived, LILE bearing fluids and partially melted to yield boninitic primary magmas (Crawford *et al.*, 1989). The requirement for the formation of boninites is (1) a refractory source (containing enstatite and olivine) and (2) conditions allowing the incongruent melting of enstatite (either low pressure melting at <5Kb or a high H₂O content or a high concentration of network modifying cations such as Na, K) (pers comm, van der Laan, 1998). The incongruent melting of enstatite, sometimes combined with the crystallisation of forsteritic olivine, causes a gradual enrichment of SiO₂ in the melt with increased degree of partial melting. In this way a melt with a relatively high SiO₂ and MgO content can be produced.

A.4.1 Dabi Volcanics, Cape Vogel, Papua New Guinea

The geology of Cape Vogel has been described by Dallwitz *et al.* (1966), Dallwitz (1968) and Smith and Davis (1976). The four samples analysed from this locality are tholeiites associated with boninites and high magnesian andesites of the Dabi Volcanics (Jenner, 1982). It is important to note that these samples were ground in agate.

The samples analysed are classified as tholeiites and are basic (LB86), andesitic (LB51 = high potassium, 47802 = low K) and dacitic/rhyodacitic (47798) (Winchester and Floyd, 1971; Pearce and Cann, 1973). Primitive mantle normalised REE plots show flat trends (Figure 5.7) and extended plots show marked negative Nb anomalies and slightly positive Ta anomalies for three of the samples (Figure 5.8). No Zr, Hf or Ti anomalies are apparent.

A.4.2 Pacquet Harbour Group, Newfoundland, Canada

The boninites of the Appalachians are chemically very similar to those found in the western Pacific Ocean (Coish, 1989). The Pacquet Harbour Group rocks are high-Ca boninites with relatively high concentrations of SiO₂ and high CaO/Al₂O₃ ratios. These rocks are characterised by low Ti, Zr, Y and REE relative to MORB, high MgO, Ni, Cr and low Al₂O₃, Zr/Sm > N-MORB, U-shaped, primitive mantle normalised REE patterns (Figure 5.8) and Low ϵ_{Nd} (Coish, 1989, Piercey *et al.*, 1997).

The major and trace element chemistry can be explained by the melting of a harzburgite with enough clinopyroxene to give the necessary Al₂O₃ and CaO contents. The U-shaped REE pattern requires either a phase in the residue that preferentially holds onto the middle REE relative to the LREE and HREE, or the depletion of the source area in mid- to light-REE with a re-enrichment of only LREE. The low ϵ_{Nd} values indicate an addition of enriched fluid to the source rock (Coish, 1989).

Primitive mantle normalised extended plots for these samples show similar characteristics to those for the Dabi tholeiites, with negative Nb anomalies and positive Ta anomalies. Slightly positive Zr and Hf anomalies are also apparent in Figure 5.8.

A.4.3 Boninites from Bonin Island and Boninite-Related Rocks from Japan

Two samples have been analysed from the Chichi-jima Island group of the Bonin (Ogasawara) Islands, which are part of the outer Izu-Mariana Arc (Jenner, 1982). Jenner (1982) has described typical boninites from this area as *glassy, feldspar-free, olivine-bronzite andesites*, with some *clinoenstatite bearing varieties*. Sample 1129-4 is andesitic and although it has a MgO content of < 11 wt%, is thought to be a boninite due to its high

Zr/Sm ratio, and slightly U-shaped primitive mantle normalised REE plot (Figure 5.7). Sample 1127-5 is more felsic than 1129-4, with a SiO₂ content of 69 wt%, classifying this rock as a rhyolite/dacite. A slightly U-shaped, primitive mantle normalised REE pattern and high Zr/Sm ratios are apparent in 1127-5, suggesting that this sample be derived from boninitic parent magma by fractional crystallisation or by assimilation of crustal material. Extended primitive mantle normalised plots for these samples show negative Nb and Ta anomalies, positive Zr and Hf anomalies and a negative Ti anomaly for sample 1127 (Figure 5.8).

A sanukitoid sample from Japan has also been analysed. This sample is not a boninite but is thought to be primary mantle derived andesite that formed in an island arc environment (Tatsumi and Ishizaka, 1981). Jenner (1982) regards these rocks as derivatives of a depleted peridotite and perhaps as rocks related to boninites by a common petrogenetic origin (partial melting of a peridotite at pressures <15kb and temperatures of 1100-1400°C). This sample shows negative Sr, Nb, Zr and Ti anomalies with no apparent Hf or Ta anomalies (Figure 5.8).

A.5 Ocean Island Volcanic Rocks

Gran Canaria (Canary Islands) is located off the NW coast of Africa, and is made up of Miocene (12-15Ma) and Pliocene-Quaternary (0-6Ma) mafic volcanics including picrites, tholeiites, alkali basalts, basanites, nephelinites and melilite nephelinites (Hoernle and Schmincke, 1993a). There is an extremely wide compositional range of magmas that are erupted from a single volcano. All the magmas are thought to have been derived from the same source and differences in the trace and major element chemistry

reflect differences in the pressure and temperature of segregation, the volatile content and the fractionation and accumulation processes during transport to the surface (Hoernle and Schmincke, 1993b). It is thought by Hoernle and Schmincke (1993a) that olivine and clinopyroxene are the major fractionating phases in basalts; plagioclase, Fe-Ti-oxides and apatite fractionation or accumulation may play a role in the derivation of the most evolved mafic volcanics. The mafic volcanics originated at $P > 3.0 \text{ GPa}$ (within the garnet stability field).

A study by Wolff (1984) on phonolitic magma erupted on Tenerife, Canary Islands, showed a high degree of variation of Nb/Ta (9-23) during differentiation. Nb/Ta are said to have varied consistently with any element chosen as a fractionation parameter. It was thought that this variation was due to sphene fractionation and possibly the change of Nb valence from 5^+ to 3^+ . It is now known from experimental studies that sphene can fractionate Nb and Ta to a high degree ($D_{\text{Nb}}/D_{\text{Ta}} = 0.3$, Green and Pearson, 1987) supporting Wolff's hypothesis. Fe-Ti-oxides are also constituent phenocrystal phases in the phonolites (Wolff, 1984) and could also have played a role in the fractionation of Nb and Ta ($D_{\text{Nb}}/D_{\text{Ta}}$: rutile = 0.6, ilmenite = 0.7-0.8, magnetite = 0.9, Green and Pearson, 1987).

The most evolved rock (RN-2) shows a negative Ti anomaly, contrasting with the more primitive samples. All samples show slightly negative Zr and Hf anomalies and negative Sr and Rb anomalies.

A.6 Continental Crust

The continental crust is defined as the upper part of the silicate Earth above the Mohorovicic Discontinuity (Wedepohl, 1995). Issues of interest for this study are the negative Nb and Ta anomalies often found in continental rocks and the often sub-chondritic Nb/Ta ratios (Green, 1995).

The HFSE have been central to the understanding of crustal growth processes, for example, the Nb/U ratios of Hoffman (1988) and Sylvester *et al.* (1997) and as mentioned in section 2.2.4 the negative Nb and Ta anomalies in both continental crust and island arc magmatism provide evidence for related geneses.

In this study, seven sediments were analysed, derived from the Gagnon terrane (Knob Lake Group, Labrador) deposited in the Early Proterozoic on the passive continental margin of the Superior Craton (Van Gool, 1991). The Gagnon terrane consists of basement-dominated and metasedimentary material which together represent continental crust in this study. A more thorough study on the Nb/Ta ratios of continental crust was recently carried out by Barth *et al.* (1998) using Australian shales to represent continental crust. These values determined gave Nb/Ta ratios close to those of Plank and Langmuir (1998) (Nb/Ta = 14, Nb = 14). The values derived from this present work show a spread of Nb/Ta ratios (4.1- 9.4) with Nb concentrations (8-25 $\mu\text{g g}^{-1}$) more compatible with the results of Taylor and McLennan (1985) (Nb/Ta = 11, Nb = 25 $\mu\text{g g}^{-1}$).

A.7 Ultramafic Samples

A.7.1 Xenoliths

Two samples derived from xenoliths from Sangeang Api volcano (Sumbawa, Indonesia) were analysed. Sangeang Api is a volcano of the Sunda Arc, Indonesia.

A.7.2 Troodos Ophiolite, Cyprus

The Troodos ophiolite complex is located on Cyprus in the Mediterranean Sea.

It is a classic ophiolite described by Rautenschlein *et al.* (1985) as

.... an association of harzburgite, overlain by layered cumulated, high level intrusives and a mafic sheet dike complex merging into mafic volcanics.

It is thought that it was formed in an extensional environment, affected by a subduction zone, but never closely associated with a well-developed island arc (Rautenschlein *et al.*, 1985).

APPENDIX II

DATA SET

Key to sample locations:

GC – Gran Canaria Island, Gran Canaries
X – Island arc xenoliths from Sangeang Api
Oph – Cyprus (ophiolite)
San – Sanukitoid
BI – Bonin Island boninites
DV – Dabi Volcanics (tholeiites from Papua New Guinea)
PHG – Pacquet Harbour Group boninites
F – Flores, Indonesia
Tambora – Sumbawa island, Indonesia
Rindjani – Lombok island, Indonesia
Tjerimai – Java, Indonesia
Tonga – Tonga Ridge, SW Pacific
Ambrym - Vanuatu
Tanna - Vanuatu
Ata – Lau Basin, island arc related
Lau – Southern Lau Basin (Valu Fa)
SLB – South Lau Basin natural glasses
CLB – Central Lau Basin natural glasses
Jb-1a – Japanese geostandard reference material
MI – Macquarie Island
MI ng – Macquarie Island natural glass
Leg82 – Azores Triple Junction
Leg82 ng – Azores Triple Junction natural glass
Eclogite – New Zealand
Sediments – Gagnon Terrane, Labrador
Noritic dyke - Greenland

Sample#	A7-E	A7-G	A8-A	A8-C	A8-F	A8-H	B10-A	B10-C
ID	GC	GC	GC	GC	GC	GC	X	X
SiO2	41	50	44	42	39	44	48	43
TiO2	3.81	1.98	4.3	3.9	3.6	4.4	0.43	1.58
Al2O3	9.8	17.1	12.0	11.5	9.6	12.2	3.4	8.2
FeO	10.6	5.0	10.0	10.2	11.4	9.8	7.9	13.9
MnO	0.00	0.17	0.00	0.00	0.00	0.00	0.20	0.28
MgO	12.4	3.0	9.4	9.8	12.9	9.4	23.1	11.3
CaO	12.0	6.0	11.6	11.4	12.0	11.7	15.5	18.6
Na2O	2.5	4.8	2.2	2.8	1.92	2.1	0.00	0.54
K2O	0.24	2.63	0.62	0.84	0.28	0.57	0.00	0.10
Mg#	0.54	0.38	0.48	0.49	0.53	0.49	0.75	0.45
Rb	0.41	45	1.50	21	4.6	1.68	0.05	0.63
Sr	137	2778	241	1116	926	556	74	242
Y	3.0	40	4.5	24	23	10.0	6.0	17.4
Zr	45	913	83	265	238	92	13	54
Nb	21	246	36	73	76	48	1	2
Ba	84	2679	151	606	579	285	57	225
La	8	251	11	59	52	27	2.3	13.3
Ce	25	421	34	134	121	72	7	34
Pr	2.3	41	3.3	15.6	14.3	7.5	1.16	4.8
Nd	141	134	85	64	58	76	6	23
Sm	0.00	21	0.00	11.7	11.4	25	1.79	6.1
Eu	1.93	6.3	2.3	3.4	3.4	3.2	0.56	1.73
Gd	0.00	14.9	0.00	8.5	8.7	0.00	1.75	5.7
Tb	0.27	2.2	0.37	1.10	1.16	0.71	0.27	0.80
Dy	0.83	12.1	1.24	5.9	5.8	2.6	1.53	4.4
Ho	0.13	2.1	0.20	0.94	0.95	0.42	0.26	0.80
Er	1.17	5.7	1.44	2.4	2.1	1.87	0.70	1.95
Tm	0.03	0.79	0.06	0.30	0.24	0.11	0.09	0.25
Yb	0.00	5.08	0.00	1.76	1.41	5.10	0.49	1.45
Lu	0.03	0.73	0.04	0.25	0.20	0.08	0.07	0.22
Hf	0.61	29	1.27	6.9	6.2	1.72	0.69	2.7
Ta	0.81	15.5	1.58	3.9	4.1	2.15	0.16	0.16
Pb	0.09	1.22	0.01	0.03	0.03	0.01	0.02	0.09
Th	0.78	49	1.01	5.3	4.9	2.4	0.31	1.23
U	0.19	15.30	0.28	1.76	1.30	0.59	0.10	0.44
Nb/Ta	27	16	23	19	19	22	5	11
Zr/Hf	73	32	65	38	38	53	19	20

Sample#	C5-A	C5-C	B2-B	B7-A	B7-B	C1-F	C1-G	C2-B
ID	Oph	Oph	San	BI	BI	DV	DV	DV
SiO2	48	56	54	69	59	57	52	65
TiO2	0.28	0.52	0.93	0.24	0.20	1.02	1.28	0.94
Al2O3	6.2	14.2	16.8	13.3	14.5	14.2	14.4	13.0
FeO	8.3	6.6	7.5	5.6	7.2	10.0	8.1	7.1
MnO	0.18	0.13	0.16	0.13	0.16	0.22	0.17	0.09
MgO	32	10.1	6.3	1.36	6.2	6.2	8.8	2.8
CaO	4.2	10.9	9.2	4.8	8.2	5.0	12.0	6.9
Na2O	0.30	0.92	2.2	2.7	2.2	2.4	2.2	2.5
K2O	0.00	0.22	0.94	0.92	0.46	2.0	0.13	0.21
Mg#	0.79	0.61	0.46	0.20	0.46	0.38	0.52	0.28
Rb	0.06	2.3	35	0.00	0.00	0.00	0.00	0.00
Sr	51	168	298	126	74	102	149	97
Y	7.6	13.4	23	7.6	5.4	17.3	19.1	18.5
Zr	15.73	28	94	43	21	45	49	39
Nb	0.91	1.24	11.6	0.89	0.44	1.26	4.36	1.06
Ba	10.8	18.3	317	64	22	90	21	33
La	0.84	1.36	16.6	2.2	1.03	2.7	4.0	2.5
Ce	2.4	3.69	35	4.76	2.4	7.0	11.2	6.5
Pr	0.41	0.60	4.1	0.71	0.37	1.08	1.56	1.00
Nd	2.3	3.3	16.7	3.3	2.2	5.9	7.4	5.1
Sm	0.82	1.21	4.0	0.95	0.46	1.95	2.5	1.84
Eu	0.32	0.53	1.24	0.29	0.18	0.74	1.03	0.71
Gd	1.13	1.76	4.1	0.98	0.58	2.3	2.6	2.4
Tb	0.21	0.35	0.72	0.19	0.10	0.49	0.54	0.49
Dy	1.41	2.4	4.7	1.25	0.75	2.9	3.6	3.3
Ho	0.32	0.54	1.00	0.35	0.17	0.69	0.79	0.69
Er	0.92	1.62	3.0	1.04	0.54	1.85	2.11	2.26
Tm	0.14	0.24	0.42	0.14	0.09	0.29	0.33	0.31
Yb	0.95	1.67	2.7	1.15	0.62	1.90	2.07	1.99
Lu	0.14	0.26	0.41	0.22	0.10	0.30	0.33	0.34
Hf	0.62	1.05	3.21	1.56	0.62	1.66	1.55	1.23
Ta	0.04	0.08	1.69	0.10	0.04	0.24	0.33	0.24
Pb	0.08	0.03	0.77	0.40	0.38	0.48	0.02	0.42
Th	0.11	0.17	4.3	0.27	0.12	0.31	0.32	0.25
U	0.07	0.10	1.55	0.25	0.09	0.11	0.11	0.11
Nb/Ta	22	16	7	9	12	5	13	4
Zr/Hf	26	27	29	27	34	27	32	32

Sample#	C2-D	C5-G	C6-A	C6-D	6-F; SP 5.9	C6-H	C7-F	B10-F
ID	DV	PHG	PHG	PHG	PHG	PHG	PHG	F
SiO2	60	62	55	45	58	54	51	53
TiO2	0.82	0.11	0.14	0.26	0.22	0.14	0.07	0.73
Al2O3	16.3	0.00	10.7	0.00	0.00	10.3	12.5	19.3
FeO	6.7	0.00	7.3	0.00	0.00	5.9	6.2	7.2
MnO	0.11	0.17	0.22	0.18	0.15	0.22	0.19	0.16
MgO	3.3	17.8	14.2	18.7	19.9	11.9	21	5.5
CaO	8.3	7.9	9.4	10.0	8.3	14.6	6.5	9.7
Na2O	2.6	0.00	1.55	0.00	0.00	1.23	0.28	2.4
K2O	0.12	0.00	1.06	0.00	0.00	0.08	0.06	0.35
Mg#	0.33	1.00	0.66	1.00	1.00	0.67	0.77	0.43
Rb	0.00	0.00	12.76	0.00	0.00	0.00	0.70	0.00
Sr	94	36	73	120	86	251	7	275
Y	25	2.0	3.0	5.6	3.9	3.3	1.9	11.7
Zr	32	13.5	16.6	21	14.7	14.8	10.3	27
Nb	0.69	1.10	1.14	1.28	1.08	1.14	0.83	0.88
Ba	24	11.3	239	50	19.4	29	9.24	91.9
La	2.3	1.14	1.42	1.52	1.53	1.83	1.04	3.55
Ce	5.7	2.8	2.8	3.5	3.2	3.8	2.5	8.9
Pr	0.87	0.31	0.34	0.44	0.40	0.43	0.28	1.24
Nd	4.4	1.68	2.2	2.4	2.5	2.7	2.0	6.1
Sm	1.42	0.31	0.31	0.62	0.39	0.42	0.26	1.92
Eu	0.63	0.12	0.16	0.30	0.21	0.20	0.12	0.72
Gd	2.2	0.29	0.33	0.65	0.56	0.40	0.27	2.0
Tb	0.39	0.06	0.05	0.14	0.10	0.07	0.04	0.35
Dy	3.3	0.29	0.45	0.91	0.68	0.52	0.28	2.2
Ho	0.71	0.08	0.10	0.22	0.16	0.12	0.07	0.47
Er	2.2	0.21	0.35	0.66	0.54	0.41	0.22	1.25
Tm	0.31	0.04	0.06	0.11	0.09	0.06	0.04	0.20
Yb	2.1	0.34	0.45	0.71	0.60	0.53	0.28	1.28
Lu	0.36	0.07	0.08	0.13	0.11	0.08	0.05	0.20
Hf	1.10	0.47	0.42	0.60	0.41	0.42	0.29	0.94
Ta	0.32	0.86	0.62	1.06	0.74	1.10	0.38	0.13
Pb	0.13	0.06	0.00	0.00	0.02	0.00	0.18	0.91
Th	0.18	0.36	0.31	0.30	0.28	0.46	0.27	0.47
U	0.10	0.14	0.11	0.13	0.21	0.22	0.20	0.20
Nb/Ta	2	1	2	1	1	1	2	7
Zr/Hf	29	28	39	34	36	36	36	29

Sample#	48054	48001	B3-J	B4-B	B4-D	B4-J	A1-A	A1-C
ID	Tambora	Rindjsni	Tjerimai	Tjerimai	Tjerimai	Tjerimai	Tonga	Tonga
SiO2	54	48	56	61	59	54	53	59
TiO2	0.67	0.69	0.82	0.64	0.78	0.88	0.86	1.18
Al2O3	19.5	10.7	18.1	16.6	17.3	17.1	18.6	17.1
FeO	5.4	8.8	7.0	5.5	6.0	7.7	8.3	7.3
MnO	0.19	0.16	0.20	0.10	0.17	0.16	0.22	0.18
MgO	2.0	12.3	3.5	3.8	3.9	5.0	4.8	3.1
CaO	4.9	14.2	8.2	6.5	7.3	9.0	9.8	7.0
Na2O	3.9	0.86	3.2	3.1	3.2	2.9	2.8	3.4
K2O	4.9	0.46	1.36	1.94	1.77	1.43	0.27	0.25
Mg#	0.27	0.58	0.34	0.41	0.39	0.39	0.37	0.30
Rb	121	6.38	48	35	53	40	1.78	1.19
Sr	781	425	393	232	270	339	127	128
Y	19.6	11.0	25	14.4	18.8	17.1	21	35
Zr	105	31	118	96	108	77	39	76
Nb	7.7	2.1	6.0	4.4	5.6	4.0	0.87	1.24
Ba	1100	273	332	231	286	250	41	54
La	35	8.80	22.47	13.9	16.3	16.7	1.37	2.8
Ce	62	19	45	26	33	32	4.89	8.53
Pr	7.4	2.6	5.7	3.2	3.9	4.0	0.92	1.68
Nd	26	9.6	23	12.4	15.7	16.9	5.4	9.5
Sm	5.4	2.5	5.7	2.6	3.5	3.7	2.2	3.6
Eu	1.61	0.89	1.51	0.66	0.98	1.09	0.83	1.16
Gd	4.3	2.3	5.0	2.3	3.3	3.1	3.1	5.0
Tb	0.71	0.42	0.79	0.36	0.51	0.52	0.56	0.96
Dy	3.8	2.1	4.9	2.3	3.3	3.0	4.0	6.3
Ho	0.82	0.46	1.04	0.47	0.68	0.61	0.88	1.41
Er	2.2	1.11	3.0	1.37	1.93	1.89	2.7	4.2
Tm	0.33	0.17	0.43	0.19	0.28	0.25	0.42	0.64
Yb	1.99	0.92	2.9	1.39	1.99	1.66	2.6	4.2
Lu	0.34	0.17	0.48	0.22	0.30	0.27	0.42	0.66
Hf	3.1	1.04	3.9	2.39	3.1	2.1	1.51	2.9
Ta	0.38	0.09	0.40	0.30	0.35	0.25	0.05	0.09
Pb	2.7	0.01	1.09	0.17	0.33	0.92	0.68	0.93
Th	9.8	1.56	6.9	5.71	6.6	5.2	0.11	0.22
U	2.9	0.38	1.42	1.06	1.38	1.02	0.10	0.24
Nb/Ta	20	24	15	15	16	16	19	14
Zr/Hf	34	30	30	40	35	37	26	26

Sample#	B9-B	B9-C	B9-D	B9-E	B9-F	B9-G	B9-H	B9-I
ID	Ambrym	Ambrym	Tanna	Tanna	Tanna	Tanna	Tanna	Tanna
SiO2	53	53	50	53	50	52	52	57
TiO2	0.93	0.74	0.81	0.71	0.37	0.60	0.61	0.79
Al2O3	16.5	15.0	18.5	16.7	8.8	13.8	13.9	17.1
FeO	7.5	6.7	9.1	8.2	6.0	8.4	8.2	7.0
MnO	0.18	0.19	0.22	0.17	0.15	0.20	0.19	0.16
MgO	5.9	8.9	6.4	6.9	18.1	8.4	8.8	2.7
CaO	9.7	10.3	11.4	10.3	14.2	12.8	12.8	6.7
Na2O	2.7	2.2	1.75	2.1	0.47	1.58	1.32	3.8
K2O	1.83	1.11	0.60	0.89	0.21	0.53	0.49	2.7
Mg#	0.44	0.57	0.41	0.45	0.75	0.50	0.52	0.28
Rb	0.00	0.00	0.00	0.00	0.00	0.00	0.00	0.00
Sr	585	419	403	594	184	337	414	554
Y	14.4	13.6	11.2	11.1	5.0	12.6	18.2	19.2
Zr	62	47	22	24	8.53	23	29	77
Nb	3.1	2.1	0.31	0.43	0.18	0.34	0.45	1.30
Ba	386	246	153	197	70	80	113	493
La	10.9	7.8	3.7	4.3	1.52	2.5	5.0	12.7
Ce	25	17.5	9.1	10.1	4.1	6.2	9.4	30
Pr	3.3	2.4	1.31	1.46	0.58	0.98	1.90	4.1
Nd	14.1	10.3	6.2	6.6	2.9	5.0	9.7	18.0
Sm	3.3	2.8	1.80	1.69	0.68	1.46	2.7	4.0
Eu	1.16	0.89	0.76	0.58	0.35	0.57	1.03	1.23
Gd	2.8	2.5	1.88	1.69	0.94	1.87	3.3	3.7
Tb	0.46	0.40	0.33	0.27	0.14	0.35	0.59	0.55
Dy	2.8	2.6	2.1	1.66	0.93	1.95	3.8	3.4
Ho	0.58	0.51	0.46	0.38	0.20	0.49	0.81	0.71
Er	1.53	1.55	1.22	1.04	0.51	1.33	2.4	2.1
Tm	0.25	0.22	0.19	0.17	0.09	0.21	0.31	0.33
Yb	1.45	1.62	1.13	1.03	0.45	1.24	2.3	2.14
Lu	0.25	0.23	0.20	0.17	0.09	0.21	0.33	0.31
Hf	2.1	1.57	0.71	0.76	0.31	0.83	1.29	2.4
Ta	0.17	0.14	0.02	0.03	0.01	0.03	0.02	0.05
Pb	0.14	0.15	0.28	0.11	0.00	0.14	0.29	3.28
Th	1.42	0.99	0.44	0.69	0.13	0.21	0.31	1.83
U	0.61	0.39	0.22	0.42	0.10	0.14	0.21	1.08
Nb/Ta	19	15	16	15	26	11	21	25
Zr/Hf	29	30	32	32	28	27	23	32

Sample#	B9-J	C4-D	C4-F	C4-E	C4-G	D1-4#10	D2-7#18	D2-8#8
ID	Tanna	Ata	Ata	Ata	Ata	Lau	Lau	Lau
SiO2	50	55	52	48	51	55	54	54
TiO2	0.75	0.69	0.72	0.16	0.64	1.33	1.56	1.54
Al2O3	17.8	17.3	17.8	13.2	15.2	19.1	16.4	16.7
FeO	8.9	8.5	10.4	6.0	10.5	10.1	11.5	11.4
MnO	0.19	0.14	0.19	0.11	0.22	0.20	0.18	0.19
MgO	6.7	4.0	4.2	13.0	7.6	2.9	3.7	3.6
CaO	12.2	9.9	9.9	18.0	12.3	7.0	7.9	7.8
Na2O	1.59	2.3	2.1	0.40	1.52	2.9	2.7	3.1
K2O	0.24	0.60	0.56	0.11	0.38	0.40	0.40	0.36
Mg#	0.43	0.32	0.29	0.68	0.42	0.23	0.24	0.24
Rb	0.00	8.8	9.1	0.49	7.8	7.7	6.8	6.4
Sr	308	245	301	112	266	162	176	174
Y	11.56	18.31	17.97	2.93	12.02	29	27	27
Zr	17.7	37	33	1.76	21	61	53	51
Nb	0.21	0.64	0.55	0.03	0.42	1.18	0.96	0.95
Ba	138	181	172	11	113	95	92	91
La	2.1	4.7	4.5	0.18	3.4	4.9	4.5	4.4
Ce	5.9	11.2	11.3	0.61	8.5	12.9	11.8	11.3
Pr	0.91	1.74	1.78	0.11	1.29	2.2	2.1	2.0
Nd	4.5	7.7	8.3	0.63	5.3	10.1	9.7	9.3
Sm	1.45	2.5	2.7	0.28	1.82	3.5	3.4	3.2
Eu	0.62	0.84	1.00	0.16	0.73	1.35	1.38	1.3
Gd	1.70	2.8	2.9	0.38	1.95	4.1	4.0	4.0
Tb	0.32	0.54	0.56	0.08	0.38	0.88	0.86	0.85
Dy	2.2	3.4	3.4	0.54	2.2	5.3	5.3	5.1
Ho	0.46	0.74	0.75	0.12	0.52	1.30	1.23	1.19
Er	1.31	2.2	2.06	0.33	1.35	3.5	3.5	3.3
Tm	0.20	0.34	0.35	0.05	0.22	0.57	0.54	0.52
Yb	1.27	2.1	2.1	0.29	1.32	3.4	3.2	3.2
Lu	0.21	0.35	0.35	0.04	0.23	0.57	0.58	0.55
Hf	0.63	1.50	1.30	0.08	0.77	2.22	2.01	1.94
Ta	0.01	0.04	0.03	0.00	0.02	0.09	0.06	0.06
Pb	0.10	0.78	0.20	0.01	0.52	0.27	0.64	0.57
Th	0.25	0.54	0.42	0.01	0.34	0.46	0.38	0.40
U	0.15	0.24	0.19	0.02	0.17	0.20	0.22	0.17
Nb/Ta	17.11	17.07	17.41	14.85	18.19	13.70	14.83	14.65
Zr/Hf	28.04	24.82	25.33	20.73	26.98	27.47	26.09	26.14

Sample#	D2-1#17	D1-2#4	D1-13#7	D1-7#20	SLB 127	SLB 79	SLB 54	SLB 58
ID	Lau	Lau	Lau	Lau	Lau	Lau	Lau	Lau
SiO2	54	55	53	54				
TiO2	1.75	1.60	1.38	1.37				
Al2O3	16.7	17.7	19.6	18.0				
FeO	11.5	10.7	10.4	10.6				
MnO	0.19	0.21	0.17	0.21				
MgO	3.7	3.3	3.3	3.2				
CaO	8.0	7.5	7.3	7.3				
Na2O	2.9	2.7	2.4	3.1				
K2O	0.36	0.40	0.46	0.48				
Mg#	0.24	0.24	0.24	0.23				
Rb	6.1	6.9	7.1	7.8	8.1	12.0	3.9	7.4
Sr	159	149	149	150	216	155	122	172
Y	29	30	29	29	16.9	51	18.4	34
Zr	56	61	60	60	28	121	34	77
Nb	0.94	1.08	1.03	1.04	0.45	1.65	0.45	1.19
Ba	94	93	95	91	97	150	51	88
La	4.2	4.6	4.3	4.3	3.4	7.2	2.1	4.7
Ce	11.0	11.9	11.4	11.6	8.3	19.0	5.3	13.1
Pr	1.89	2.0	1.95	1.97	1.23	3.0	0.90	2.1
Nd	9.3	9.9	9.4	9.6	6.7	16.6	4.5	11.4
Sm	3.5	3.5	3.3	3.4	2.09	5.4	1.78	3.8
Eu	1.22	1.25	1.27	1.24	0.75	1.57	0.71	1.38
Gd	4.1	4.2	4.2	4.1	2.6	7.3	2.4	4.7
Tb	0.85	0.86	0.82	0.82	0.43	1.29	0.45	0.79
Dy	5.4	5.2	5.3	5.1	3.1	9.2	3.2	6.0
Ho	1.22	1.21	1.19	1.22	0.67	1.90	0.68	1.30
Er	3.5	3.4	3.4	3.5	2.0	5.8	2.1	3.8
Tm	0.52	0.55	0.53	0.53	0.29	0.86	0.29	0.55
Yb	3.3	3.4	3.4	3.2	2.0	5.9	2.0	3.7
Lu	0.56	0.57	0.56	0.56	0.30	0.92	0.30	0.57
Hf	2.1	2.2	2.3	2.1	0.9	3.6	1.1	2.4
Ta	0.05	0.08	0.07	0.07	0.07	0.13	0.07	0.08
Pb	0.3	0.2	0.2	1.0	1.3	1.7	1.2	1.2
Th	0.36	0.47	0.37	0.36	0.43	0.68	0.18	0.42
U	0.17	0.18	0.16	0.16	0.18	0.29	0.07	0.20
Nb/Ta	17	14	15	15	6	12	7	14
Zr/Hf	26	28	27	29	30	34	32	33

Sample#	SLB 53	SLB 142	SLB 133	CLB 18	CLB 51	CLB 10	CLB 7
ID	Lau	Lau	Lau	Lau	Lau	Lau	Lau
SiO2							
TiO2							
Al2O3							
FeO							
MnO							
MgO							
CaO							
Na2O							
K2O							
Mg#							
Rb	7.1	6.8	7.4	0.93	0.89	4.72	0.70
Sr	157	173	173	85	74	119	78
Y	26	27	33	32	29	29	26
Zr	58	56	70	68	50	75	48
Nb	0.82	0.89	1.06	1.10	1.04	4.93	0.85
Ba	72	85	104	8.0	8.0	41	6.5
La	3.6	3.9	4.7	2.3	1.69	4.6	1.48
Ce	10.2	10.4	12.8	8.3	6.0	11.9	5.3
Pr	1.60	1.66	2.1	1.48	1.09	1.74	0.93
Nd	8.2	8.7	11.1	8.6	6.5	9.1	5.7
Sm	2.8	3.0	3.8	3.3	2.7	2.8	2.2
Eu	0.98	1.14	1.31	1.19	0.99	1.07	0.93
Gd	3.6	4.2	4.7	4.2	3.9	3.9	3.5
Tb	0.65	0.67	0.86	0.80	0.66	0.69	0.63
Dy	4.6	4.8	5.8	5.7	5.0	5.3	4.5
Ho	0.96	1.04	1.25	1.21	1.08	1.08	0.94
Er	2.8	3.0	3.8	3.4	3.2	3.3	2.9
Tm	0.42	0.44	0.53	0.51	0.48	0.42	0.45
Yb	2.8	3.0	3.8	3.6	3.2	3.1	2.9
Lu	0.45	0.45	0.57	0.54	0.48	0.46	0.43
Hf	1.7	1.8	2.2	2.0	1.6	2.0	1.5
Ta	0.06	0.07	0.07	0.08	0.07	0.34	0.06
Pb	0.96	1.15	1.30	0.45	0.29	0.79	0.33
Th	0.31	0.35	0.41	0.09	0.07	0.50	0.08
U	0.14	0.16	0.19	0.04	0.03	0.14	0.06
Nb/Ta	13	14	15	13	15	15	15
Zr/Hf	34	31	32	34	32	38	32

Sample#	CLB 46	CLB 42	Jb-1a	B5-B	B5-C	B5-D	B5-F	C1-H
ID	Lau	Lau	Jb-1a	MI	MI	MI	MI	MI
SiO2			56	52	51	52	53	51
TiO2			1.32	1.06	1.10	1.38	1.01	1.17
Al2O3			15.0	19.1	19.2	15.1	18.2	16.5
FeO			6.0	3.9	3.9	8.2	4.5	6.5
MnO			0.00	0.10	0.14	0.18	0.12	0.16
MgO			8.0	8.1	8.0	7.4	7.6	9.6
CaO			9.8	12.4	12.3	11.4	10.9	10.1
Na2O			2.1	2.2	2.4	2.9	3.5	2.0
K2O			1.26	0.23	0.25	0.49	0.19	0.98
Mg#			0.57	0.68	0.67	0.48	0.63	0.60
Rb	0.91	0.76	1.21	1.38	4.9	10.8	3.2	0.00
Sr	79	79	395	140	290	140	277	157
Y	33	25	19.0	12.1	23	25	17.2	18.2
Zr	65	46	110	42	83	72	56	58
Nb	1.21	0.89	26	8.7	19.0	10.3	10.2	4.2
Ba	8.1	6.9	447	59	202	58	46	301
La	1.97	1.52	33.19	5.2	16.7	7.3	6.4	3.8
Ce	7.0	5.4	59	10.4	37	16.0	13.7	10.8
Pr	1.26	0.99	6.3	1.42	4.7	2.2	1.82	1.54
Nd	7.5	5.6	23	5.7	21	11.0	8.6	7.0
Sm	3.0	2.3	4.4	1.62	5.5	3.1	2.4	2.2
Eu	1.08	0.92	1.19	0.58	1.90	1.13	0.84	0.87
Gd	4.3	3.2	3.8	1.66	5.6	3.5	2.6	2.7
Tb	0.78	0.59	0.62	0.27	0.96	0.70	0.46	0.52
Dy	5.5	4.4	3.6	1.94	6.3	4.6	3.1	3.3
Ho	1.24	0.94	0.67	0.39	1.40	0.99	0.64	0.72
Er	3.8	2.8	1.96	1.22	4.0	2.8	1.84	2.0
Tm	0.56	0.40	0.28	0.17	0.56	0.39	0.27	0.31
Yb	3.7	2.9	1.79	1.01	3.8	2.7	1.74	1.99
Lu	0.56	0.42	0.28	0.17	0.52	0.38	0.25	0.30
Hf	1.88	1.50	3.1	1.01	3.7	2.1	1.63	1.46
Ta	0.08	0.07	1.46	0.45	1.73	0.58	0.57	0.26
Pb	0.50	0.40	0.02	0.00	0.00	0.13	0.17	19.3
Th	0.12	0.07	7.6	0.63	2.3	0.79	0.76	0.24
U	0.07	0.03	1.42	0.14	0.71	0.18	0.20	0.10
Nb/Ta	14	13	17	19	11	18	18	16
Zr/Hf	35	31	36	42	22	35	34	40

Sample#	C1-I	C1-J	46776	60794	40428.52	60701.62	608255	B6-G
ID	MI	MI	MI	MI	MI ng	MI ng	MI ng	Leg82
SiO2	49	50	50	50	50	48	48	55
TiO2	0.51	1.07	1.09	1.15	1.70	1.32	1.79	1.62
Al2O3	23.5	18.7	19.3	17.3	15.3	16.5	17.1	15.0
FeO	3.7	5.3	5.1	7.3	8.8	7.8	7.9	9.7
MnO	0.09	0.14	0.12	0.14	0.17	0.15	0.13	0.21
MgO	5.9	7.8	6.9	8.7	6.8	8.1	6.2	4.2
CaO	13.7	11.9	13.2	10.2	10.7	12.4	10.8	8.5
Na2O	2.1	3.0	3.0	3.0	3.2	2.9	3.8	3.1
K2O	0.11	0.28	0.87	0.70	0.58	0.56	1.16	0.37
Mg#	0.61	0.60	0.57	0.54	0.43	0.51	0.44	0.30
Rb	0.00	0.00	10.65	16.26	23.57	18.65	35.61	0.00
Sr	178	201	396	218	230	310	467	162
Y	9.7	16.0	17.2	20.0	28	20	27	29
Zr	20.9	55	65	64	111	72	136	58
Nb	2.0	14.1	24	16.7	35	32	67	0.85
Ba	28	103	213	151	184	187	395	95
La	1.67	8.7	14.3	10.6	19.7	18.2	38	4.4
Ce	4.6	19.5	26	20.63	41.52	35	71	11.7
Pr	0.62	2.4	3.2	2.7	5.4	4.4	8.3	1.97
Nd	3.0	9.5	13.2	11.5	19.5	15.7	30	9.7
Sm	1.02	2.5	3.0	3.0	5.0	3.7	6.2	3.5
Eu	0.51	0.97	1.11	1.07	1.76	1.42	2.2	1.26
Gd	1.34	2.5	3.1	3.5	4.9	3.7	5.6	4.3
Tb	0.25	0.45	0.54	0.60	0.96	0.68	1.00	0.79
Dy	1.55	3.0	3.3	3.9	5.4	3.9	5.7	5.5
Ho	0.38	0.64	0.69	0.83	1.25	0.91	1.22	1.16
Er	1.10	1.69	2.01	2.42	3.39	2.3	3.3	3.5
Tm	0.15	0.25	0.33	0.35	0.52	0.36	0.49	0.53
Yb	1.19	1.71	1.89	2.3	3.1	2.2	2.9	3.4
Lu	0.16	0.24	0.29	0.33	0.53	0.36	0.50	0.52
Hf	0.63	1.52	1.91	2.1	3.1	2.0	4.0	2.0
Ta	0.11	0.77	1.48	1.04	2.1	1.93	4.3	0.05
Pb	19.7	2.8	0.00	0.00	1.39	0.99	2.2	0.20
Th	0.13	1.01	0.00	1.94	2.8	2.4	5.6	0.38
U	0.05	0.29	0.00	0.62	0.78	0.66	1.40	0.18
Nb/Ta	18	18	16	16	17	16	16	17
Zr/Hf	33	36	34	31	36	35	34	28

Sample#	B6-H	B6-I	B6-J	10.82	108.82	120.82	131.82	2.82
ID	Leg82	Leg82	Leg82	Leg82 ng				
SiO2	55	57	57	51	51	50	50	51
TiO2	1.57	1.57	1.60	1.41	1.58	1.57	1.26	1.62
Al2O3	14.9	15.2	15.4	14.2	14.4	14.4	15.0	14.4
FeO	10.7	8.3	7.7	11.0	10.3	10.5	9.9	10.6
MnO	0.22	0.21	0.20	0.19	0.20	0.18	0.17	0.20
MgO	4.0	3.9	4.0	7.1	6.8	7.2	7.9	6.6
CaO	8.2	8.1	8.3	11.3	11.2	11.2	11.8	11.0
Na2O	3.3	3.3	3.3	2.6	2.7	2.6	2.4	2.9
K2O	0.37	0.45	0.43	0.11	0.16	0.12	0.12	0.19
Mg#	0.27	0.32	0.34	0.39	0.40	0.41	0.44	0.38
Rb	0.00	0.00	0.00	1.79	3.71	1.27	1.50	3.33
Sr	154	161	160	88	93	98	89	97
Y	27	30	27	33	29	29	28	37
Zr	51	60	52	66	71	67	60	92
Nb	0.80	0.97	0.87	2.8	2.2	2.3	2.9	2.5
Ba	88	96	95	21.8	33	11.7	16.3	41
La	4.1	4.5	4.1	3.1	3.1	2.9	3.0	3.7
Ce	11.0	12.1	11.3	9.1	9.8	9.5	8.7	11.2
Pr	1.77	2.0	1.83	1.6	1.82	1.78	1.58	2.1
Nd	9.3	10.0	9.0	8.2	8.8	8.6	7.8	10.8
Sm	3.0	3.6	2.6	3.3	3.4	3.4	3.0	4.1
Eu	1.23	1.35	1.23	1.27	1.29	1.33	1.14	1.48
Gd	3.3	4.4	4.0	4.5	4.1	4.3	4.0	5.6
Tb	0.69	0.74	0.69	0.97	0.89	0.90	0.85	1.13
Dy	4.6	5.4	5.0	6.2	5.5	5.4	5.2	7.0
Ho	1.01	1.18	1.05	1.45	1.29	1.31	1.24	1.66
Er	3.0	3.3	3.2	4.0	3.4	3.5	3.3	4.5
Tm	0.42	0.49	0.50	0.63	0.54	0.55	0.52	0.71
Yb	2.9	3.6	3.2	3.7	3.2	3.3	3.2	4.3
Lu	0.46	0.56	0.45	0.63	0.55	0.55	0.53	0.72
Hf	1.72	1.98	1.89	2.5	2.3	2.2	2.2	3.1
Ta	0.05	0.07	0.06	0.18	0.13	0.14	0.18	0.17
Pb	0.50	0.29	0.08	0.39	0.71	0.38	0.39	0.70
Th	0.32	0.33	0.34	0.21	0.12	0.13	0.17	0.16
U	0.16	0.19	0.16	0.07	0.05	0.05	0.06	0.05
Nb/Ta	17	13	15	16	16	16	16	15
Zr/Hf	29	30	28	27	31	30	28	29

Sample#	65.82	85.82	91.82	Z5-2-2-	Z6-50-14-	Z6-55-3(1)	Z6-55-3(2)	Z6-55-4-
ID	Leg82 ng	Leg82 ng	Leg82 ng	eclogite	eclogite	eclogite	eclogite	eclogite
SiO2	51	50	50	43	46	53	57	56
TiO2	1.31	1.47	1.50	1.88	2.4	0.94	0.79	1.54
Al2O3	14.9	14.7	14.6	0.00	0.00	0.00	0.00	0.00
FeO	8.7	9.8	10.0	0.00	0.00	0.00	0.00	0.00
MnO	0.17	0.18	0.18	0.18	0.20	0.21	0.20	0.27
MgO	8.1	7.7	7.7	36.93	9.18	9.76	2.39	3.31
CaO	11.5	11.0	11.0	12.23	9.00	9.27	9.35	12.33
Na2O	2.4	2.7	2.6	0.00	0.00	0.00	0.00	0.00
K2O	0.28	0.32	0.34	0.00	0.00	0.00	0.00	0.00
Mg#	0.48	0.44	0.43	1.00	1.00	1.00	1.00	1.00
Rb	5.99	8.14	8.98	0.00	0.00	0.00	0.00	0.00
Sr	154	174	173	38	281	68	69	97
Y	22.8	29	25.7	29	43	15.1	14.8	16.8
Zr	64	92	79	78	111	72	69	55
Nb	9.5	16.0	15.2	2.3	4.0	5.8	6.0	8.0
Ba	72	98	90.16	4.91	4.43	49.56	47.11	6.40
La	7.8	11.1	10.3	1.74	6.1	12.9	13.2	4.8
Ce	17.0	22.6	21.5	5.4	17.6	27.4	28.9	12.4
Pr	2.5	3.3	3.1	1.00	3.1	3.5	3.7	1.53
Nd	10.4	13.9	12.6	5.7	17.4	15.1	15.1	8.4
Sm	3.2	4.0	3.6	2.3	7.3	3.3	3.7	2.3
Eu	1.11	1.40	1.38	0.98	2.28	0.85	0.87	0.55
Gd	3.6	4.7	4.0	3.8	7.8	3.0	2.8	2.4
Tb	0.69	0.92	0.79	0.79	1.25	0.48	0.52	0.41
Dy	4.2	5.6	4.9	5.5	7.9	3.0	2.7	3.0
Ho	0.95	1.31	1.17	1.16	1.71	0.59	0.59	0.65
Er	2.6	3.5	2.9	3.3	5.0	1.63	1.72	2.0
Tm	0.41	0.55	0.47	0.52	0.72	0.18	0.26	0.24
Yb	2.4	3.3	2.9	3.1	4.7	1.50	1.49	1.61
Lu	0.40	0.57	0.49	0.47	0.71	0.23	0.24	0.28
Hf	2.1	3.1	2.5	2.2	3.5	2.4	2.2	1.57
Ta	0.60	1.02	0.91	0.15	0.24	0.34	0.37	0.51
Pb	0.66	0.68	0.67	0.03	0.08	0.09	0.14	0.03
Th	0.71	1.12	1.01	0.10	0.72	3.1	3.04	0.52
U	0.22	0.33	0.34	0.09	0.46	0.96	1.10	0.07
Nb/Ta	16	16	17	15	17	17	17	16
Zr/Hf	30	30	32	36	32	30	31	35

Sample#	Jang 87-279	Jang 87-283	Jang 87-51	Jang 87-86	Jang 87-48	Jang 88-74	Jang 88-85	B1-C
ID	Sediments	Sediments	Sediments	Sediments	Sediments	Sediments	Sediments	norite dyke
SiO2	51	47	57	60	51	54	55	51
TiO2	1.54	2.70	0.84	0.85	76	77	63	0.92
Al2O3	14.7	14.4	18.9	22.2	15.6	22.5	21.7	14.5
FeO	11.6	13.3	6.9	4.8	11.7	7.8	7.5	10.0
MnO	0.22	0.18	0.10	0.09	0.05	0.08	0.05	0.00
MgO	6.7	7.5	5.0	3.7	10.6	5.4	4.1	7.3
CaO	1.34	2.8	1.01	0.70	52	49	32	11.0
Na2O	1.37	2.0	2.5	1.27	0.59	1.61	0.98	0.92
K2O	4.3	3.7	4.5	5.8	4.7	4.8	4.5	0.17
Mg#	0.36	0.36	0.42	0.43	0.48	0.41	0.36	0.42
Rb	132	107	115	118	163	125	103	1.16
Sr	87	191	142	70	49	35	43	89
Y	22.8	30.5	10.9	19.1	4.0	15.2	12.5	18.7
Zr	181	245	204	235	151	65	55	46
Nb	25	20.5	21.6	19.1	10.5	8.0	8.2	3.3
Ba	588	672	917	1299	203	345	396	33
La	31	39	8.6	33	40	42	17.9	2.97
Ce	81	89	25	100	83	87	36	8.37
Pr	8.8	10.9	2.45	9.02	8.4	10.3	3.94	1.34
Nd	34	41	9.1	31	25	35	12.9	6.6
Sm	6.2	8.0	1.75	5.3	3.0	6.4	2.2	2.2
Eu	1.34	2.11	0.49	1.10	0.43	1.12	0.58	0.75
Gd	4.8	6.5	1.35	4.2	1.70	4.2	2.1	2.9
Tb	0.84	1.10	0.26	0.63	0.19	0.61	0.44	0.53
Dy	4.8	6.1	1.72	3.8	0.88	3.2	2.6	3.5
Ho	1.06	1.39	0.45	0.86	0.17	0.64	0.52	0.78
Er	3.1	3.8	1.51	2.5	0.41	1.65	1.34	2.2
Tm	0.50	0.66	0.26	0.46	0.06	0.24	0.19	0.31
Yb	3.4	4.4	2.1	2.7	0.44	1.44	1.20	2.1
Lu	0.53	0.75	0.36	0.51	0.07	0.21	0.18	0.34
Hf	6.0	7.5	6.7	8.0	5.4	2.3	1.83	1.62
Ta	2.7	2.8	2.8	3.0	2.2	1.95	1.29	0.19
Pb	0.04	0.16	0.05	0.06	0.30	0.29	0.03	0.00
Th	9.2	8.2	18.3	19.2	19.4	9.0	9.5	0.30
U	7.3	5.2	7.2	4.8	0.61	1.14	1.54	0.16
Nb/Ta	9	7	8	6	5	4	6	18
Zr/Hf	30	33	31	29	28	29	30	29

REFERENCES

- Abbey, S., 1983. Studies in 'standard samples' of silicate rocks and minerals, 1969-1982. *Geological Survey Canada, Paper 83-15*.
- Adam, J., Green, T.H. and Sie, S.H., 1993. Proton microprobe determined partitioning of Rb, Sr, Ba, Y, Zr, Nb and Ta between experimentally produced amphiboles and silicate melts with variable F content. *Chemical Geology*, **109**, 29-49.
- Ayres, J.C. and Watson, E.B., 1993. Rutile solubility and mobility in supercritical aqueous fluids. *Contributions to Mineralogy and Petrology*, **114**, 321-330.
- Baker, M.B., Hirschmann, M.M., Ghiorso, M.S. and Stolper, E.M., 1995. Compositions of near-solidus peridotite melts from experiments and thermodynamic calculations. *Nature*, **375**, 308-311.
- Barberi, F., Bigioggero, B, Boriani, A., Cattaneo, M., Lavallin, A., Cioni, R., Eva, C., Gelmini, R., Giorgetti, F., Laccarino, S., Innocenti, F., Marinelli, G., Slejko, D. and Sudradjnt, A., 1987. The Island of Sumbawa; a major structural discontinuity in the Indonesian arc. *Bollettino della Societa Geologica Italiana*, **106 (4)**, 547-620.
- Barth, M.G., Rudnick, R.A. and Taylor, S.R., 1998. Tracking the budget of Nb and Ta in the Continental Crust. GERM abstracts.
- Brenan, J.M., Shaw, H.F., Phinney, D.L. and Ryerson, F.J., 1994. Rutile-aqueous fluid partitioning of Nb, Ta, Hf, Zr, U and Th: implications for high field strength element depletions in island-arc basalts. *Earth and Planetary Science Letters*, **128**, 327-339.

- Briqueu, L. Bougault, H. and Joron, J.L., 1984. Quantification of Nb, Ta, Ti and V anomalies in magmas associated with subduction zones: petrogenetic implications. *Earth and Planetary Science Letters*, **68**, 297-308.
- Bryan, W.B., Stice, G.D. and Ewart, A., 1972. Geology, petrography and geochemistry of the volcanic islands of Tonga. *Journal of Geophysical Research*, **77** (8), 1566-1585.
- Cabanis, B. and Lecolle, M., 1989. Le diagramme La/10-Y/15-Nb/8: un outil pour la discrimination des series volcaniques et la mise en evidence des processus de melange et/ou de contamination crustale. *C.R. Academique Science Series, II*, **309**, 2023-2029.
- Coish, R.A., 1989. Boninitic lavas of the Appalachian ophiolites: a review. In *Boninites*. Crawford, A.J. (Ed). Unwin Hyman, Boston.
- Coryell, C.D., Chase, J.W. and Winchester, J.W., 1963. A procedure for the geological interpretation of terrestrial rare-earth abundance patterns. *Journal of Geophysical Research*, **68**, 559-566.
- Crawford, A.J., Falloon, T.J. and Green, D.H., 1989. Classification, petrogenesis and tectonic setting of boninites. In *Boninites*. Crawford, A.J. (Ed). Unwin Hyman, Boston.
- Dallwitz, W.B., 1968. Chemical composition and genesis of clinoenstatite-bearing volcanic rocks from Cape Vogel, Papua: a discussion. 23rd International Geological Congress, 2, 229-242.
- Dallwitz, W.B., Green, D.H. and Thompson, J.E., 1966. Clinoenstatite in a volcanic rock from the Cape Vogel area, Papua. *Journal of Petrology*, **7**, 375-403.

- Duncan, R.A. and Varne, R., 1988. The age and distribution of the igneous rocks of Macquarie Island. *Papers and Proceedings of the Royal Society of Tasmania*, **122(1)**, 45-50.
- Eggins, S.M., Rudnick, R.L. and McDonough, W.F., 1998. The composition of peridotites and their minerals: a laser ablation ICP-MS study. *Earth and Planetary Science Letters*, **154**, 53-71.
- Eggins, S.M., Woodhead, J.D., Kinsley, L.P.J., Mortimer, G.E., Sylvester, P., McCulloch, M.T., Hergt, J.M. and Handler, M.R., 1997. A simple method for the precise determination of ≥ 40 trace elements in geological samples by ICPMS using enriched isotope internal standardisation. *Chemical Geology*, **134**, 311-326.
- Elinson, S.V. and Petrov, K.I., 1965. *Analytical Chemistry of Zirconium and Hafnium*. Vinogradov, A.P. (Ed) Ann Arbor-Humphrey Science Publishers, Ann Arbor, London.
- Ewart, A. and Hawkesworth, C.J., 1987. The Pleistocene-recent Tonga-Kermadec Arc lavas; interpretation of new isotopic and rare earth data in terms of a depleted mantle source model. *Journal of Petrology*, **28(3)**, 495-530.
- Fairbrother, F., 1967. *The Chemistry of Niobium and Tantalum*. Amsterdam Elsevier Publishers.
- Fassett, J.D. and Paulsen, P.J., 1989. Isotope dilution mass spectrometry for accurate elemental analysis. *Analytical Chemistry*, **61 (10)**; 643A-649A.
- Faure, G., 1986. *Principles of Isotope Geology*. Second edition. John Wiley and Sons Inc.

- Fedorowich, J.S., Richards, J.P., Kerrich, R. and Fan, J., 1993. A rapid method for REE and trace-element analysis using laser sampling ICP-MS on direct fusion whole-rock glasses. *Chemical Geology*, **106**: 229-249.
- Floyd, P.A. and Winchester, J.A., 1975. Magma-type and tectonic setting discrimination using immobile elements. *Earth and Planetary Science Letters*, **27**, 211-218.
- Foley, S.F. and Wheller, G.E., 1990. Parallels in the origin of the geochemical signatures of island arc volcanics and continental potassic igneous rocks: The role of residual titanites. *Chemical Geology*. **85**: 1-18.
- Gibalo, I.M., 1970. *Analytical Chemistry of Niobium and Tantalum*. Ann Arbour, Humphrey Science Publishers.
- Gladney, E.S., Burns C.E. and Roelandts, I., 1983. 1982 compilation of elemental concentrations in eleven United States Geological Survey rock standards. *Geostandards Newsletter*, **7**; 3-226.
- Glaney, E.S., Jones, E.A., Nickell, E.J. and Roelandts, I., 1990. 1988 compilation of elemental concentration data for USGS basalt BCR-1. *Geostandards Newsletter*, **14** (2), 209-360.
- Govindaraju, K., 1994. Compilation of working values and sample description for 383 geostandards. *Geostandards Newsletter*, **18**, 1-158.
- Govindaraju, K. and de la Roche, H., 1977. Rapport (1966-1976) sur les elements en trace dans trois standards geochimiques du CRPG: Basalte BR et granites, GA et GH. *Geostandards Newsletter*, **1**; 67-100.
- Green, T.H. and Pearson, N.J., 1986. Ti-rich accessory phase saturation in hydrous mafic-felsic compositions at high P,T. *Chemical Geology*, **54**: 185-201.

- Green, T.H. and Pearson, N.J., 1987. An experimental study of Nb and Ta partitioning between Ti-rich minerals and silicate liquids at high pressure and temperature. *Geochemica et Cosmochemica Acta*, **51**, 55-62.
- Green, D.H. and Ringwood, A.E., 1967. An experimental investigation of the gabbro to eclogite transformation and its petrological applications. *Geochemica et Cosmochemica Acta*, **31**, 767-833.
- Green, T.H., Sie, S.H., Ryan, C.G. and Cousens, D.R., 1989. Proton microprobe determination of Nb, Ta, Zr, Sr and Y between garnet, clinopyroxene and basaltic magma at high pressure and temperature. *Chemical Geology*, **74**, 201-216.
- Green, T., 1995. Significance of the Nb/Ta as an indicator of geochemical processes in the crust-mantle system. *Chemical Geology*, **120**, 347-359.
- Griffin, B.J. and Varne, R., 1980. The Macquarie Island ophiolite complex: Mid-Tertiary oceanic lithosphere from a major ocean basin. *Chemical Geology*, **30**, 285-308.
- Guenther, D., Longerich, H.P. and Jackson, S.E., 1995. A new enhanced sensitivity quadrupole inductively coupled plasma mass spectrometer (ICP-MS). *Canadian Journal of Applied Spectroscopy*, **40(4)**, 111-116.
- Hall, G.E.M. and Plant, J.A., 1992. Analytical errors in the determination of high field strength elements and their implications in tectonic interpretations studies. *Chemical Geology*, **95**, 141-156.
- Hall, G.E.M. and Pelchat, J-C., 1990. Determination of zirconium, niobium, hafnium and tantalum at low levels in geological materials by inductively coupled plasma mass spectrometry. *Journal of Analytical Atomic Spectrometry*, **5**; 339-349.

- Harris, N.B.W., Pearce, J.A. and Tindle, A.G., 1986. Geochemical characteristics of collision-zone magmatism. *In* Coward, M.P. and Reis, A.C. (eds) *Collision Tectonics. Special Publication of the Geological Society*, **19**, 67-81.
- Hart, S.R. and Dunn, T., 1992. Experimental cpx/melt partitioning of 24 trace elements. *Contributions to Mineralogy and Petrology*, **113**, 1-8.
- Hawkesworth C.J. and Ellam, R.M., 1989. Chemical fluxes and wedge replenishment rates along recent destructive plate margins. *Geology*, **17**, 46-49.
- Hawkesworth, C.J., Hergt, J.M., Ellam, R.M. and McDermott, F., 1991. Element fluxes associated with subduction related magmatism. *Philosophical Transactions of the Royal Society of London, A*, **335**, 393-405.
- Hawkins Jr, J.W., 1995. Geology of the Lau Basin. *In* *Backarc Basins: Tectonics and Magmatism*. Brian Taylor (Ed.). Plenum Press, New York.
- Hertogen, J., Sachtleben, Th. and Jenner, G.A., 1985. Trace element geochemistry and petrogenesis of basalts from deep sea drilling project sites 556-559 and 561-564. *Reprinted from* Bougault, H., Cande, S.C. *et al.*, 1985. *Initial reports of the Deep Sea Drilling Project, Volume LXXXII*, Washington (US Government Printing Office).
- Hoernle, K. and Schmincke, H-U., 1993a. The petrology of the tholeiites through melilite nephelinites on Gran Canaria, Canary Islands; crystal fractionation, and depths of melting. *Journal of Petrology*, **34** (3), 573-597.
- Hoernle, K. and Schmincke, H-U., 1993b. The role of partial melting in the 15-Ma geochemical evolution of the Gran Canaria; a blob model for the Canary hotspot. *Journal of Petrology*, **34** (3), 599-626.

- Hofmann, A.W., 1988. Chemical differentiation of the Earth: the relationship between mantle, continental crust and oceanic crust. *Earth and Planetary Science Letters*, **90**, 297-314.
- Horn, I., 1995. Die Bestimmung des Verteilungsverhaltens der HFSE, LREE und ausgewählter Uebergangselemente zwischen Spinell und Schmelzen: Ein experimentelle Studie. PhD dissertation, Georg-August-Universitaet zu Goettingen.
- Horn, I., Longerich, H.P. and Jackson, S.E. (1996). Breaking the ppb detection limit using laser ablation microprobe ICP-MS. *V.M. Goldschmidt Conference, 1996, Journal of Conference Abstracts*, **1(1)**, Cambridge Publications; 274.
- Ionov, D.A. and Hofmann, A.W., 1995. Nb-Ta-rich mantle amphiboles and micas: Implications for subduction-related metasomatic trace element fractionations. *Earth and Planetary Science Letters*, **131**, 341-356.
- Irvine, T.N. and Baranger, W.R.A., 1971. A guide to the chemical classification of the common volcanic rocks. *Canadian Journal of Earth Sciences*, **8**, 523-548.
- Jackson, S.E., Longerich, H.P., Dunning, G.R. and Fryer, B.J., 1992. The application of laser-ablation microprobe – inductively coupled plasma – mass spectrometry (LAM-ICP-MS) to *insitu* trace element determinations in minerals. *Canadian Mineralogist*, **30**; 1049-1064.
- Jeffries, T.E., 1996. *Investigations of mineral analysis by laser ablation inductively coupled plasma mass spectrometry*. PhD thesis, Chapter 4: Laser ablation characteristics in mineral analysis. University of Aberystwyth, UK, 48-108.
- Jenner, G.A., 1981. Geochemistry of the high-Mg andesites from Cape Vogel, Papua New Guinea. *Chemical Geology*, **33**, 307-332.

- Jenner, G.A., 1982. *Petrogenesis of High-Mg Andesites. An Experimental and Geochemical Study with Emphasis on High-Mg Andesites from Cape Vogel, PNG.* University of Tasmania, Hobart.
- Jenner, G.A., 1996. Trace element geochemistry of igneous rocks: geochemical nomenclature and analytical geochemistry. In Wyman, D.A. (Ed). *Trace Element Geochemistry of Volcanic Rocks: Applications for Massive Sulphide Exploration.* Geological Association of Canada Short Course Notes **12**, 51-79.
- Jenner, G.A., Cawood, P.A., Rautenschlein, M. and White, W.M., 1987. Composition of back-arc basin volcanics, Valu Fa Ridge, Lau Basin: Evidence for a slab-derived component in their mantle source. *Journal of Volcanology and Geothermal Research*, **32**, 209-222.
- Jenner, G.A., Longerich, H.P., Jackson, S.E. and Fryer, B.J., 1990. ICP-MS - A powerful tool for high precision trace element analysis in Earth Sciences: Evidence from analysis of selected U.S.G.S. reference samples, *Chemical Geology*, **83**; 133-148.
- Jochum, K.P. and Jenner G.A., 1994. Trace element analysis of Geological Survey of Japan silicate reference materials: Comparison of SSMS with ICP-MS data and a critical discussion of compiled values. *Fresenius' Journal of Analytical Chemistry*, **350**, 310-318.
- Jochum, K.P., Seufert, H.M. and Thirlwall, M.F., 1989a. High sensitivity Nb analysis by spark-source mass spectrometry (SSMS) and calibration with of XRF Nb and Zr. *Chemical Geology*, **81**, 1-16.

- Jochum, K.P., McDonough, W.F., Palme, H. and Spettel, B., 1989b. Compositional constraints on the continental lithospheric mantle from trace elements in spinel peridotite xenoliths. *Nature*, **340**, 548.
- Jochum, K.P., Seufert, H.M., Midinet-Best, S., Rettmann, E., Schoenberger, and Zimmer, M., 1988. Multi-element analysis by isotope dilution-spark source mass spectrometry (ID-SSMS). *Fresenius Zeitschrift fuer Analytische Chemie*, **331**; 104-110.
- Jochum, K.P., Seufert, H.M., Spettel, B. and Palme, H., 1986. The solar system abundances of Nb, Ta and Y and the relative abundances of refractory lithophile elements in differentiated planetary bodies. *Geochemica et Cosmochemica Acta*, **50**, 1173-1183.
- Kelemen, P.B., Johnson, K.T.M., Kinzler, R.J. and Irving, A.J., 1990. High-field-strength element depletions in arc basalts due to mantle-magma interaction. *Nature*. 345: 521.
- Keller, O.L. and Chetham-Strode, A. 1966. A study by raman spectroscopy of complex ions formed by tantalum (V) in the system Ta(V)-HF-NH₄F-H₂O. *Inorganic Chemistry*, **3** (3), 367-372.
- Keppler, H., 1996. Constraints from partitioning experiments on the composition of subduction-zone fluids. *Nature*, **380**, 237-240.
- Krauskopf, K., 1967. *Introduction to Geochemistry*. McGraw Hill, New York.
- Lee, D.C. and Halliday, A.N., 1995. Hafnium-tungsten chronometry and the timing of terrestrial core formation. *Nature*, **378**; **6559**, 771-774.

- Lide, D.R. (Ed), 1996. *CRC Handbook of Chemistry and Physics*. National Institute of Standards and Technology.
- Linnen, R.L. and Keppler, H., 1997. Columbite solubility in granitic melts: consequences for the enrichment and fractionation of Nb and Ta in the Earth's crust. *Contributions to Mineralogy and Petrology*, **128**, 213-227.
- Longerich, H.P., 1989. The application of isotope dilution to inductively coupled plasma-mass spectrometry. *Atomic Spectroscopy*, **10** (4); 112-115.
- Longerich, H.P., Horn, I. and Jackson, S.E. (1997). ICP torch bonnet for reduction of air entrainment and background of polyatomic ions. *Abstract, European Winter Conference on Plasma Spectroscopy, Gent, Belgium*.
- Loock, G., 1992. *Character and distribution of the Indian Ocean mantle domain: A study of the mantle source compositions of Lau Basin volcanics (SW Pacific) and Indian Ocean mid-ocean ridge basalts*. PhD dissertation, University of Cologne.
- Maaløe and Aoki, 1977. The major element composition of the upper mantle estimated from the composition of lherzolites. *Contributions to Mineralogy and Petrology*, **63**, 161-173.
- McCulloch, M.T. and Gamble, J.A., 1991. Geochemical and geodynamical constraints on subduction zone magmatism. *Earth and Planetary Science Letters*, **102**, 358-374.
- McDonough, W.F., 1991. Partial melting of subducted oceanic crust and isolation of its residual eclogitic lithology. *Philosophical Transactions of the Royal Society of London, Series A*, **335**, 407-418.

- Monzier, M, Robin, C., Eissen, J-P. and Cotten, J., 1997. Geochemistry vrs seismo-tectonics along the volcanic New Hebrides Central Chain (SW Pacific). *Journal of Volcanology and Geothermal Research*. **78 (1-2)**, 1-29.
- Moore, L.J., Moody, J.R., Barnes, I.L., Gramich, J.W., Murphy, T.J., Paulsen, P.J. and Shields, W.R., 1973. Trace determination of Rubidium and strontium in silicate standard reference materials. *Analytical Chemistry*, **45**, 2384-2387.
- Morris, J.D. and Hart, S.R., 1983. Isotopic and incomaptible element constraints on the genesis of island arc volcanics from Cold Bay and Amak Island, Aleutians, and implications for mantle source. *Geochemica et Cosmochemica Acta*, **47**, 2015-2030.
- Mukherji, A.K., 1970. *Analytical Chemistry of Zirconium and Hafnium. International Series of Monographs in Analytical Chemistry*, **40**. Belcher, R and Frieser, M. (Eds). Pergamon Press.
- Münker, C., 1998. Nb/Ta fractionation in a Cambrian arc/back arc system, New Zealand: source constraints and application of refined ICPMS techniques. *Chemical Geology*, **144**, 23-45.
- Murton, B.J., Peete, D.W., Arculus, R.J., Pearce, J.A. and Van der Lann, S., 1992. Trace-element geochemistry of volcanic rocks from site 786: the Izu-Bonin forearc region. In *Proceedings of the Ocean Drilling Program, Scientific results, Sites 778-786, Bonin/Mariana region*. Fryer, P., Pearce, J.A., Stokking, L.B., *et al.* (Eds), pp. 211-235.

- Nicholls, I.A., 1974. A direct fusion method of preparing silicate rock glasses for energy dispersive electron microprobe analysis. *Chemical Geology*, **14**: 151-157.
- Odling, N.W.A., 1995. A fusion method for preparing glass samples of peridotitic and picritic rock compositions for bulk analysis. *Mineralogical Magazine*, **59**: 267-271.
- Pearce, J.G., Perkin, W.T., Westgate, J.A., Gorton M.P., Jackson, S. E., Neal, C. R., Chenery, S.P. (1997). A Compilation of new and published major and trace element data for NIST SRM 610 and NIST SRM 612 glass reference materials. *Geostandards Newsletter*, **21** (1), 115-144.
- Pearce, J.A. and Cann, J.R., 1973. Tectonic setting of basic volcanic rocks determined using trace element analyses. *Earth and Planetary Science Letters*, **19**, 290-300.
- Pearce, J.A. and Peate, D.W. 1995. Tectonic implications of the composition of volcanic arc magmas. *Annual Review of Earth and Planetary Sciences*, **23**, 251-285.
- Pearce, J.A., 1982. Trace element characteristics in lavas from destructive plate boundaries. In Thorpe, R.S. (Ed), *Andesites*, Wiley, Chichester, 524-548.
- Pearce, J.A., Harris, N.W.B. and Tindle, A.G., 1984. Trace element discrimination diagrams for the tectonic interpretation of granitic rocks. *Journal of Petrology*, **25**, 956-983.
- Piercey, S.J., Jenner, G.A. and Wilton, D.H.C., 1997. The stratigraphy and geochemistry of the Southern Pacquet Harbour Group, Baie Verte Peninsula, Newfoundland: Implications for mineral exploration. *Current Research, Newfoundland Department of Mines and Energy, Geological Survey, Report*, **97-1**, 119-139.

- Plank, T and Langmiur, C.H., 1998. The chemical composition of subducting sediment and its consequences for the crust and mantle. *Chemical Geology*, in press.
- Poitrasson, F., Pin, C., Telouk, P. and Imbert, J-L., 1993. Assessment of a simple method for the determination of Nb and Ta at sub- $\mu\text{g/g}$ level in silicate rocks by ICP-MS. *Geostandards Newsletter*, **17 (2)**, 209-215.
- Potts, P.J., 1987. *A Handbook of Silicate Rock Analysis*. Blackie Academic and Professional; an imprint of Chapman and Hall.
- Potts, P.J., Thorpe, O. Williams and Watson, J.S., 1981. Determination of the rare earth element abundances in 29 international rock standards by instrumental neutron activation analysis: a critical appraisal of calibration errors. *Chemical Geology*, **34**; 331-352.
- Rautenschlein, M., Jenner, G.A., Hertogen, J., Hofmann, A.W., Kerrich, R., Schmincke, H.-U. and White, W.M., 1985. Isotopic and trace element composition of volcanic glasses from Akaki Canyon, Cyprus: implications for the origin of the Troodos ophiolite. *Earth and Planetary Science Letters*, **75**, 369-383.
- Rea, D.K. and Ruff, L.J., 1996. Composition and mass flux of sediment entering the world's subduction zones: Implications for global sediment budgets, great earthquakes, and volcanism. *Earth and Planetary Science Letters*, **140**, 1-12.
- Reeves, R.D. and Brooks, R.R., 1978. *Trace Element Analysis of Geological Materials*. In: *A Series of Monographs on Analytical Chemistry and Its Applications*. **Vol 51**. Elving, P.J. and Winefordner, J.D. (Eds). John Wiley & Sons.

- Reid, J.E., Horn, I., Longerich, L.P., Forsythe, L. and Jenner, G.A., 1998. Determination of the High Field Strength Elements (Zr, Nb, Hf, and Ta) and Selected Rare Earth Elements (La, Ce, Pr, Sm, Gd, Ho, Tm, and Lu) in a Flux-Free Fusion of Whole Rock Samples using Laser Ablation-Inductively Coupled Plasma-Mass Spectrometry (LA-ICP-MS) with Combined External and Isotope Dilution Calibration. *Geostandards Newsletter*, submitted.
- Robin, C., Eissen, J-P. and Monzier, M., 1994. Ignimbrites of basaltic andesite and andesite composition from Tanna, New Hebrides arc. *Bulletin of Volcanology*, **56** (1), 10-22.
- Rollinson, H., 1993. *Using Geochemical Data: evaluation, presentation, interpretation*. Longman Scientific and Technical. 174-193.
- Rudnick, R.L., McDonough, W.F. and Chappel, B.W., 1991. Carbonatite metasomatism in the northern Tanzanian mantle: petrographic and geochemical characteristics. *Earth and Planetary Science Letters*, **114**, 463-475.
- Ryerson, F.J. and Watson, E.B., 1987. Rutile saturation in magmas: implications for Ti-Nb-Ta depletion in island-arc basalts. *Earth and Planetary Science Letters*. **86**, 225-239.
- Saunders, A.D., Tarney, J., Marsh, N.G. and Wood, D.A., 1980. Ophiolites as ocean crust or marginal basin crust: a geochemical approach, in, Panayiotou, (ed.), *Ophiolites: Proceedings of the International Ophiolite Symposium Cyprus 1979*, Ministry of Agriculture and Natural Resources, Geological Survey Department, Cyprus, p. 193-204.

- Saunders, A.D., Tarney, J. and Weaver, S.D., 1980. Traverse geochemical variations across the Antarctic Peninsula: Implications for the genesis of calc-alkaline magmas. *Earth and Planetary Science Letters*, **46**, 344-360.
- Schroeder, B., Thompson, G., Sulanowska, M. and Ludden, J.N., 1980. Analysis of geological materials using an automated x-ray fluorescence system. *X-ray Spectrometry*, **9**; 198-205.
- Sen, C. and Dunn, T., 1994. Dehydration melting of a basaltic composition amphibolite at 1.5-2.0GPa: Implications for the origin of adakites, *Contributions to Mineralogy and Petrology*, **117**, 394-409.
- Shannon, R.D., 1976. Revised effective ionic radii in halides and chalcogenides. *Acta Crystallographica*, **32**.
- Smith, I.E.M. and Davies, H.L., 1976. *Geology of the southeastern Papua*. PhD. Thesis, Australian National University, Canberra, A.C.T. (unpublished).
- Stolz, A.J., Jochum, K.P., Spettel, B. and Hofmann, A.W., 1996. Fluid- and melt-enrichment in the sub-arc mantle: Evidence from Nb/Ta variations in island-arc basalts. *Geology*, **24(7)**, 587-590.
- Sun, S.-s. and McDonough, W.F., 1989. Chemical and isotopic systematics of ocean basalts: implications for mantle composition and processes. In Saunders, A.D. and Norry, M.J. (eds). *Magmatism in the Ocean Basins. Geological Society Special Publications* No. **42**, 313-345.
- Sweeney, R.J., Green, D.H. and Sie, S.H., 1992. Trace and minor element partitioning between garnet and amphibole and carbonatitic melt. *Earth and Planetary Science Letters*, **113**, 1-14.

- Sylvester, P.J., Cambell, I.H. and Bowyer, D.A., 1997. Niobium/Uranium evidence for early formation of the continental crust. *Science*, **275**, 521-523.
- Takahashi, E., 1986. Melting of a dry peridotite KLB-1 up to 14Gpa: Implications on the origin of peridotitic upper mantle. *Journal of Geophysical Research*, **91 (B9)**, 9367-9382.
- Tatsumi, Y. and Ishazaka, K., 1981. Existence of andesitic primary magma: an example from Southwest Japan. *Earth and Planetary Science Letters*, **53**, 124-130.
- Taylor, S.R. and McLennan, 1985. *The Continental Crust; It's Composition and Evolution*. Blackwell.
- Taylor, S.R. and Gorton, M.P., 1977. Geological application of spark source mass spectrometry – III. Element sensitivity, precision and accuracy. *Geochemica et Cosmochemica Acta*, **41**, 1375-1380.
- Taylor, W.R. and Green, D.H., 1988. Measurement of reduced peridotite-C-O-H solidus and implications for redox melting of the mantle. *Nature*, **332**, 349-352.
- Thirlwall, M.F., Smith, T.E., Graham, A.M., Theodorou, N., Hollings, P., Davidson, J.P. and Arculus, R.J., 1994. High field strength element anomalies in arc lavas: Source or process? *Journal of Petrology*, **35**, 819-38.
- Van Gool, J.A.M., 1992. The Grenville Front Foreland Fold-and-Thrust Belt in Southwestern Labrador: Mid-Crustal Structural and Metamorphic Configuration of a Proterozoic Orogenic Thrust Wedge. PhD dissertation, Memorial University of Newfoundland.

- Von Huene, R. and Scholl, D.W., 1991. Observations at convergent margins concerning sediment subduction, subduction erosion, and the growth of continental crust. *Reviews of Geophysics*, **29** (3), 279-316.
- Wallace, M.E. and Green, D.H., 1988. An experimental determination of primary carbonatite composition. *Nature*, **335**, 343-346.
- Wedepohl, K.H., 1995. The composition of the Continental Crust. *Geochemica et Cosmochemica Acta*, **59**, 1217-1232.
- Whitford, D.J., 1975. Strontium isotopic studies of the volcanic rocks of the Sunda arc, Indonesia, and their petrogenetic implications. *Geochemica et Cosmochemica Acta*, **39**, 1287-1302.
- Winchester, J.A. and Floyd, P.A., 1977. Geochemical differentiation of different magma series and their differentiation products using immobile elements. *Chemical Geology*, **20**, 325-343.
- Wolff, J.A., 1984. Variation in Nb/Ta during differentiation of phonolitic magma, Tenerife, Canary Islands. *Geochemica et Cosmochemica Acta*, **48**, 1345-1348.
- Wood, D.A., 1980. The application of a Th-Hf-Ta diagram to problems of tectonomagmatic classification and to establishing the nature of crustal contamination of basaltic lavas of the British Tertiary volcanic province. *Earth and Planetary Science Letters*, **50**, 11-30.
- Wyllie, P.J. and Sekine, T., 1982. The formation of mantle phlogopite in subduction zone hybridisation. *Contributions to Mineralogy and Petrology*, **79**, 375-380.

Xie, Q. and Kerrich, R., 1995. Application of isotope dilution for the precise measurement of Zr and Hf in low abundance samples and international reference materials by inductively coupled plasma mass spectrometry: Implications for Zr (Hf) / REE fractionations in komatiites. *Chemical Geology*, **123**; 17-27.

